Impact of Stratospheric Intrusions, Regional Wildfires, and Long-Range Transport Events on Air Quality in the Western United States

Leo Miguel Paolo M. Baylon

A dissertation
submitted in partial fulfillment of the
requirements for the degree of

Doctor of Philosophy

University of Washington

2017

Reading Committee:

Daniel A. Jaffe, Chair

Lyatt Jaeglé

Joel A. Thornton

Program Authorized to Offer Degree:
Department of Atmospheric Sciences

University of Washington

Abstract

Impact of Stratospheric Intrusions, Regional Wildfires, and Long-Range Transport Events on Air Quality in the Western United States

Leo Miguel Paolo M. Baylon

Chair of the Supervisory Committee:

Professor Daniel A. Jaffe

Department of Atmospheric Sciences

Baseline ozone refers to observed concentrations of tropospheric ozone at sites that have a negligible influence from local emissions. In 2004, the Mount Bachelor Observatory (MBO) was established to examine baseline air masses as they arrive to North America from the west. In the western U.S., air quality is impacted by local, regional, and trans-Pacific sources, which can be natural or anthropogenic. Because of increasing baseline O_3 and tighter air quality standards, it is therefore important to understand the nature and the impact of high-ozone events on urban air quality in the western U.S.

This dissertation is focused on three types of high-ozone events that we typically observe at MBO and in other surface sites in the western U.S.: (1) upper troposphere/lower stratosphere (UT/LS) episodes, (2) biomass burning (BB) plumes, and (3) long-range transport (LRT) events.

First, I looked at an anomalously high-O_3 springtime episode in May 2012, where I observed an O_3 increase of 2.0–8.5 ppbv in monthly average maximum daily 8–hour average O_3 mixing ratio (MDA8 O_3) at MBO and numerous other sites in the western U.S. compared to previous years. This shift in the O_3 distribution had a strong effect on the number of exceedance days. I also observed a good correlation between daily MDA8 variations at MBO and at downwind sites. This is consistent with previous studies that show that under specific meteorological conditions, synoptic variation in O_3 at MBO can be observed at other surface sites in the western U.S. At MBO, the elevated O_3 concentrations in May 2012 are associated with low CO values and low water vapor values, consistent with transport from the upper troposphere/lower stratosphere (UT/LS). The Real-time Air Quality Modeling System analyses indicate that a large flux of O_3 from the UT/LS in May 2012 contributed to the observed enhanced O_3 across the western U.S. Results from this component suggest that a network of mountaintop observations, LiDAR and satellite observations of O_3 could provide key data on daily and interannual variations in baseline O_3.

Second, I studied BB events that I observed at MBO during the summer of 2015. Regional BB has the potential to increase ozone in the western U.S. especially during summer. I explored the photochemical environment in BB plumes, which remains poorly understood. Because I am interested in understanding the effect of aerosols only (as opposed to the combined effect of aerosols and clouds), I carefully selected three cloud-free days in August and investigate the photochemistry in these plumes. At local mid-day (solar zenith angle, SZA =

35°), $j(NO_2)$ values were slightly higher (0.2-1.8%) in the smoky days compared to the smoke-free day, presumably due to enhanced scattering by the smoke aerosols. At higher SZA (70°), BB aerosols decrease $j(NO_2)$ by 14-21%. I also observe a greater decrease in the actinic flux at 310-350 nm, compared to 350-420 nm, presumably due to absorption in the UV by brown carbon. I compare my measurements with results from the TUV5.2 model and find a good agreement during cloud-free conditions. I perform sensitivity runs and find that $j(NO_2)$ is not sensitive to O_3 column input. If I keep single scattering albedo and aerosol optical depth constant, an increase in the total ozone from 280 to 400 DU leads to only a 0.8% decrease in $j(NO_2)$. Finally, I used the extended Leighton relationship to estimate mid-day HO_2 and RO_2 concentrations and $P(O_3)$ in the fire plumes. I calculate HO_2 and RO_2 values from 49-185 pptv, and compute ozone production rates of ~2 ppbv/hour in these fire plumes.

Finally, I looked at an LRT event on Spring 2015. I observed O_3 and CO enhancements of up to 40 ppbv and 80 ppbv, respectively, at MBO. I also used measurements from the NOAA WP-3D Orion research aircraft during the Shale Oil and Natural Gas Nexus (SONGNEX) campaign in Spring 2015. One of the flights during the SONGNEX campaign intercepted the Siberian plume. Ground-based, satellite, and LiDAR data suggest that the Siberian plume was transported at high elevation, did not encounter a high-pressure system that would have led to air subsidence, and therefore did not cause any surface O_3 enhancement. I compare our measurements at MBO with aircraft observations and conclude that the Siberian airmass split into two plumes in the eastern Pacific. One plume moved eastward and was sampled by MBO. The other moved over to Alaska and then down to the U.S. Midwest; this second plume was intercepted by the aircraft. $\Delta\sigma_{sp}/\Delta CO$ enhancement ratios for the Siberian 2015 plume were higher than similarly aged plumes in previous studies, owing to dust and the absence of

particulate matter loss because of the relatively intact nature of the Siberian plume. $\Delta O_3/\Delta CO$ ratio observed at MBO was higher than the aircraft because of PAN decomposition. I look at the plume's reactive nitrogen speciation using data from the aircraft and find that ~75% of the NOy is stored as PAN. For ozone production to take place, the plume has to warm up (i.e., descend) to re-form NOx. But given the high elevation of the plume and stable atmospheric conditions, this likely did not take place.

The results of this dissertation have important policy implications. They suggest that at the current standard, high-ozone events such as BB plumes, UT/LS episodes, and LRT events would affect the attainment status of a site if they were not identified as exceptional events, which the EPA defines as an uncontrollable event that affected air quality. Understanding the nature and year-to-year variability of these events is therefore critical for an effective implementation of the US NAAQS. Long-term measurements aimed at observing exceptional events would be valuable. MBO is the only high-elevation site on the U.S. West Coast that routinely observes high-O_3 events in the FT; however, it provides measurements at only a single point. High-frequency measurements of O_3, water vapor and CO at a network of mountaintop sites would be valuable at observing exceptional events. Vertical profiles of O_3 and water vapor from LiDAR and ozonesondes, and satellite retrievals would also be helpful. This network of mountaintop observations, LiDAR and satellite observations of ozone could also provide key data on daily and interannual variations in baseline O_3. Forecasting exceptional events would be possible using high-resolution chemical transport models that have been evaluated and verified with free troposphere observations.

TABLE OF CONTENTS

LIST OF FIGURES

Chapter 2

Chapter 3

Chapter 4

LIST OF TABLES

Chapter 2

Chapter 3

Chapter 4

Acknowledgements

I am grateful to a lot of people for helping me get through the past six years.

First, I would like to thank Dan Jaffe for being an exceptional mentor. He has challenged me to become a better scientist, has allowed me to choose the direction of my research, and has provided words of advice and encouragement – science-related or otherwise – that I will forever be grateful for. I would also like to thank him for the opportunity to teach in UW-Bothell. I am also grateful to each of my committee members – Becky Alexander, Lyatt Jaeglé, and Joel Thornton – for providing insights on improving my manuscripts. I appreciate their patience and helpful advice.

I would like to acknowledge my friends in Seattle for providing me a home away from home. To Grads11, for being a fun group of classmates and friends. To the Jaffe Research Group, for being an amazing group of scientists. To my volleyball friends, for keeping me sane, for cheering me up during those grad school lows, and for celebrating with me during those grad school highs.

Finally, I would like to thank my family back home in the Philippines. For always being there in spirit. And for the never-ending love and support. This is for all of you.

CHAPTER 1

INTRODUCTION

Baseline ozone refers to observed concentrations of tropospheric ozone at sites that have a negligible influence from local emissions. In 2004, the Mount Bachelor Observatory (MBO; 2.8 km above sea level) was established by the University of Washington Atmospheric Chemistry group to examine baseline air masses as they arrive to North America from the west. In the western U.S., free tropospheric springtime ozone has been increasing since the 1990s, likely due to increasing precursor emissions in Asia and long-range transport to the western U.S. Biomass burning, both regional and long-range transport in origin, has also been shown to impact air quality in the region. In the context of increasing baseline ozone and tighter air quality standards, it is therefore important to understand the nature and the impact of these high-ozone episodes on urban air quality in the western U.S. These events would affect the attainment status of a site if they were not identified as exceptional events, which the U.S. Environment Protection Agency (EPA) describes as an unusual or natural event that affects air quality but is not reasonably controlled.

This dissertation is focused on three types of high-ozone events that we typically observe at MBO and in other surface sites in the western U.S.: (1) upper troposphere/lower stratosphere (UT/LS) events, (2) biomass burning (BB) plumes, and (3) long-range transport (LRT) episodes. But before each type of event is examined in detail in Chapters 2, 3, and 4, respectively, a discussion of the sources of air pollution in the western U.S. is warranted.

1.1 AIR QUALITY IN THE WESTERN UNITED STATES

Air quality in the western U.S. is impacted by local, regional, and trans-Pacific sources of pollution (Baylon et al., 2016; Cooper et al., 2009; Fine et al., 2015; Jaffe et al., 2008b; Jaffe, 2011; Jaffe et al., 2013; Jaffe and Ray, 2008; Lu et al., 2016; Swartzendruber et al., 2008; Timonen et al., 2013; Wigder et al., 2013a). These sources can be natural or anthropogenic.

The U.S. Environment Protection Agency (EPA) has set primary National Ambient Air Quality Standards (NAAQS) for six major pollutants, including ozone. These standards are set at levels to protect human health. The current ozone NAAQS requires that the three-year average of the fourth-highest annual maximum 8-hour ozone concentration (MDA8) be 70 ppbv or below (U.S. EPA, 2015). If these standards are not met, then a region is designated as a "nonattainment area." The state is then required to submit a state implementation plan (SIP) which outlines the steps that it needs to take in order to improve its air quality.

Tropospheric ozone is not emitted directly into the air but is produced from the interaction of nitrogen oxides ($NOx = NO + NO_2$) and volatile organic compounds (VOCs) in the presence of sunlight (Finlayson-Pitts and Pitts, 2000). It is a health hazard to sensitive individuals (Bell et al., 2006). People most at risk include children, older adults, people with asthma, and people who are active outdoors. Breathing ozone can trigger a variety of health problems including coughing, throat irritation, chest pain, and airway inflammation. It can also worsen bronchitis, emphysema, and asthma, leading to increased medical care and premature mortality (www.epa.gov/ozone-pollution). Ozone is the third strongest anthropogenic greenhouse gas (Henderson et al., 2012) and is the main source of hydroxyl radicals that drive the oxidizing capacity of the atmosphere (Monks et al., 2009). It damages food crops, forests and other ecosystems (Fiscus et al., 2005).

The U.S. EPA defines U.S. background ozone as concentrations that would be observed in the U.S. in the absence of anthropogenic emissions from the continental U.S. (U.S. EPA, 2006). This therefore requires the use of atmospheric models and must be informed and evaluated based on observational data (McDonald-Buller et al., 2011). On the other hand, baseline ozone refers to observed concentrations of tropospheric ozone at sites that have a negligible influence from local emissions (Dentener et al., 2011; Parrish et al., 2012). High-elevation sites such as Mt. Bachelor Observatory (MBO; 2.8 km a.s.l.) are able to sample free tropospheric (FT) air devoid of local anthropogenic emissions, and are therefore able to measure baseline ozone.

The U.S. EPA has a nationwide network of ground-based monitoring sites that measure CO, NOx, particulate matter ($PM_{2.5}$ and PM_{10}), lead, SO_2, and O_3. State, tribal, and local agencies use these data to ensure that the NAAQS are met. Ozone correlations between these sites are indicative of large-scale factors that influence ozone mixing ratios in the area (Jaffe and Ray, 2008). For example, significant correlations between surface and free tropospheric (FT) ozone reflect ozone transport from the FT to the surface (Baylon et al., 2016; Jaffe, 2011). This can be important for urban cities, where ozone from the upper troposphere/lower stratosphere (UT/LS) can contribute to elevated ozone in downwind surface sites (Baylon et al.; 2016; Wigder et al., 2013a). Stratospheric intrusions have been shown to increase the MDA8 ozone values at urban and rural sites, and therefore contribute to exceedances of the NAAQS for ozone (Ambrose et al., 2011; Baylon et al., 2016; Langford et al., 2017).

Wildfires also impact air quality in the western U.S. especially during summer. They are an important source of CO, NOx, and VOCs, and therefore have the potential for significant ozone formation during the fire season (Val Martín et al., 2006). During summers 1989-2010,

wildfires enhanced summer mean MDA8 ozone in the western U.S. by 0.3-1.5 ppbv, but with large interannual variability (Lu et al., 2016). Daily episodic enhancements could reach 10-20 ppbv at individual sites and 31% of the summer days from 1989-2010 with MDA8 ozone above 70 ppbv would not occur in the absence of wildfires (Lu et al., 2016). Jaffe et al. (2008a) showed that summer burned area (BA) is significantly correlated with ozone at 9 rural Clean Air Status and Trends Network (CASTNET) and National Park Service (NPS) sites. For each 1 million acres burned in the western U.S. during summer, they estimated that the daytime mean ozone was enhanced across the region by 2.0 ppbv (Jaffe et al., 2008a). Wildfires also increase the number of exceedance days across the western U.S. (Jaffe, 2011). Aside from ground observations and computer models, statistical tools are also helpful in quantifying the impact of wildfires on urban ozone mixing ratios (Jaffe et al., 2013).

The influence of Siberian biomass burning on surface air quality in North America was first observed by Jaffe et al. (2004). Typical transport times of ALRT events are 7-10 days (Bertschi and Jaffe, 2005). Siberian fires during the summer of 2003 resulted in CO and ozone enhancements of 23-37 ppbv and 5-9 ppbv, respectively, at 10 surface stations in Alaska, Canada and the Pacific Northwest, and therefore led to exceedances in ozone air quality in the region (Jaffe et al., 2004). Similarly, particulate matter concentrations were well-correlated between high- and low-elevation sites (Timonen et al., 2013). This suggests that ALRT episodes can be seen in both FT and BL. Long-range transport of Asian pollution plumes to the western U.S. has been identified not only by aircraft and satellite measurements but also in chemical transport models (Jaffe et al., 1999; Fiore et al., 2009; Brown-Steiner and Hess, 2011; Lin et al., 2012b; Huang et al., 2013; Verstraeten et al., 2015).

Aside from UT/LS, BB, and LRT/Siberian events, meteorological factors like enhanced temperatures, reduced cloud fraction, and increased stagnation can also lead to elevated ozone concentrations (Jaffe and Zhang, 2017). These factors enhanced MDA8 ozone values by 3-13 ppbv across much of the western U.S. in June 2015. Some sites had as many as 16 days above the NAAQS threshold of 70 ppbv (Jaffe and Zhang, 2017).

In the U.S., ozone precursor emissions have declined. However, springtime ozone mixing ratios have been increasing in the western U.S. since the 1990s likely due to increasing Asian emissions (Cooper et al., 2009) and long-range transport to the eastern Pacific. Ozone precursor emissions from Asia have tripled in the past 25 years due to a rapid economic growth (Granier et al., 2011; Hilboll et al., 2013). It is estimated that transport of ozone and its precursors from China to the western U.S. has offset about 43% of the reduction in free tropospheric ozone that was expected from the emissions reductions associated with federal, state, and local air quality policies in the U.S. between 2005 and 2010 (Verstsaeten et al., 2015). Global chemistry-climate model (GFDL-AM3) hindcasts over 1980-2014 show that springtime ozone at rural sites in the western U.S. has increased at a rate of 0.2-0.5 ppbv/year (Lin et al., 2017). Asian NOx emissions contributed as much as 65% to modeled springtime background increases, larger than the ozone decreases expected from a 50% decrease in US NOx emissions (Lin et al., 2017). High-ozone events can therefore significantly affect the ability of a site to achieve air quality objectives. However, the EPA has a method for excluding these high-ozone events from consideration, and this is described below.

1.2 EPA'S EXCEPTIONAL EVENT RULE

Under the U.S. Clean Air Act (CAA), states and cities are required to meet the U.S. National Ambient Air Quality Standard (NAAQS) for ozone and other pollutants. Currently, the standard for ozone requires that the fourth highest annual MDA8 ozone, averaged over 3 years, be below 70 ppbv. However, when "unusual or natural events that affect air quality but are not reasonably controlled" takes place, the U.S. EPA has a mechanism for excluding these exceptional events from consideration. If the air quality in a geographic area meets the NAAQS, it is called an attainment area; if it does not meet the national standard, it is called a nonattainment area. To demonstrate these "exceptional events", states and cities must show three things (https://www.epa.gov/air-quality-analysis/treatment-air-quality-data-influenced-exceptional-events):

1. That the event affected air quality in such a way that there exists a clear causal relationship between the specific event and the monitored exceedance or violation;
2. That the event was not reasonably controlled or preventable; and
3. That the event was caused by human activity that is unlikely to recur at a particular location or was a natural event.

Nonattainment areas are required to draft a plan known as a state implementation plan (SIP) in order to improve air quality. Once a nonattainment area meets the standards, it will then be classified as a "maintenance area."

1.3 PHOTOCHEMISTRY IN BIOMASS BURNING PLUMES

Wildfires are an important source of CO, NOx and VOCs and therefore have the potential for significant ozone formation during the fire season (Val Martín et al., 2006). Because ozone is not directly emitted by wildfires but is instead produced from precursors, understanding the chemistry of these species is important. NOx is typically the limiting precursor in ozone production from wildfires (Mauzerall et al., 1998; Singh et al., 2012). This is because there are large sources of VOCs in wildfires. NOx concentrations in fire plumes are affected by fuel nitrogen content, fire combustion efficiency, and photochemical production and loss of species such as peroxyacetyl nitrate (PAN) (Alvarado et al., 2010; Wigder et al., 2013). Total reactive nitrogen is represented by NOy ($NO + NO_2 + HNO_3 + PAN + HONO + NO_3 + N_2O_5$ + aerosol nitrate +…). Model simulations show that VOCs, especially oxygenated VOCs (OVOCs), lead to complex effects on net ozone production (Mason et al., 2001). While it has been previously shown (Sillman, 1999) that ozone production is independent of VOCs in the NOx-sensitive (low-NOx) regime for urban plumes, Mason et al. (2001) concluded from their modeling studies that this may not be true for wildfire plumes. Most of the NOx emissions in the atmosphere come in the form of NO, and the photolysis of NO_2 regenerates O_3. Thus, for net O_3 formation to occur, NO must be converted to NO_2 by reactions with HO_2 and RO_2. In the VOC-sensitive (high-NOx) regime, O_3 production decreases with increasing NOx but increases with increasing VOC. In the NOx-sensitive (low-NOx) regime, O_3 formation increases with increasing NOx. While previous studies have shown that O_3 production in this regime is largely independent of VOC, Mason et al. (2001) showed in their modeling study that it can sometimes be VOC-dependent, depending on the initial NOx concentrations.

Pfister et al. (2006) used observations and model simulations to estimate the amount of O_3 produced by Alaskan and Canadian wildfires in the summer of 2004. The enhancement of O_3 with respect to CO for BB plumes was found to be 3–4 times smaller than for anthropogenic pollution due to the lower initial NOx/CO ratios for these sources. Other studies have found that ozone formation ranges from very low in fresh plumes to low in moderately aged plumes to high in well-aged plumes (Val Martín et al., 2006). In their review of 132 published studies, Jaffe and Wigder (2012) showed that the observed enhancement of ozone relative to CO for boreal and temperate fires was, on average, 0.018, 0.15 and 0.22 ppbv/ppbv for plumes aged 1–2 days, 2–5 days and more than 5 days, respectively, but there was large variability from fire to fire. Factors affecting the variability of ozone production included fire emissions (type of species emitted), combustion efficiency, chemical and photochemical reactions, aerosol effects on chemistry, solar radiation and meteorological patterns (Jaffe and Wigder, 2012).

An important reservoir of NOx in the atmosphere is PAN, which can be transported over long distances and can thermally decompose back to NOx as the plume descends to warmer temperatures (Jacob, 1999; Kotchenruther et al., 2001). The first observational evidence of rapid PAN formation in boreal smoke plumes showed that 40% of initial NOx emissions were converted to PAN in the first few hours after plume emission (Alvarado et al., 2010). Later, this NOx would be released from the thermal decomposition of PAN and could be involved again in O_3 production. Because of large production of PAN from wildfires (Wigder et al., 2014), a large fraction of the initial NOx is sequestered as PAN.

Numerous studies have evaluated the effects of aerosols on photolysis rates and O_3 formation. These effects are dependent on different factors. First is the type of aerosol. Model simulations by Dickerson et al. (1997) show that scattering particles in the boundary layer (BL)

can increase photolysis rates and can therefore accelerate ozone production. However, UV-absorbing aerosols such as mineral dust and soot have also been found to reduce ozone mixing ratios by up to 24 ppbv (Dickerson et al., 1997). Simulations in Mexico City by Castro et al. (2001) suggest a large reduction in NO_2 photolysis rates (10-30%) and surface ozone mixing ratios (30-40 ppbv) due to urban aerosols. Using a three-dimensional regional chemical transport model, Tang et al. (2003) found that the accumulated impact of biomass burning aerosols from Southeast Asia, which contain large amounts of carbonaceous material, is to reduce surface ozone mixing ratios by about 6 ppbv. Another important factor is the vertical location of the aerosols with respect to the point of observation. Model simulations near Mexico City during the MILAGRO campaign suggest that aerosols enhance actinic flux, and therefore photolysis rates, above the BL and reduce actinic flux near the surface (Palancar et al., 2013). Alvarado et al. (2015) looked at model simulations over the Williams fire in California and found that $j(NO_2)$ is lowest in the bottom of the plume, reduced in the middle of the plume, and enhanced above the plume. In a modeling study that looked at wildfires in the western U.S., Jiang et al. (2012) found that reductions in downward shortwave radiation reaching the surface due to fire aerosols cause decreases in $j(NO_2)$ in the fire source region by as much as 75% and therefore reductions in ozone mixing ratios by as much as 15%.

Most of these studies rely on model simulations of photochemistry. Very few were based on in-situ measurements aimed at exploring the photochemical environment in BB plumes. This dissertation aims to fill this knowledge gap. My goal is to understand the photochemistry in biomass burning plumes by looking at field measurements of actinic flux, aerosols, and NOx at MBO, a mountaintop research station located on the summit of a dormant volcano in central Oregon (Jaffe et al., 2005).

1.4 THE MOUNT BACHELOR OBSERVATORY

The Mount Bachelor Observatory (MBO) is a mountaintop site (2.8 km a.s.l.) established in 2004 by the University of Washington Atmospheric Chemistry group to examine baseline air as it arrives in the West Coast of the U.S. (Jaffe et al., 2005). The Observatory is located on the summit of Mt. Bachelor, an extinct volcano in the Cascade mountain range of central Oregon. Mt. Bachelor is located in the Deschutes National Forest and is home to a ski resort, which provides access and power.

Data at MBO has been used for multi-year studies of ozone (Gratz et al., 2015), CO (Gratz et al., 2015), CO_2 (McClure et al., 2016), NOx (Reidmiller et al., 2010), and PAN (Fischer et al., 2011b). Recently, data at MBO has also been used to explore the presence of bacteria in the troposphere (Klein et al., 2016). During Spring 2011, long-range transport of bacteria have been observed at MBO in trans-Pacific plumes (Smith et al., 2011; Smith et al., 2012; Smith et al., 2013). Backtrajectories suggest that these microorganisms come from China or Japan.

Over the 10-year period from 2004-2013, the median and 95th percentile springtime (April-May) ozone at MBO increased by 0.76 ± 0.61 ppbv yr^{-1} and 0.87 ± 0.73 ppbv yr^{-1}, respectively (Gratz et al., 2015). These trends are somewhat larger, but within the uncertainty bounds, of the positive trends in springtime FT O_3 in the western U.S. reported by Cooper et al. (2012). The rise in springtime ozone is likely associated with increasing ozone precursor emissions in Asia and long-range transport to the western U.S.

We typically perform field campaigns at MBO during spring and summer. UT/LS and ALRT events typically happen during winter and spring when transport is most favorable. BB events in the western U.S., on the other hand, mostly occur during summer and early autumn.

The first ALRT events at MBO were observed during Spring 2004. These events were characterized by low water vapor and significantly elevated concentrations of CO, total gaseous mercury (TGM) and ozone (Weiss-Penzias et al., 2006). ALRT has been shown to affect mercury (Weiss-Penzias et al., 2007; Jaffe and Strode, 2008; Strode et al., 2008) and PAN (Wolfe et al., 2007) concentrations at MBO.

A couple of studies have demonstrated springtime trends in NOy species, such as peroxyacetyl nitrate (PAN). During Spring 2006, PAN, an important NOx reservoir, was measured at MBO. On average, PAN levels were substantially higher in the free troposphere (FT) air relative to the boundary layer (BL) air, suggesting that MBO is strongly affected by distant pollution sources under the right meteorological conditions (i.e., when transport occurs via the FT). Zhang et al. (2009) used the GEOS-Chem chemical transport model to quantify the contribution of Asian pollution at MBO during Spring 2008. The mean observed concentration at MBO is 54±10 ppbv compared with 53±9 ppbv in the model. The contribution of ozone produced over Asian in the model is 13±3.6 ppbv at MBO. Fischer et al. (2010a) argued that variability in PAN during Spring 2008 was predominantly a function of synoptic-scale processes. Two Asian plumes were observed and both were associated with elevated PAN, CO, ozone, and aerosol scattering.

Similarly, Redimiller et al. (2010) looked at NOx measurements at MBO during one autumn and three springtime (2007-2009) periods. Springtime mean values for NOx were 119, 117, and 91 pptv, for 2007, 2008, and 2009. Decline in NOx is attributed to higher geopotential heights over the Gulf of Alaska, warmer temperatures over the Aleutian Islands/Gulf of Alaska, and much weaker winds throughout the N Pacific in 2009. During autumn 2008, NOx concentrations were 175±548 pptv. The highly non-normal distribution of autumn data resulted

from periods of very high NOx levels from wildfires in the western U.S. This is in contrast to springtime when the smaller positive (right) tail of the NOx distribution is driven largely by ALRT.

Fischer et al. (2010b) identified 7 plumes of Asian origin and observed variability in the scattering Angstrom exponent. The average Angstrom exponent was significantly larger than the same parameter observed closer to Asia. Therefore, they hypothesized that the aerosol size distribution shifts toward smaller particles during trans-Pacific transport. Also, the average single scattering albedo (SSA) observed in Asian plumes at MBO (0.88) was slightly larger than the mean observations closer to the Asian coast. Moreover, intensive aerosol properties varied from plume to plume, which indicates that even after transport, the aerosols are not necessarily well-mixed and the plumes can be layered.

A couple of studies at MBO have extensively looked at the aerosol properties of wildfire plumes observed at MBO. For example, a high-resolution time-of-flight aerosol mass spectrometer (HR-AMS) was deployed at MBO in summer 2013 to characterize the impact of wildfire emissions on aerosol loading in the PNW, as part of the Biomass Burning Observation Project (BBOP) (Zhou et al., 2017). Their results show that during fire-impacted periods, the average PM_1 was 22.4±17.7 $\mu g/m^3$, mostly due to organic aerosols that dominated the PM composition. During clean periods, the average PM_1 was only 3.7$\mu g/m^3$ and the aerosols contained a high mass fraction of ammonium sulfate. Findings suggest that BB emissions undergo substantial chemical processing which starts immediately after emission and continues during atmospheric transport.

In a recent paper, Laing et al. (2016) looked at 19 wildfire events observed at MBO during summer of 2015. Six of the 19 events were influenced by Siberian fires that were

transported to MBO over 4-10 days. The remainder of the events were from wildfires in Northern California and Southwestern Oregon, with transport times ranging from 3 to 35 hours. Siberian events had significantly higher $\Delta\sigma_{abs}/\Delta CO$ enhancement ratio, higher mass absorption efficiency ($\Delta\sigma_{abs}/\Delta PM_1$), lower single scattering albedo (ω), and lower absorption Angstrom exponent (AAE) when compared to the regional events. It was suggested that MBO sampled the portion of the plume that has been lofted to higher elevation via pyroconvection, thereby preferentially sampling more flaming combustion emissions. In general, flaming conditions produce more BC which explain the enhanced absorption in the Siberian events. Similarly, Collier et al. (2016) studied the regional and near-field influences of wildfire emissions on ambient aerosol concentrations and chemical properties using MBO as fixed site and an aircraft. Regional characteristics of BB aerosols were strongly correlated with modified combustion efficiency (MCE). They suggest that MCE can be a useful metric for describing aerosol properties of wildfire emissions.

Organic carbon (OC) and elemental carbon (EC) from particulate matter were measured at MBO by Timonen et al. (2014) from March to September 2012. Average concentrations of OC and EC in the FT were low (OC 1.87 $\mu g/m^3$; EC 0.07 $\mu g/m^3$), but much higher during pollution episodes. The highest OC and EC concentrations were measured during BB episodes (3h average OC up to 146 $\mu g/m^3$; EC up to 5.5 $\mu g/m^3$). Elevated concentrations were also measured during ALRT events (OC up to 3.6 $\mu g/m^3$ EC up to 1.1 $\mu g/m^3$).

Wigder et al. (2013b) looked at 32 wildfires observed at MBO during June-September 2004-2011. Observed enhancement ratio of $\Delta PM_1/\Delta CO$ ranged from 0.06 to 0.42 $\mu g/m^3$/ppbv; $\Delta O_3/\Delta CO$ ranged from 0.01 to 0.51 ppbv/ppbv for the 13 plumes with a significant $\Delta O_3/\Delta CO$ enhancement ratio ($R^2 >= 0.30$). A specific fire event was associated with significant ozone

production. This event was transported in a FT air mass, suggesting that conversion of NOx to PAN may be a factor affecting O_3 production. Two of these wildfire plumes were mixed with urban emissions from the Seattle/Tacoma metropolitan area, and had relatively higher $\Delta O_3/\Delta CO$ compared to other wildfire plumes transported similar distances.

NOy speciation has also been investigated at MBO. Briggs et al. (2016) looked at 23 wildfire plumes observed during the summer of 2012 and 2013 at MBO. The observed NOx, PAN, and aerosol nitrate represented 6-48%, 25-57%, and 20-69% of the observed NOy in the aged plumes, respectively, and other species represented on average 11% of the observed NOy. The high proportion of PAN in the observed plumes suggests that there may have been added ozone production in the plumes as they were transported further downwind.

Baylon et al. (2015) looked at 19 wildfire events that were observed in the summers of 2012 and 2013 at MBO. We observed a negative correlation between $\Delta O_3/\Delta CO$ and $\Delta NOx/\Delta NOy$ ($r = -0.72$). This showed that the degree of NOx oxidation is a key predictor of ozone production. The highest $\Delta NOx/\Delta NOy$ (0.57 pptv/pptv) was associated with ozone loss (ozone titration). Low $\Delta NOx/\Delta NOy$ values (ranging from 0.049 to 0.15 pptv/pptv) are generally associated with ozone enhancement. We also found that even if $\Delta O_3/\Delta CO$ is low, ΔO_3 may still be significant if CO enhancements are large. We then explored events that are not associated with any O_3 enhancement/loss. Out of 19 fire events, 3 belong to this category. We discovered that these events are either BL-influenced (O_3 deposition), associated with low $\Delta NOy/\Delta CO$ ratios, and/or associated with minimal photochemistry (due to nighttime transport). Absolute ozone enhancements ranged from 3.8 to 32 ppbv, while ozone production efficiencies (OPEs) ranged from 2.1 to 17. However, because PAN comprises most of the reactive nitrogen in fire plumes, the calculated OPEs underestimated the true ozone mixing ratios. OPEs may therefore

be misleading indicators of ozone production in wildfires. Finally, we segregated the data into plume/non-plume time periods. From this we found that the average O_3 mixing ratio was significantly higher in fire plumes compared to non-plume time periods, and the noontime NO/NO_2 ratios were also higher. This later result gives insight into the photochemical environment in the fire plumes, which until now remains poorly understood.

Ambrose et al. (2011) identified 25 high-ozone events (8h averaged ozone mixing ratio was > 70 ppbv) at MBO. These events were transported to MBO in the FT and were driven mostly by subsidence of ozone-rich air masses from the UT/LS, ALRT, and mixed ALRT + UT/LS influences. UT/LS events were depleted in CO compared to monthly median values. Levels of O_3 and CO tended to be anti-correlated during UT/LS events, consistent with transport from clean regions in the UT. Conversely, ALRT events were characterized by enhancements in CO. Unlike for UT/LS events, levels of ozone and CO during ALRT events tended to be correlated, consistent with photochemical ozone production in polluted air masses transported across the Pacific. Mixed ALRT + UT/LS exhibited characteristics that were intermediate between those of the ALRT and UT/LS events.

1.5 RESEARCH QUESTIONS

In the western U.S., free tropospheric springtime ozone has been increasing since the 1990s, likely due to increasing precursor emissions in Asia and long-range transport to the western U.S. Biomass burning, both regional and long-range transport in origin, has also been shown to impact air quality in the region. In the context of increasing baseline ozone and tighter air quality standards, it is therefore important to understand the nature and the impact of these high-ozone episodes on air quality in the western U.S. These events would affect the attainment

status of a site if they were not identified as exceptional events. This dissertation is focused on three types of high-ozone events that we typically observe at MBO and in other surface sites in the western U.S.: (1) UT/LS events, (2) BB plumes, and (3) LRT episodes. While most analysis revolves around observations at MBO, I will use data from a variety of platforms – surface measurements, aircraft data, radiosonde observations, satellite retrievals, and model simulations – to understand the chemistry and transport mechanisms of these high-ozone events. Specifically, I am to answer the following research questions.

For the UT/LS episode discussed in Chapter 2:

- How variable is springtime O_3 at MBO?
- Did the high FT O_3 in Spring 2012 seen at MBO result in enhancements at the surface in the western U.S.?
- How did these high-O_3 periods influence the distribution of MDA8 values and contribute to air quality exceedances at surface sites?
- What is the spatial and temporal relationship between MDA8 values measured at nearby stations across the western U.S.?
- What was the cause for high springtime O_3 in 2012?

For the BB events discussed in Chapter 3:

- Can we identify variations in j and NO/NO_2 ratios due solely to BB smoke?
- What is the level of agreement between observations and TUV model for clear-sky conditions for $j(NO_2)$ and $j(O^1D)$?
- What are the instantaneous O_3 production rates and $HO_2 + RO_2$ concentrations in P/NP?

For the Siberian LRT event discussed in Chapter 4:

- Were the aircraft and MBO observations consistent with respect to the enhancement ratios?
- What caused the high $\Delta O_3/\Delta CO$ and $\Delta\sigma_{sp}/\Delta CO$ ratios for the Siberian 2015 fires?
- How does the reactive nitrogen speciation of the plume relate to O_3 production and $\Delta NOy/\Delta CO$?
- Was there O_3 production and if so, was this O_3 mixed into the boundary layer? What was the role of UT/LS mixing?

1.6 DISSERTATION OVERVIEW

Chapter 2 describes a UT/LS episode that affected air quality in the western U.S. on Spring 2015. I observed an O_3 increase of 2.0–8.5 ppbv in monthly average maximum daily 8–hour average O_3 mixing ratio (MDA8 O_3) at MBO and numerous other sites in the western U.S. compared to previous years. I also observed a good correlation between daily MDA8 variations at MBO and at downwind sites. At MBO, the elevated O_3 concentrations in May 2012 are associated with low CO values and low water vapor values, consistent with transport from the upper troposphere/lower stratosphere (UT/LS). Furthermore, I run the Real-time Air Quality Modeling System (RAQMS) analyses and find that a large flux of O_3 from the UT/LS in May 2012 contributed to the observed enhanced O_3 across the western U.S.

Chapter 3 looks at BB events that we observed at MBO on Summer 2015, a huge fire season in the Pacific Northwest. I explored the photochemical environment in BB plumes, which remains poorly understood, and my results suggest that BB plumes increase local noontime $j(NO_2)$ on average and decrease photolysis rates at high solar zenith angles. I compare

my measurements with cloud-free simulations from the TUV5.2 model. I also use the extended Leighton relationship to estimate the HO_2 and RO_2 concentrations and the ozone production rates in BB plumes.

Chapter 4 describes a Siberian LRT event that was observed at MBO during Spring 2015. I observed O_3 and CO enhancements of up to 40 ppbv and 80 ppbv, respectively, at MBO. I compare our mountaintop measurements with observations from one of the flights during the Shale Oil and Natural Gas Nexus (SONGNEX) campaign. I calculate the $\Delta O_3/\Delta CO$ and $\Delta\sigma_{sp}/\Delta CO$ ratios of the Siberian 2015 fires, and compare them to similarly aged fires from previous studies. Ground-based, satellite, and LiDAR data suggests that the Asian plume was transported at high elevation and therefore did not cause any surface O_3 enhancements in the western U.S.

Chapter 5 provides conclusions of this dissertation and recommendations for future work.

Appendix A lists my co-authors and their contributions. Appendix B provides GOES-WEST images of MBO on August 2015. Appendix C includes forward dispersion runs on April 2015 from the HYbrid Single Particle Lagrangian Integrated Trajectory (HYSPLIT) model. Finally, Appendix D provides AOD forecasts from the Navy Aerosol Analysis and Prediction System (NAAPS) Global Aerosol Model.

CHAPTER 2

INTERANNUAL VARIABILITY IN BASELINE OZONE AND ITS RELATIONSHIP TO SURFACE OZONE IN THE WESTERN U.S.

(published as Baylon et al., Environ. Sci. Tech., 2016)

2.1 INTRODUCTION

Ozone is an important tropospheric constituent for multiple reasons. First, it is the third strongest anthropogenic greenhouse gas (Henderson et al., 2012). Second, it is the main source of hydroxyl radicals that drive the oxidizing capacity of the atmosphere (Monks et al., 2009). Third, surface ozone is a health hazard particularly to sensitive individuals and is associated with premature mortality (Bell et al., 2006; Gryparis et al., 2004). Finally, ozone damages food crops, forests and other ecosystems (Fiscus et al., 2005). In the U.S., the current ozone National Ambient Air Quality Standard (NAAQS) requires that the fourth-highest annual maximum daily average 8–hour (MDA8) ozone concentration be 70 ppbv or below, averaged over 3 years (U.S. EPA, 2015). From a NAAQS attainment perspective, as the O_3 standard is lowered springtime becomes increasingly important in the western U.S. (Jaffe, 2011).

Ozone is a secondary pollutant that is formed in the troposphere from the interaction of nitrogen oxides ($NOx = NO + NO_2$) and volatile organic compounds (VOCs) in the presence of sunlight (Finlayson-Pitts and Pitts, 1986). It is destroyed via reactions involving water vapor and photolysis (Monks et al., 2009). Ozone also originates from the stratosphere and can be transported to the surface (Langford et al., 2009). In the north-eastern Pacific, the direct transport of ozone produced from Asian emissions, including secondary production from Asian

peroxyacetyl nitrate (PAN) and NOx, accounts for at least 16% of tropospheric ozone during spring (Jaeglé et al., 2003). Furthermore, enhanced O_3 due to Asian pollution is routinely seen in the free troposphere (FT) at MBO as the air masses arrive to North America (Ambrose et al., 2011; Jaffe et al., 2005).

In the U.S., domestic anthropogenic emissions of ozone precursors NOx, CO and VOCs have declined from 1990 to 2010 by 49%, 58% and 44%, respectively (U.S. EPA, 2012). This should have resulted in ozone reductions across the country. However in the western U.S., FT springtime ozone has increased significantly from 1995 to 2011 at the rate of 0.41 ± 0.27 ppbv/yr (Cooper et al., 2012). This increase in O_3 is likely due to increasing precursor emissions in Asia and long-range transport to the western U.S. (Cooper et al., 2010; Cooper et al., 2012; Gratz et al., 2015).

The Mount Bachelor Observatory (MBO) was started in 2004 to examine baseline air as it arrives in the West Coast of the U.S. (Jaffe et al., 2005). It is a high-elevation site (2.8 km a.s.l) located in central Oregon. At MBO, the median and 95th percentile springtime (April-May) O_3 have increased by 0.76 ppbv/yr and 0.87 ppbv/yr, respectively, from 2004–2013 (Gratz et al., 2015). These trends are somewhat larger, but within the uncertainty bounds, of the positive trends in springtime FT O_3 in the western U.S. reported by Cooper et al. (2012).

The U.S. Environmental Protection Agency (EPA) defines U.S. background ozone as concentrations that would be observed in the U.S. in the absence of anthropogenic emissions from the continental U.S. (U.S. EPA, 2006). This therefore requires the use of atmospheric models (McDonald-Buller et al., 2011). Baseline ozone refers to observed concentrations of tropospheric ozone at sites that have a negligible influence from local emissions (Dentener et al., 2011; Parrish et al., 2012).

In the context of increasing baseline O_3 and tighter air quality standards, it is important to understand the sources and the role that baseline O_3 plays on urban air quality in the western U.S. For example, enhanced O_3 from 25 events (defined as days with MDA8 O_3 > 70 ppbv) observed from 2004–2009 were transported to MBO in the FT and were driven mostly by subsidence of O_3-rich air mass from the upper troposphere/lower stratosphere (UT/LS), Asian long-range transport (ALRT) and mixed UT/LS + ALRT (Ambrose et al., 2011). During UT/LS events, levels of O_3 and CO were anti-correlated. On the other hand, during ALRT events, O_3 and CO tend to be correlated (Ambrose et al., 2011). Wildfires can also cause high-O_3 events at MBO (Baylon et al., 2015; Wigder et al., 2013a). They are an important source of CO, NOx and VOCs and therefore have the potential for significant ozone formation during spring and summer (Val Martin et al., 2006).

Under specific meteorological conditions, FT O_3 can influence surface observations (Fine et al., 2015; Jaffe et al., 2005; Jaffe, 2011; Langford et al., 2015a; Lefohn et al., 2001; Wigder et al., 2013b). For example, a deep tropopause fold brought ~215 ppbv of O_3 to the Rocky Mountains on 6 May 1999, and this led to O_3 mixing ratios exceeding 100 ppbv at a downwind surface site in Boulder (Langford et al., 2009). Higher O_3 values at several rural sites across southern Canada, the northern U.S. and northern Europe are also linked to UT/LS air masses that are transported down to the surface (Lefohn et al., 2001). On 3 exceedance days in Clark County, Nevada, stratosphere-to-troposphere transport contributed to 8–hour surface O_3 concentrations in excess of 30 ppbv (Fine et al., 2015; Langford et al., 2015a). O_3 passing through high-elevation sites like MBO can be transported to downwind urban surface sites (Wigder et al., 2013b). Modeling studies also show that stratospheric intrusions can episodically increase surface O_3 observations in the western U.S. by 20–40 ppbv (Lin et al., 2012).

Temporal correlations in O_3 across large spatial scales are indicative of a non-local O_3 source (Jaffe et al., 2008; Jaffe, 2011). An analysis of ozonesonde data from 13 midlatitude stations in North America and Europe found that the temporal correlations between pairs of stations decrease with increasing station separation distance (Liu et al., 2009). While the ozone correlation length (defined as the horizontal distance for the correlation coefficient to decrease by a factor of *e*) is longer in the stratosphere (1000–2000 km), in the troposphere the correlation length can still be substantial (500–1000 km) (Liu et al., 2009). These results suggest that the baseline contribution to surface O_3 is significant and therefore leads to significant temporal and spatial correlations at surface sites.

O_3 data have been collected continuously at MBO since 2004. We previously reported on a long-term trend in springtime O_3 (Gratz et al., 2015). Here we focus on the interannual variability (IAV) in spring and especially Spring 2012, which has some of the highest concentrations seen over the past decade. Specifically, we address the following questions:

- How variable is springtime O_3 at MBO?
- Did the high FT O_3 in Spring 2012 seen at MBO result in enhancements at the surface in the western U.S.?
- How did these high-O_3 periods influence the distribution of MDA8 values and contribute to air quality exceedances at surface sites?
- What is the spatial and temporal relationship between MDA8 values measured at nearby stations across the western U.S.?
- What was the cause for high springtime O_3 in 2012?

We focus on MDA8 O_3 values as this is the policy-relevant metric.

2.2 MATERIALS AND METHODS

Mount Bachelor Observatory (MBO; 2.8 km a.s.l.) is a mountaintop site established in 2004 by the University of Washington Atmospheric Chemistry group (Jaffe et al., 2005). The Observatory is located on the summit of Mt. Bachelor, an extinct volcano in the Cascade mountain range of central Oregon. Mt. Bachelor is located in the Deschutes National Forest and is home to a ski resort, which provides access and power. Since 2004, we have measured σ_{sp} (TSI Model 3563), O_3 (Dasibi 1008 RS UV Photometric Ozone Analyzer) and CO (May 2012 onwards: Picarro G2302 Cavity Ring-Down Spectrometer), along with measurements of meteorology, such as temperature, humidity and wind speed [see Ambrose et al. (2011) and Gratz et al. (2015) and references therein for details on σ_{sp}, O_3 and CO instrumentation]. O_3 measurements have a daily span check and have been manually calibrated every six months with an O_3 transfer standard photometer [see Gratz et al. (2015) for more details on O_3 instrumentation and calibration].

Observations of O_3 in Salt Lake City, UT (SLC; AQS ID: 49-035-3006); Great Basin NP, NV (GRB; 32-033-0101); Reno, NV (32-031-0016); Tehama, CA (06-103-0004); Boise, ID (16-001-0010, 16-001-0017); Portland, OR (41-005-0004); Siskiyou, CA (06-093-2001); and Lassen, CA (06-089-3003) were obtained from the U.S. EPA AirData archive (www.epa.gov/airdata). Ozone measurements from South Fork State Recreation Area, NV (SFSR), and Berlin-Ichthyosaur State Park, NV (BISP), were obtained from the Nevada Rural Ozone network (Gustin et al., 2015). Upper air soundings of water vapor in Salem, OR, were acquired from the University of Wyoming, Department of Atmospheric Sciences (http://weather.uwyo.edu/upperair/sounding). Figure 2.1 shows a map of the western U.S. and locations of all sites used in this analysis.

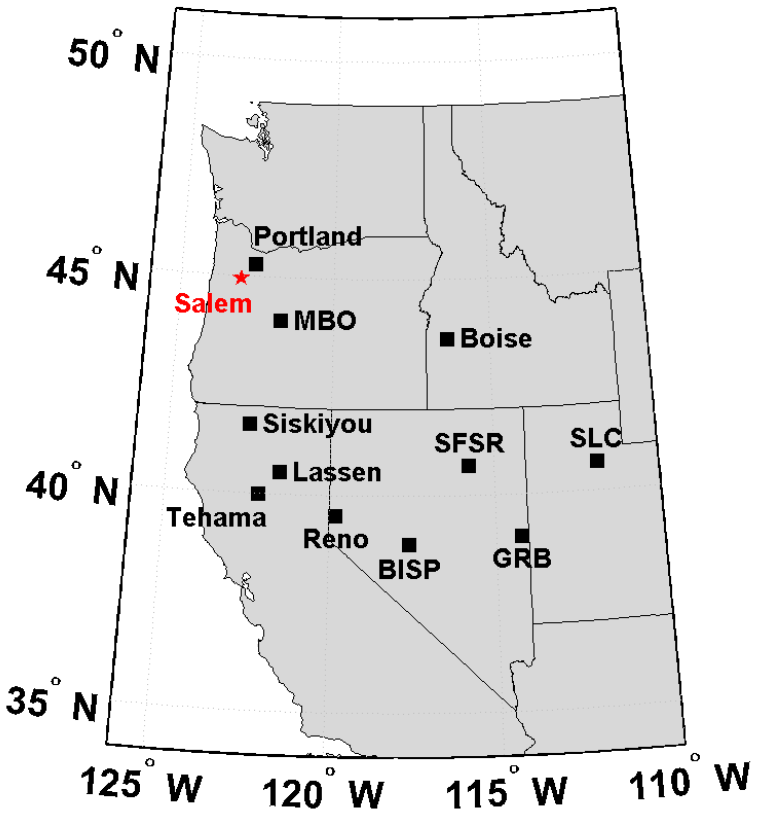

Figure 2.1. Map of selected O_3 stations (black squares) in the western U.S. Water vapor soundings from Salem (red star) are also analyzed in this study. BISP: Berlin Ichthyosaur State Park; GRB: Great Basin NP; MBO: Mt. Bachelor Observatory; SLC: Salt Lake City; SFSR: South Fork State Recreation Area.

We used the Real-time Air Quality Modeling System (RAQMS) to look at the modeled vertical profile of O_3 at MBO in May 2012 and to derive maps of tropospheric column ozone (TCO_3) and total precipitable water (TPW). RAQMS is a unified (stratosphere/troposphere), multi-scale (global to regional) online (meteorological, chemical, and aerosol) modeling system which has been developed for assimilating satellite-based observations of atmospheric chemical composition and providing real-time predictions of trace gas and aerosol distributions (Pierce et

al., 2003; Pierce et al., 2007; Pierce et al., 2009). It is a 1x1 degree global online chemistry and aerosol assimilation and forecast system extending from the surface to ~60km with 35 hybrid isentropic/eta vertical coordinates. The top 24 (stratospheric) levels are purely isentropic and begin at 379K. The lower 21 eta levels transition from isentropic in the upper troposphere/lower stratosphere to terrain following near the surface. RAQMS uses the statistical digital filter (SDF) analysis system (Stobic et al., 1985; Stobic et al., 2000) to perform an optimal interpolation (OI) based univariate assimilation of satellite ozone (OMI, MLS) and aerosol (MODIS) observations. RAQMS has been used in previous studies of UT/LS transport (Fiore et al., 2014; Langford et al., 2015b; Yates et al., 2013).

2.3 RESULTS AND DISCUSSION

2.3.1 Interannual variability (IAV) in baseline springtime O_3

Figure 2.2 shows the monthly mean MDA8 O_3 at MBO, SLC, Boise, Reno and GRB for May 2004–2014. Despite some site-to-site discrepancies, Figure 2.2 shows that the highest MDA8 values for all sites (except Boise) are recorded in 2012. The IAV (calculated as the standard deviation divided by the mean) of the monthly measured MDA8 O_3 values at MBO, SLC, Boise, Reno and GRB is 7.2%, 6.2%, 11%, 7.2% and 6.8%, respectively.

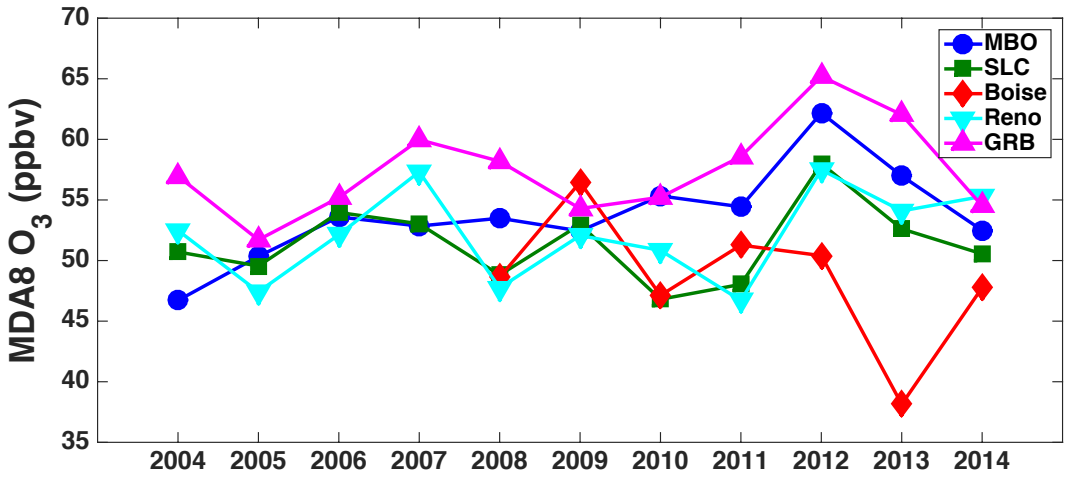

Figure 2.2. Monthly mean MDA8 O_3 at MBO, SLC, Boise, Reno and GRB for May 2004–2014. Note the elevated MDA8 O_3 values in 2012.

Table 2.1 shows the absolute and relative enhancements for April and May 2012 MDA8 O_3 over all stations. While both April and May were enhanced, the enhancements in May 2012 were much larger. Monthly mean MDA8 O_3 enhancements in May range from 2.0 to 8.5 ppbv, which represents an increase of 3.5 to 17% from the 2010, 2011, 2013 and 2014 average. Higher altitudes generally observe higher enhancements.

Table 2.1. April and May 2012 MDA8 O_3 enhancements at selected western U.S. sites. Enhancement is calculated with respect to the April and May 2010, 2011, 2013 and 2014 mean. "ND" in columns 4 and 5 denote missing April data.

Station	Station Type	Elevation (km)	Apr 2012 MDA8 O_3 enhancement (ppbv)	Ratio of Apr 2012 enhancement to Apr 2010, 2011, 2013 and 2014 mean (%)	May 2012 MDA8 O_3 enhancement (ppbv)	Ratio of May 2012 enhancement to May 2010, 2011, 2013 and 2014 mean (%)
SLC	Urban	1.3	2.9	6.1	8.5	17
GRB	Rural	2.1	2.5	4.6	7.6	13
MBO	Rural	2.8	1.7	3.1	7.4	13
Reno	Urban	1.3	1.0	2.0	5.8	11
Tehama	Rural	0.6	ND	ND	5.5	11
Boise	Urban	0.8	-2.9	-6.1	4.3	9.4
SFSR*	Rural	1.6	3.9	8.5	3.7	7.3
Portland	Urban	0.2	ND	ND	3.0	7.4
Siskiyou	Rural	0.8	-0.1	0.0	2.8	6.1
Lassen	Rural	1.8	0.2	0.0	2.6	5.2
BISP*	Rural	2.1	4.7	9.7	2.0	3.5

*Data at these sites started in 2012; therefore, the enhancement is calculated relative to the April and May 2013–2014 mean. Also note that for SFSR and BISP, there is limited available data on April 2012 (5 days) and April 2014 (6 days), respectively; therefore, the calculated April 2012 MDA8 O_3 enhancements at these sites may not be representative of the actual value.

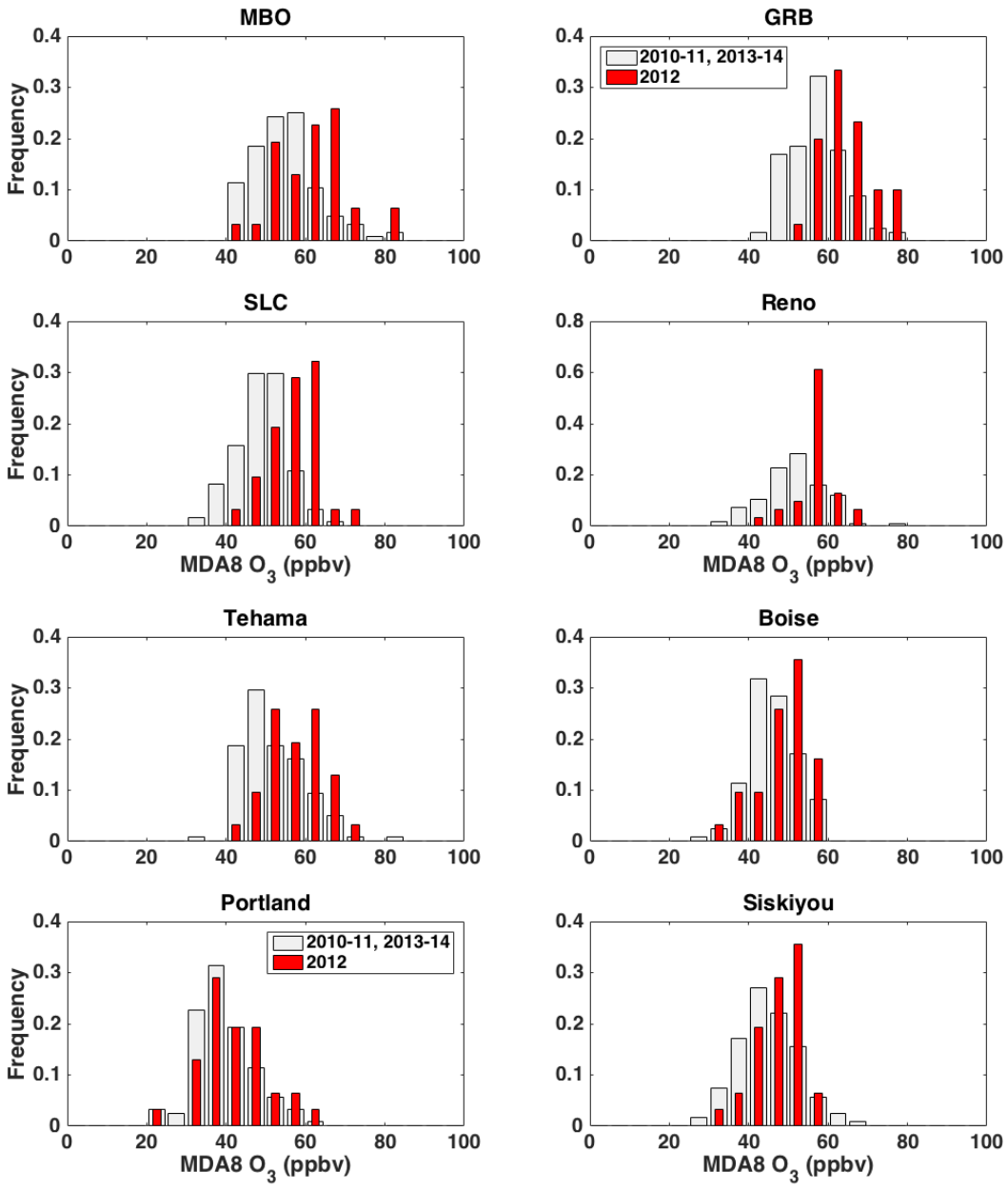

Figure 2.3. MDA8 O_3 normalized histograms for May 2010, 2011, 2013 and 2014 (gray), and May 2012 (red) at all sites. The May 2012 distribution at all sites is shifted to higher MDA8 O_3 values across the entire frequency distribution.

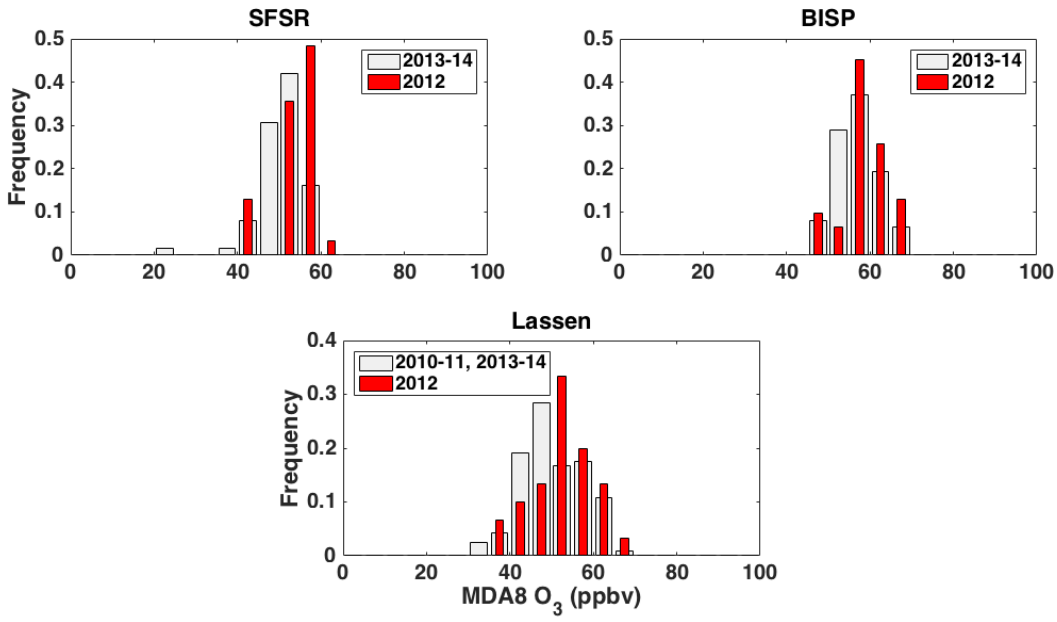

Figure 2.3 (continued). MDA8 O_3 normalized histograms for May 2010, 2011, 2013 and 2014 (gray), and May 2012 (red) at all sites. The May 2012 distribution at all sites is shifted to higher MDA8 O_3 values across the entire frequency distribution.

Because some of the sites have long-term/decadal trends, we examine the variations in the most recent 5-year period. To do this we segregated MDA8 O_3 data from the last 5 years into two groups: one for May 2010, 2011, 2013 and 2014; and another for 2012. Figure 2.3 shows normalized histograms of these datasets for all sites. The May 2012 MDA8 O_3 distribution for all sites is shifted towards higher concentrations across the entire frequency distribution. For example, at MBO, the 5th percentile, median and 95th percentile MDA8 O_3 values are shifted by 6.0, 8.8 and 6.4 ppbv, respectively; while at SLC, they are shifted by 11.5, 9.0 and 6.5 ppbv, respectively. See Table 2.2 for a complete profile on all sites.

Table 2.2. 5th percentile, median and 95th percentile MDA8 O_3 values at all sites, grouped into: (a) May 2010, 2011, 2013 and 2014; and (b) May 2012. May 2012 enhancements are calculated with respect to the May 2010, 2011, 2013 and 2014 distribution.

Station		2012 MDA8 O_3 (ppbv)	2010-11, 2013-14 MDA8 O_3 (ppbv)	2012 ΔO_3 (ppbv)
SLC	5th	49.5	38.0	11.5
	Median	59.0	50.0	9.0
	95th	66.5	60.0	6.5
GRB	5th	56.0	47.0	9.0
	Median	64.0	57.0	7.0
	95th	76.6	69.0	7.6
MBO	5th	49.6	43.6	6.0
	Median	63.0	54.2	8.8
	95th	76.7	70.3	6.4
Reno	5th	48.0	38.0	10
	Median	58.0	52.0	6.0
	95th	66.0	63.9	2.1
Tehama	5th	46.5	42.0	4.5
	Median	57.0	51.0	6.0
	95th	69.5	67.2	2.3
Boise	5th	38.5	38.1	0.4
	Median	51.0	46.0	5.0
	95th	57.5	56.0	1.5
SFSR	5th	43.5	43.0	0.5
	Median	56.0	51.0	5.0
	95th	59.5	57.0	2.5
Portland	5th	32.0	29.3	2.7
	Median	42.0	39.0	3.0
	95th	58.0	54.0	4.0
Siskiyou	5th	38.0	33.0	5.0
	Median	49.0	45.0	4.0
	95th	56.0	59.0	-3.0
Lassen	5th	41.8	40.0	1.8
	Median	54.5	50.0	4.5
	95th	64.0	62.1	1.9
BISP	5th	49.0	48.1	0.9
	Median	59.0	57.5	1.5
	95th	68.5	66.0	2.5

To explore the effect of IAV in baseline O_3 on regulatory exceedance levels, we looked at the number of exceedance days (days with MDA8 O_3 above a specific threshold) from 2010 to 2014 for the current NAAQS threshold of 70 ppbv. The results (in Table 2.3) show that the shift in the O_3 distribution in May 2012 has an impact on the number of exceedance days. This is particularly observed in GRB, MBO, and Lassen – all high-elevation, rural sites – and in SLC, a high-elevation urban site.

Table 2.3. Number of spring (April–May) 2010-2014 exceedance days at all sites for the current MDA8 O_3 threshold of 70 ppbv. "ND" denotes missing data.

Station	2010	2011	2012	2013	2014
SLC	0	0	1	0	0
GRB	0	2	6	3	0
MBO	2	3	8	4	2
Reno	0	0	0	0	1
Tehama	0	0	1	1	1
Boise	0	0	0	0	0
SFSR	ND	ND	0	0	0
Portland	0	0	0	0	0
Siskiyou	0	0	1	0	0
Lassen	0	0	3	0	0
BISP	ND	ND	0	0	0

2.3.2 Relationship between O_3 at MBO and at surface sites in the western U.S.

We then explored the relationship between daily variations in MDA8 O_3 at MBO and surface stations in the western U.S. for Spring 2012. While some of these sites are occasionally

directly downwind of MBO, others are not (Wigder et al., 2013b). But nonetheless, a relationship between MBO and these sites can tell us about large-scale synoptic variations and spatial relationships. Figure 2.4 shows a time series of 3-day average April–May MDA8 O_3 at all sites. The variations in 3-day smoothed MDA8 O_3 for April–May 2012 are similar at all sites. The highest MDA8 O_3 values are observed in the first half of May. Table 2.4 summarizes the r^2 values for the 3-day smoothed MDA8 O_3 (correlations for May 2012 are in bold and italics). We also see no evidence for a time lag in O_3 relationships between any combinations of sites. This supports the notion that all sites are being impacted simultaneously by large-scale processes rather than by direct west-to-east transport.

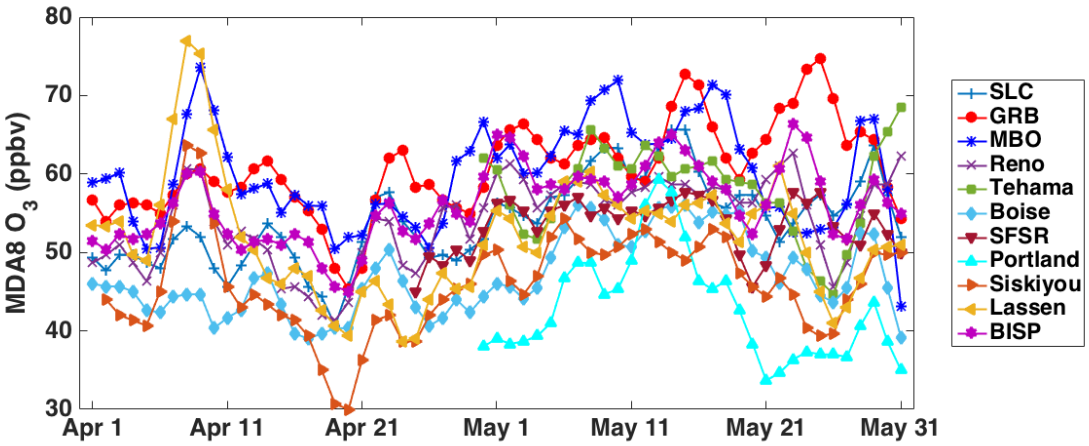

Figure 2.4. Time series of 3-day running averaged MDA8 O_3 for April and May 2012 at all sites.

Table 2.4. r^2 values for 3–day average April–May 2012 MDA8 O_3 correlations at all sites. Values in bold and italics represent only May 2012 correlations.

	SLC	GRB	MBO	Reno	Tehama	Boise	SFSR	Portland	Siskiyou	Lassen	BISP
SLC	1										
GRB	0.46 ***0.01***	1									
MBO	0.29 ***0.44***	0.11 ***0.0***	1								
Reno	0.39 ***0.0***	0.26 ***0.08***	0.25 ***0.01***	1							
Tehama	0.12 ***0.17***	-0.37 ***-0.36***	0.18 ***0.17***	0.36 ***0.39***	1						
Boise	0.72 ***0.49***	0.30 ***0.0***	0.39 ***0.62***	0.33 ***0.03***	0.14 ***0.17***	1					
SFSR	0.30 ***0.11***	0.38 ***0.23***	0.16 ***0.09***	0.18 ***0.02***	0.0 ***0.0***	0.23 ***0.06***	1				
Portland	0.60 ***0.60***	0.0 ***0.01***	0.37 ***0.40***	0.03 ***0.03***	0.21 ***0.24***	0.59 ***0.59***	0.17 ***0.17***	1			
Siskiyou	0.24 ***0.15***	0.11 ***-0.33***	0.52 ***0.38***	0.59 ***0.27***	0.64 ***0.64***	0.21 ***0.29***	0.18 ***0.04***	0.39 ***0.41***	1		
Lassen	0.05 ***0.05***	0.05 ***0.02***	0.35 ***0.21***	0.40 ***0.54***	0.36 ***0.39***	0.09 ***0.27***	0.25 ***0.05***	0.15 ***0.14***	0.71 ***0.42***	1	
BISP	0.46 ***0.05***	0.53 ***0.16***	0.22 ***0.02***	0.70 ***0.33***	0.01 ***0.01***	0.31 ***0.04***	0.62 ***0.55***	0.11 ***0.11***	0.40 ***0.02***	0.25 ***0.16***	1

The highest correlation with MBO is obtained with Boise. Boise is more often directly downwind of MBO, and 62% of the variation in Boise MDA8 on May 2012 can be explained by variations in MBO MDA8 (Wigder et al., 2013b). Forty-four percent of the variance in SLC MDA8 can be explained by variations in MBO MDA8. If we look at the April–May 2012 dataset, good correlations are also obtained between SLC and Boise (r^2 = 0.72), and SLC and GRB (r^2 = 0.46).

To examine the spatial scale of correlation in MDA8 values across the western U.S., we looked at all combinations of the daily MDA8 values at the 11 ozone stations in Figure 2.1 for Spring 2012. Figure 2.5 shows that the correlation coefficient decreases as a function of station separation distance (r = -0.61). This means that the correlation coefficient is strongest for stations that are closer together. The ozone correlation length is approximately 850 km, which is consistent with the 500-1000 km values typical in the troposphere from ozonesonde data (Liu et al., 2009). We did the same analysis but this time grouping our data into seasons (Figure 2.6), and we find the same negative trend between the correlation coefficients and station separation distance across all seasons. However, the correlation coefficients during Summer are the weakest, likely due to the influence of local pollution events. The trends during the other three seasons appear similar, with Winter having slightly better correlation coefficients between stations.

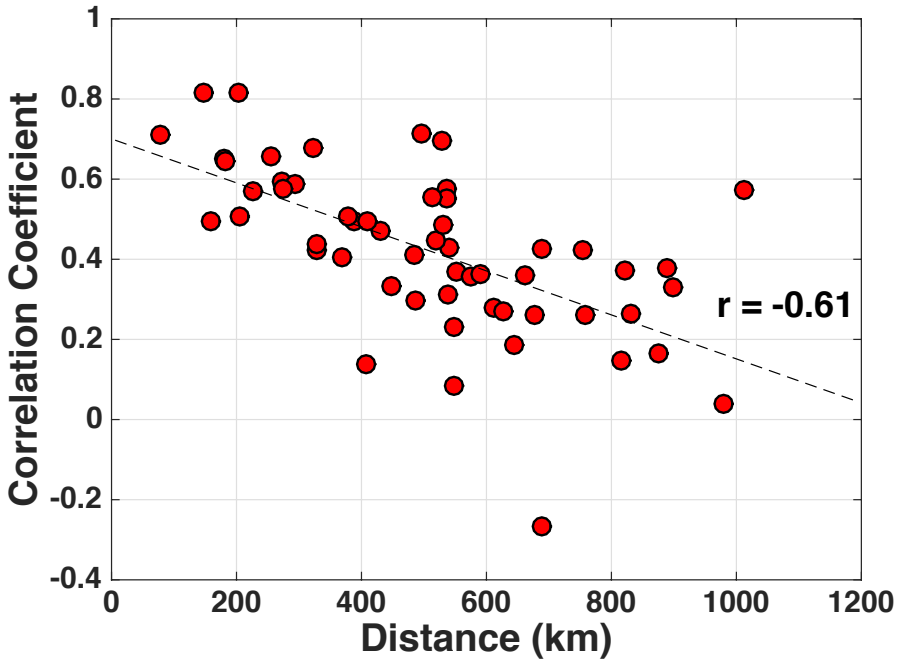

Figure 2.5. Spatial correlation coefficients of the April–May 2012 MDA8 O_3 values at the 11 O_3 stations in Figure 1, versus separation distance. A total of 55 pairs of stations were obtained.

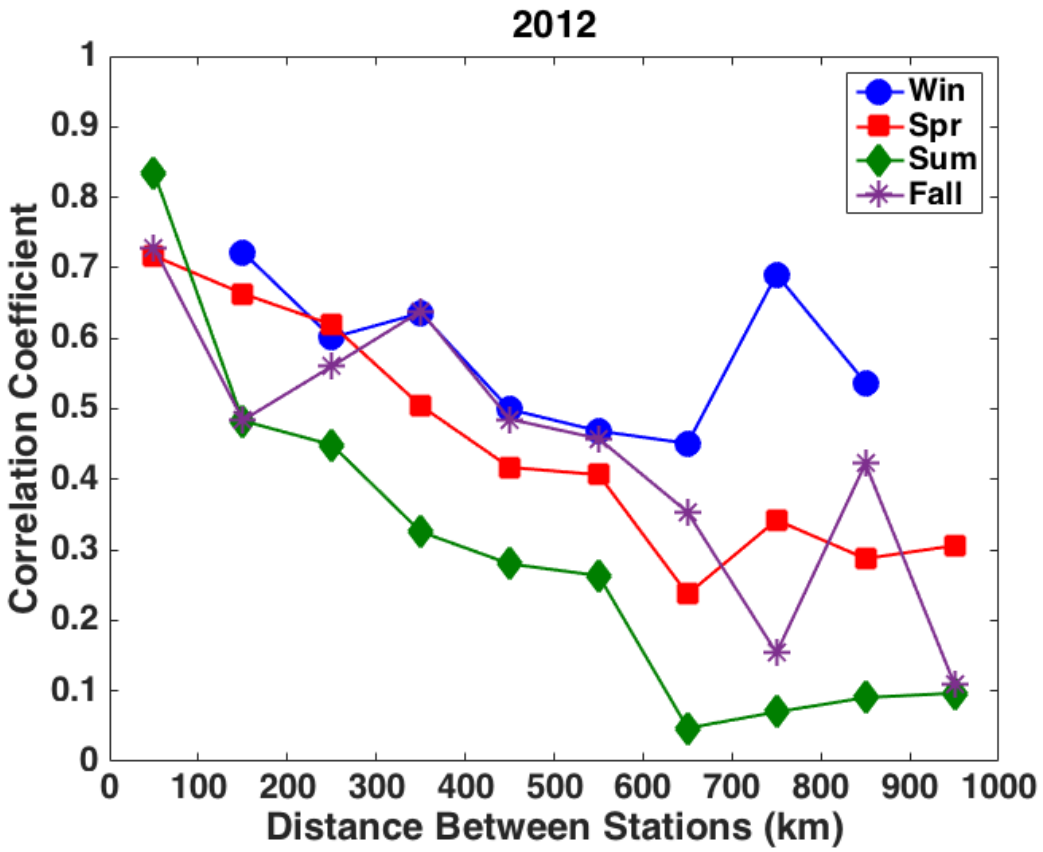

Figure 2.6. Spatial correlation coefficients of the 2012 MDA8 O_3 values at the 11 stations in Figure 2.1, versus separation distance, grouped according to season (Winter: JFM; Spring: AM; Summer: JJA; Fall: SOND). Each point represents the average of the correlation coefficients for every 100-km bin.

2.3.3 Causes for O_3 enhancement

Figure 2.7 shows a plot of daily MDA8 O_3 at MBO for May 2004–2014. High-O_3 days (yellow-red) are seen periodically throughout the data record, especially during the first half of May 2012. Figure 2.7 illustrates a broad enhancement in MDA8 O_3 in May 2012 that is consistent with Figure 4. Figure 2.8 shows a contour plot of MDA8 O_3 at MBO in May 2012 as well as hourly CO and water vapor values measured during the time when maximum average 8-

hr O_3 was observed. The elevated O_3 concentrations in May 2012 are associated with low CO values and low water vapor values – consistent with transport from UT/LS – except for May 29. Backtrajectories for the May 29 event suggest pollution transport from Asia, hence the elevated CO levels. The relatively high water vapor values on this day suggest that the air mass came from the BL before it arrived at MBO.

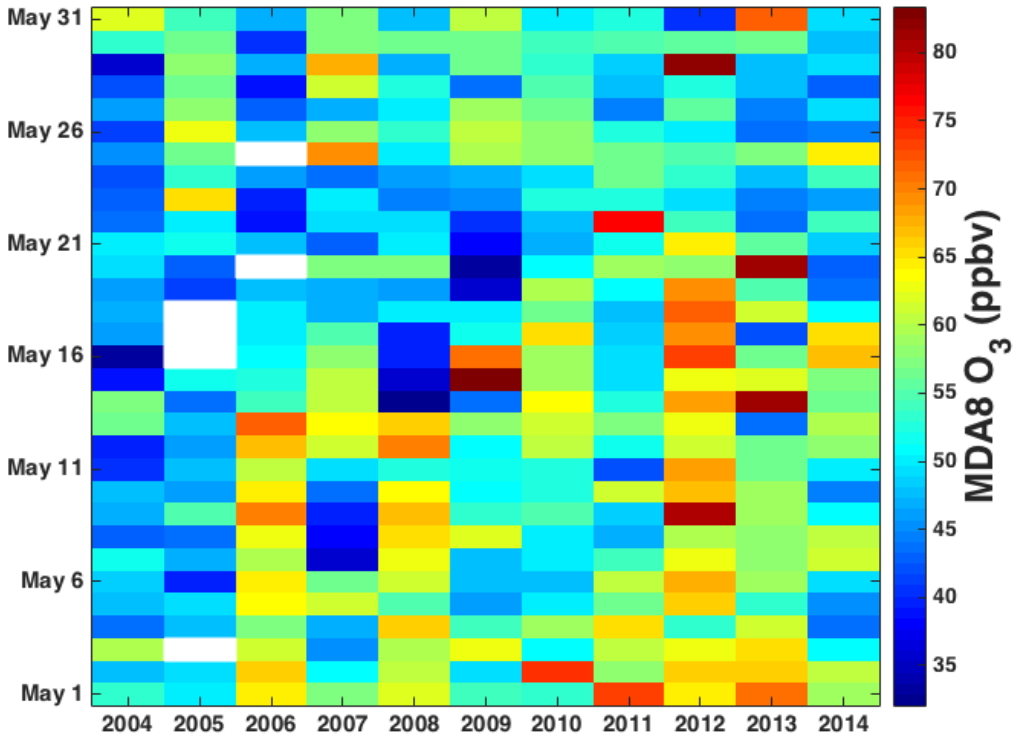

Figure 2.7. MDA8 O_3 at MBO for May 2004–2014. Missing data are plotted as white regions.

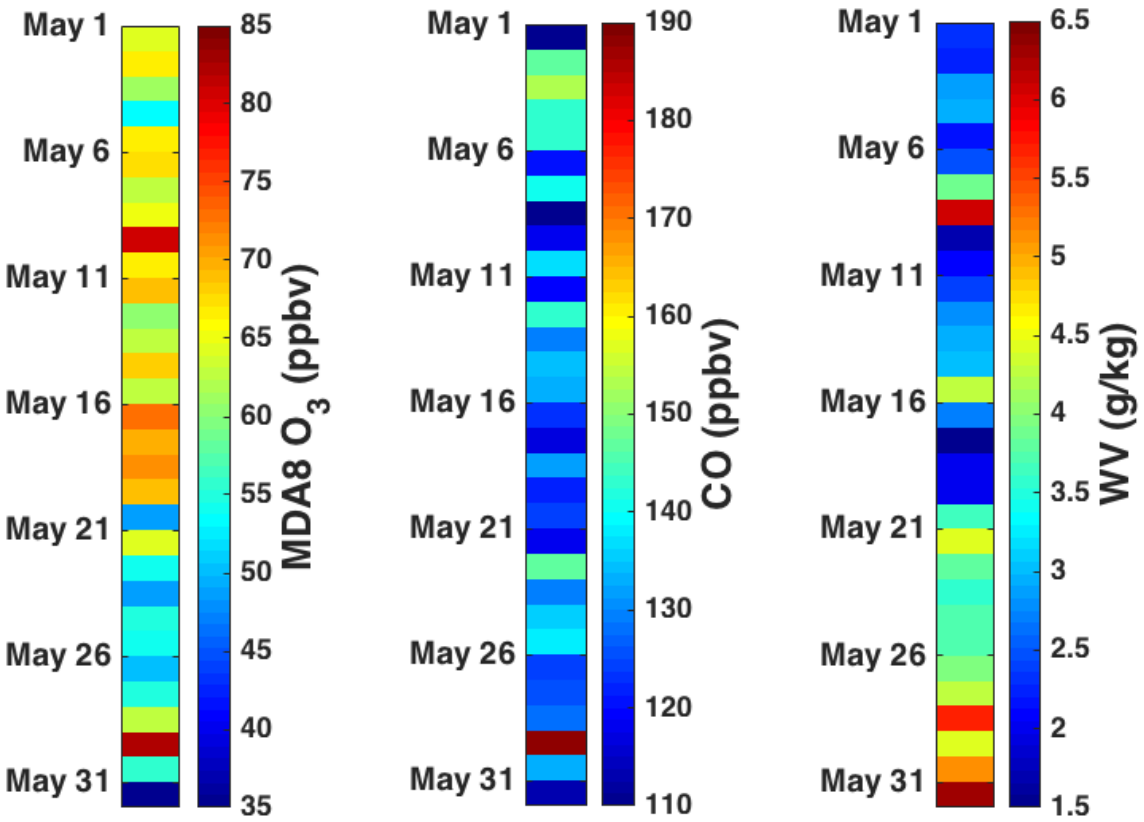

Figure 2.8. MDA8 O_3 at MBO for May 2012. Also plotted are the hourly CO and water vapor values measured when the maximum daily 8-hr average O_3 was observed.

Figure 2.9 shows the vertical profiles of water vapor in the lower FT over Salem, OR. Measurements for the May 2010, 2011, 2013 and 2014 average are plotted against the sounding data from May 2012. Based on a paired T-test, the two-tailed p-value is less than 0.0001 which means that the difference between the two datasets is statistically significant. At MBO, relatively low water vapor (mean ± 1σ: 3.5 ± 1.3 g/kg) and CO (128 ± 15 ppbv) measurements were also observed in May 2012 (see Figures 2.10 and 2.11 for plots of hourly CO and water vapor, respectively, for May 2004–2014; see Figure 2.12 for diurnal plots of O_3, water vapor and

CO for May 2012). These data all suggest enhanced subsidence and an enhanced influence from UT/LS air during May 2012.

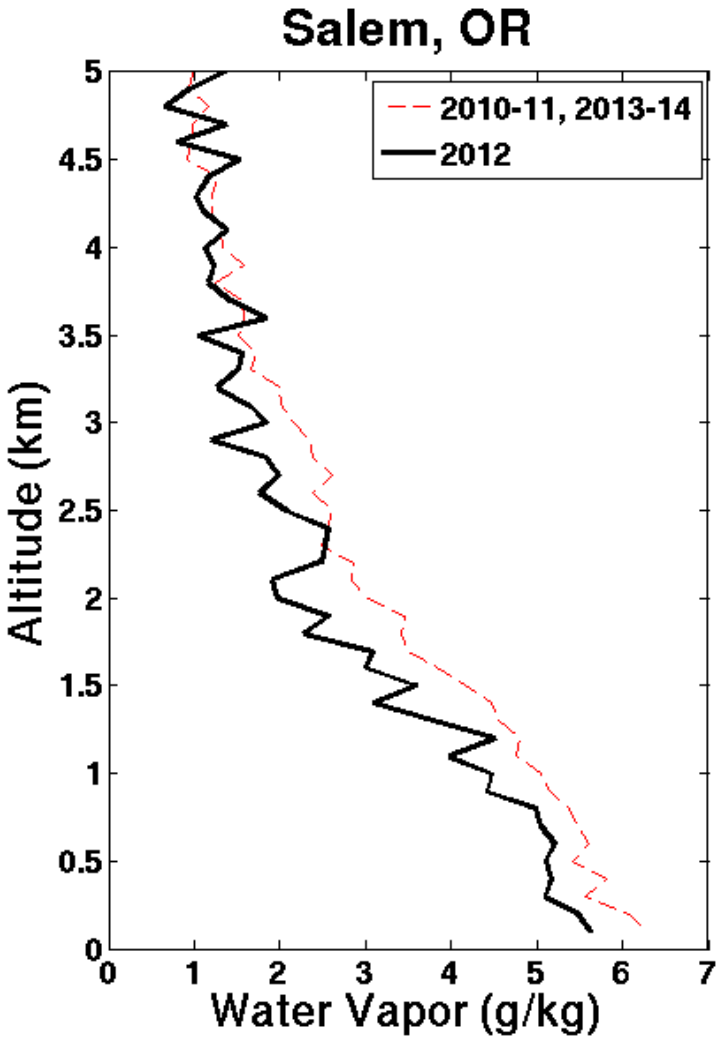

Figure 2.9. Radiosonde profiles of water vapor from Salem, OR. Measurements in May 2010, 2011, 2013 and 2014 are averaged (dashed red line) and are plotted against the average from May 2012 (solid black line). Note the unusually low water vapor values in 2012 across the lower FT.

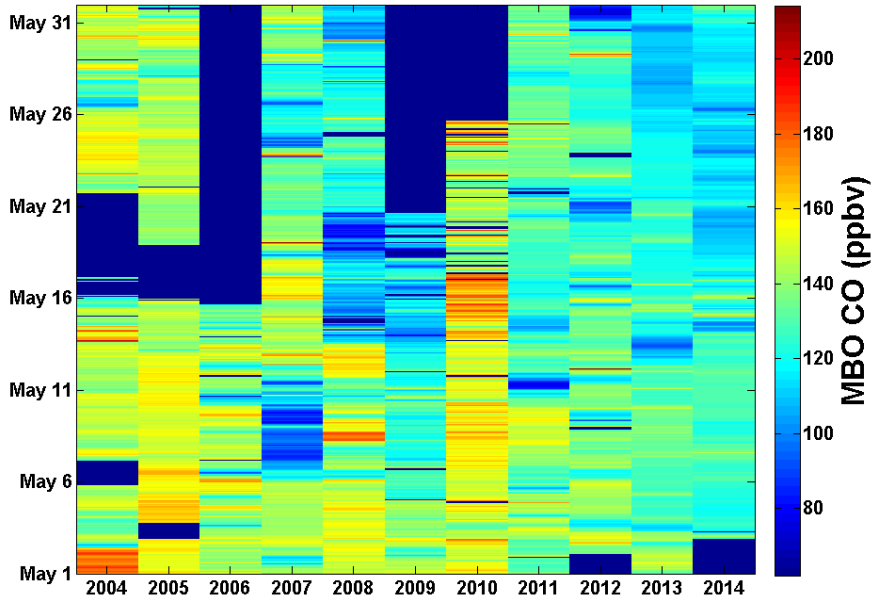

Figure 2.10. Hourly CO at MBO for May 2004–2014. Missing data are plotted as dark blue regions.

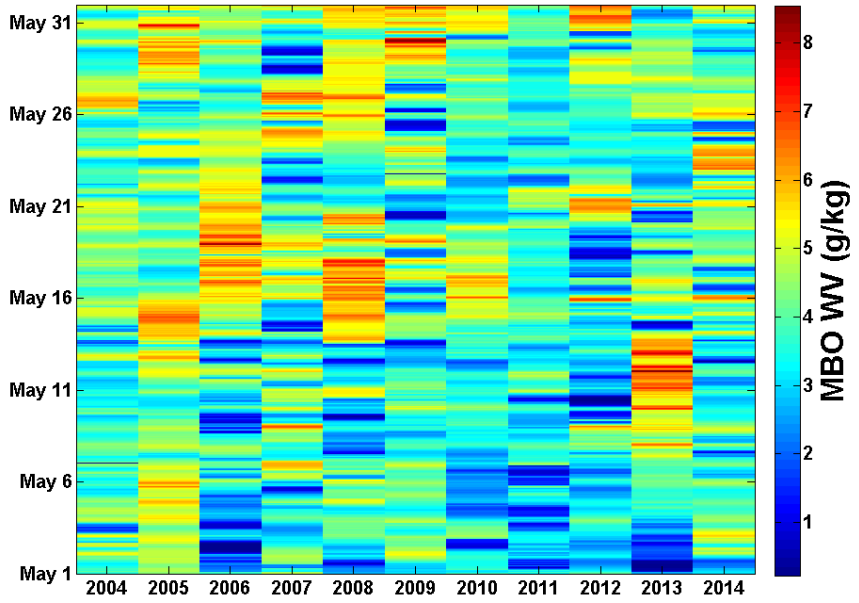

Figure 2.11. Hourly water vapor at MBO for May 2004–2014.

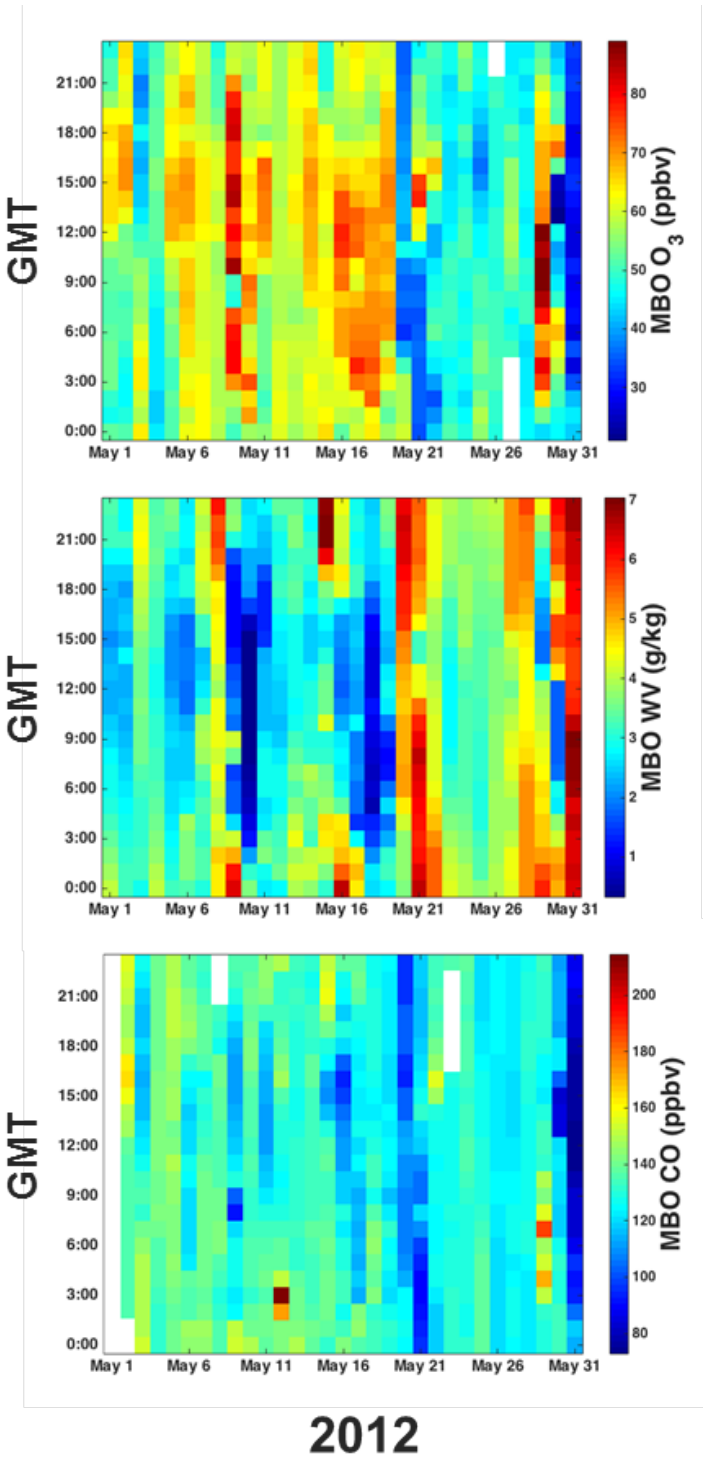

Figure 2.12. Hourly O_3, water vapor and CO at MBO for May 2012.

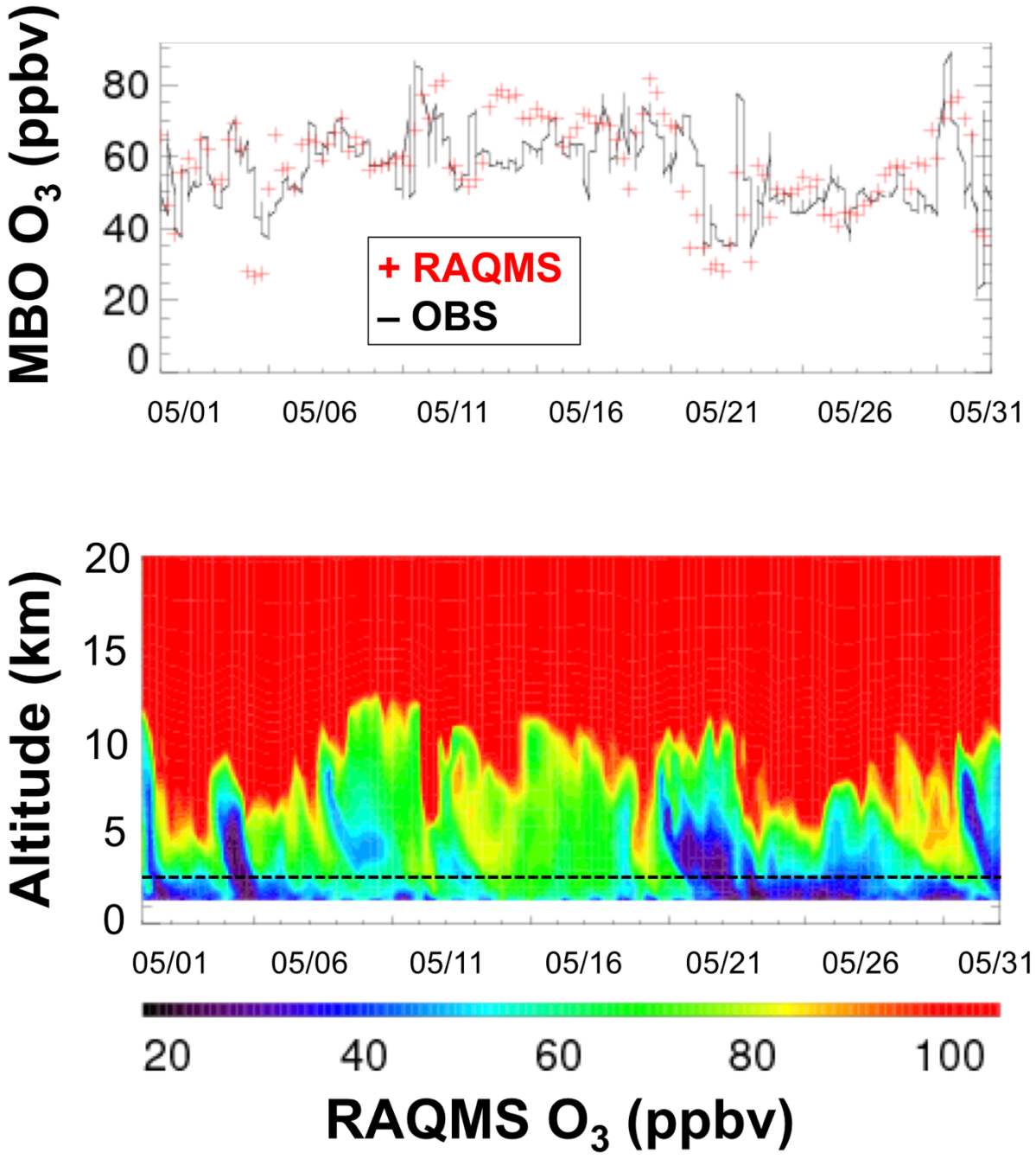

Figure 2.13. (a) Comparison between RAQMS-derived (red) and measured (black) O_3 at MBO (2.8 km a.s.l.); and (b) vertical profile of RAQMS-analyzed O_3 above MBO on May 2012. The horizontal line on (b) shows the MBO height at which RAQMS O_3 was interpolated to.

To further verify this, we look at the RAQMS-modeled vertical profile of O_3 at MBO. We first interpolate RAQMS tropospheric column ozone (TCO_3) to MBO altitude and observe that RAQMS-analyzed ozone mixing ratio correlates well with MBO measurements (r = 0.75, bias = -1.3 ppbv). Figure 2.13a shows that RAQMS O_3 captures the hourly O_3 trend at MBO fairly well. RAQMS likely underestimates surface ozone concentrations at high-altitude sites that are influenced by LRT because it doesn't resolve the true height of the surface measurements. Figure 2.13b shows the O_3 predictions from RAQMS from MBO height up to 20 km. We see periods of subsiding, high-O_3 air and these periods are associated with high O_3 measurements at MBO. An exception is May 29, where we see high O_3 at MBO but no evidence for significant transport from the UT/LS. This high-O_3 event is characterized by high CO (maximum hourly CO peak: 188 ppbv) and air mass backward trajectories that suggest an influence of ALRT.

We then look at TCO_3 and total precipitable water (TPW) maps over the western U.S. Figure 2.14 shows RAQMS TCO_3, TPW and sea level pressure for May 2012, 2013 and 2014. There is a significant enhancement in TCO_3 extending from SE Asia into the central Pacific during May 2012. This TCO_3 enhancement is associated with a stronger Aleutian Low over the Gulf of Alaska during May 2012 and is upwind from MBO.

Figure 2.15 shows a scatter plot of RAQMS TCO_3 vs TPW upwind from MBO (for the boxes shown in Figure 14: 180W-110W, 35N-50N) for May 2012, 2013 and 2014. 2012 has the highest TCO_3 (black points). The TCO_3 histograms show that 2014 had the lowest median, while 2012 and 2013 had similar medians but 2012 shows a tail extending to higher values. The TPW histograms show that 2012 had the lowest median TPW values. These observed and modeled factors—low water vapor, low CO, high O_3 in the FT—all support our conclusion that

enhanced stratosphere/troposphere exchange (STE) in 2012 contributed to the observed elevated surface O_3 across the western U.S.

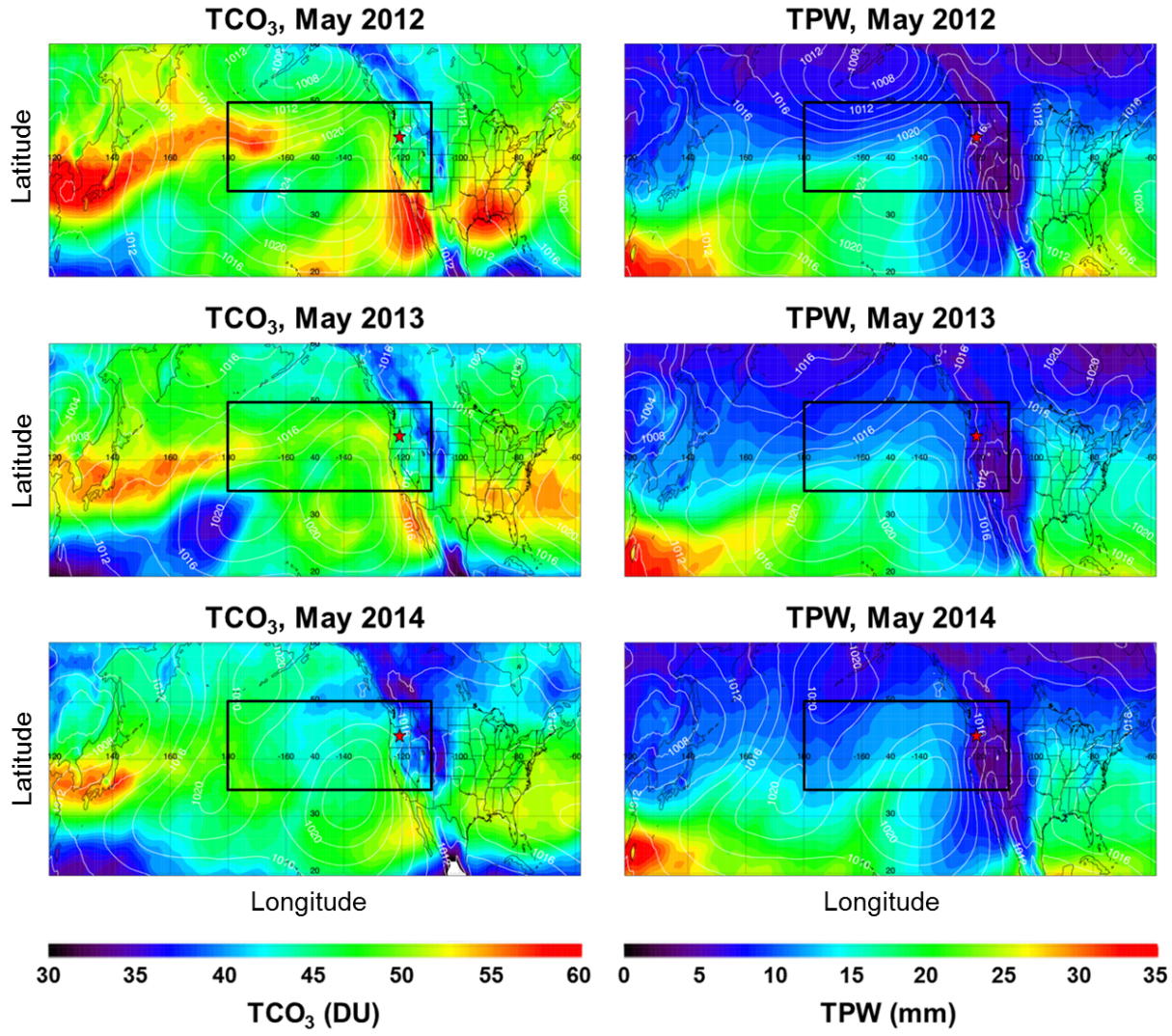

Figure 2.14. Maps of RAQMS tropospheric column ozone (TCO_3, DU) and total precipitable water (TPW, mm) for May 2012, 2013 and 2014. Mean sea level pressure (mb) is contoured in white. Location of MBO is shown as a red star.

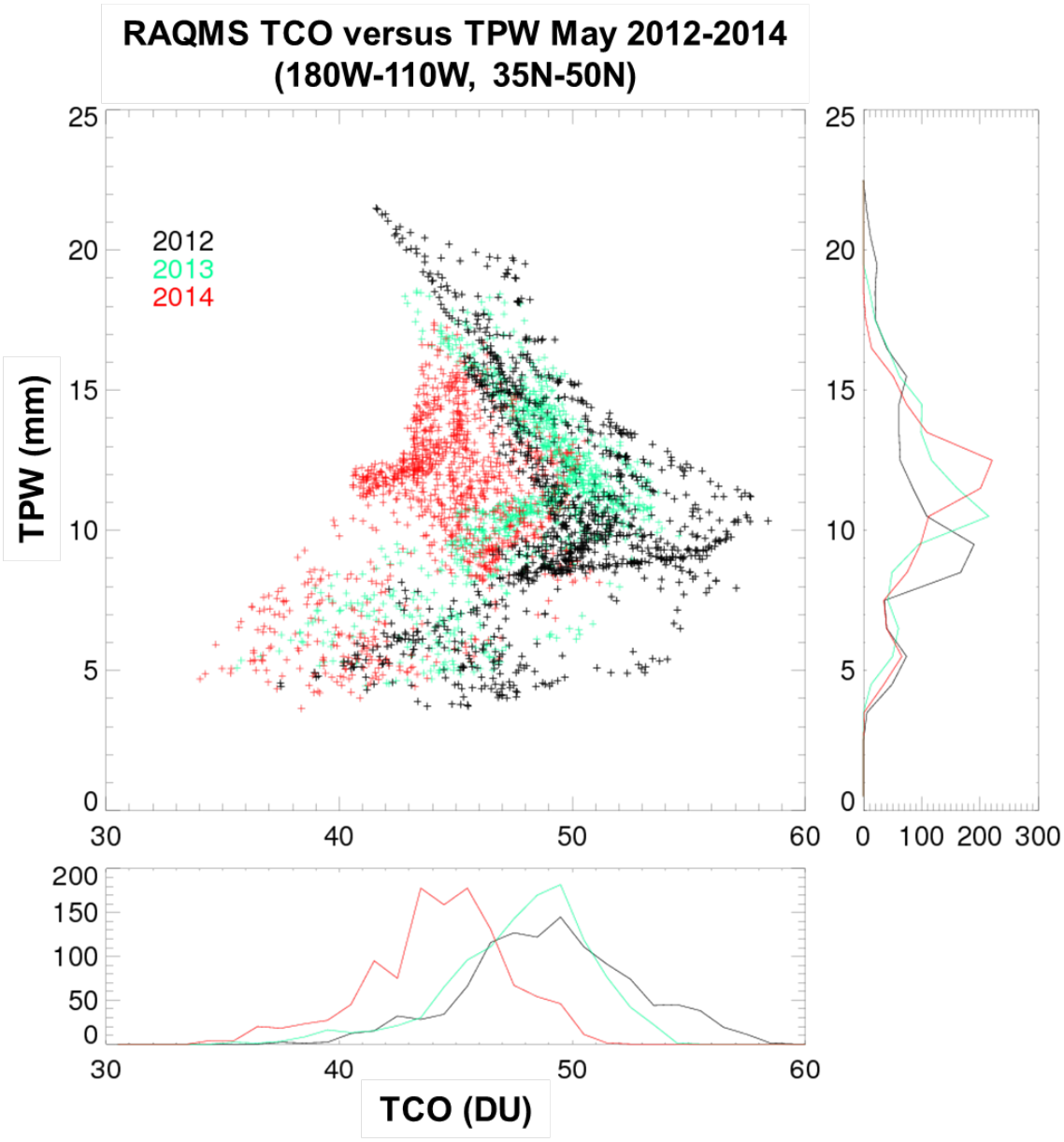

Figure 2.15. Scatter plots of RAQMS tropospheric column O_3 (TCO_3) vs total precipitable water (TPW) for May 2012, 2013 and 2014 for the boxes indicated in Figure 14. Histograms are also plotted.

Our results show that a large-scale high-O_3 period was observed in the western U.S. in Spring 2012, and this shifted the O_3 distribution to higher values across numerous sites. This

caused monthly mean MDA8 O_3 enhancements for May 2012 of 2.0–8.5 ppbv at many sites across the western U.S. compared to other years. While both April and May were enhanced, May had much larger enhancements. The modest shift in the O_3 distributions has a strong effect on the number of exceedance days. MBO, GRB, Lassen, and SLC – all high-elevation sites – exceeded the 8-hr 70 ppbv threshold on 8, 6, 3, and 1 day, respectively, in Spring 2012.

2.4 IMPLICATIONS

Despite reductions in anthropogenic U.S. emissions of O_3 precursors, FT springtime O_3 has been increasing in the western U.S. since the 1990s. On top of this increasing long-term trend, high-O_3 events also drive interannual variations of springtime O_3 in the western U.S. Because FT O_3 can contribute to surface observations under specific meteorological conditions, these high-O_3 events can potentially elevate surface O_3 to unhealthy levels.

We have shown that enhanced UT/LS events in Spring 2012 shifted the MDA8 O_3 distribution to higher values, and as a result increased the number of exceedance days across some sites in the western U.S. This suggests that under current standards, high-O_3 events such as UT/LS episodes and ALRT events could affect the attainment status of a station if they were not identified as exceptional events, which the EPA defines as an uncontrollable event that affected air quality. Understanding the nature and the year-to-year variability of exceptional events is therefore critical for an effective implementation of the US NAAQS.

Long-term measurements aimed at observing exceptional events would be valuable. MBO is the only high-elevation site on the U.S. West Coast that routinely observes high-O_3 events in the FT; however, it provides measurements at only a single point. High-frequency

measurements of O_3, water vapor and CO at a network of mountaintop sites would be valuable at observing exceptional events. Vertical profiles of O_3 and water vapor from LiDAR and ozonesondes, and satellite retrievals would also be helpful. This network of mountaintop observations, LiDAR and satellite observations of ozone could also provide key data on daily and interannual variations in baseline O_3. Forecasting exceptional events would be possible using high-resolution chemical transport models that have been evaluated and verified with free troposphere observations.

CHAPTER 3

IMPACT OF BIOMASS BURNING PLUMES ON PHOTOLYSIS RATES AND OZONE FORMATION AT THE MT. BACHELOR OBSERVATORY

(adapted from Baylon et al., submitted to J. Geophys. Res.)

3.1 INTRODUCTION

Biomass burning (BB) plumes can emit huge amounts of aerosol particles and trace gases to the atmosphere (Andreae, 1991; Crutzen and Andreae, 1990). BB aerosols are predominantly organic carbon and black carbon, with some inorganic components (Reid et al., 2005; Vakkari et al., 2014). Primary organic aerosols (POA) are emitted directly from the fires while secondary organic aerosols (SOA) are formed from the oxidation of organic gases (Akagi et al., 2011). BB plumes are rich in primary pollutants such as carbon monoxide (CO), volatile organic compounds (VOCs), and nitrogen oxides (NOx) (Real et al., 2007; Hodnebrog et al., 2012; Martins et al., 2012). Photochemical reactions of these pollutants can produce secondary pollutants, such as O_3, which can be transported over large distances (Val Martin et al., 2006; Pfister et al., 2008; Mebust et al., 2014). In the troposphere, O_3 is in a delicate balance between photolytic destruction and photochemical formation. Whether the troposphere is a net source or sink of O_3 depends on the balance between the two processes (Thompson, 1984).

The rate-limiting step in the photolytic destruction of O_3 is the reaction between $O(^1D)$ and H_2O to form OH radicals, which are important oxidizing agents in the troposphere:

$$O_3 + h\nu \rightarrow O(^1D) + O_2 \quad (1)$$

$$O(^1D) + H_2O \rightarrow 2OH \quad (2)$$

Reaction of OH with O_3 produces HO_2 which in turn reacts with O_3 resulting in a catalytic destruction cycle.

$$OH + O_3 \rightarrow HO_2 + O_2 \quad (3a)$$

$$HO_2 + O_3 \rightarrow OH + 2O_2 \quad (3b)$$

$$\text{Net:} \quad 2O_3 \rightarrow 3O_2 \quad (3c)$$

On the other hand, the rate-limiting step in the photochemical formation of O_3 is the reaction of NO with HO_2 or RO_2.

$$\begin{Bmatrix} HO_2 \\ RO_2 \end{Bmatrix} + NO \rightarrow NO_2 + \begin{Bmatrix} OH \\ RO \end{Bmatrix} \quad (4)$$

$$NO_2 + h\nu \rightarrow NO + O \quad (5)$$

$$O + O_2 + M \rightarrow O_3 + M \quad (6)$$

The photolysis rate for O_3 (Eq. 1) is termed $j(O^1D)$ while for NO_2 (Eq. 5) it is called $j(NO_2)$. Tropospheric ozone photolysis is in the 290-340 nm range, while NO_2 photolysis is in the 290-420 nm range.

Because BB plumes can produce large amounts of NOx and VOCs, they have the potential to produce O_3 downwind (Jaffe and Wigder, 2012). For example, the Siberian wildfires in 2003 caused enhancements of summertime ozone in the western U.S. from 9 to 17 ppbv (Jaffe et al., 2004). On January 2014, intense wildfires in forests located 70 km southwest of Santiago, Chile were transported by low-level winds and led to a striking decrease in visibility and a marked increase in ozone well above 80 ppbv in the urban atmosphere (Rubio et al., 2015). The September 2012 Pole Creek Fires, which originated 20 km north of Mount Bachelor Observatory (MBO, 2.8 km above sea level), resulted in ozone enhancements of 17-32 ppbv at MBO (Baylon

et al., 2015). Studies have found that ozone formation ranges can vary sharply from very low in fresh plumes to low in moderately aged plumes to high in well-aged plumes (Val Martín et al., 2006; Wigder et al., 2013). However, quantifying ozone production from wildfires is complicated by variations and uncertainties such as fire emissions (type of species emitted), combustion efficiency, meteorological patterns, chemical and photochemical reactions, aerosol effects on chemistry, and solar radiation (Jaffe and Wigder, 2012). Aside from NOx and VOCs, sunlight is an important factor for ozone production. Baylon et al. (2015) looked at wildfire plumes observed at MBO during the Summers of 2012 and 2013 and found that plumes that are not associated with ozone formation were transported during the nighttime, when there is minimal photochemistry.

Numerous studies have evaluated the effects of aerosols on photolysis rates and O_3 formation. These effects are dependent on different factors. First is the type of aerosol. Model simulations by Dickerson et al. (1997) show that scattering particles in the boundary layer (BL) can increase photolysis rates and can therefore accelerate ozone production. However, UV-absorbing aerosols such as mineral dust and soot have also been found to reduce ozone mixing ratios by up to 24 ppbv (Dickerson et al., 1997). Similarly, aerosol particles containing black carbon (BC) have been suggested to reduce surface ozone in Los Angeles by 5-8% (Jacobson et al., 1998). Simulations in Mexico City by Castro et al. (2001) suggest an even larger reduction in NO_2 photolysis rates (10-30%) and surface ozone mixing ratios (30-40 ppbv) due to urban aerosols. A more recent field campaign study by Ying et al. (2011) looked at the impact of dust aerosols in Mexico City on photolysis rates. They confirmed that dust aerosols lead to significant reductions in photolysis rates and surface concentrations of OH and O_3 in the city. Using a three-dimensional regional chemical transport model, Tang et al. (2003) found that the

accumulated impact of biomass burning aerosols from Southeast Asia, which contain large amounts of carbonaceous material, is to reduce surface ozone mixing ratios by about 6 ppbv. Smaller reductions in $j(NO_2)$ have been simulated by Li et al. (2011) for urban aerosols in Central Eastern China. They found reductions less than 10% during noontime; however, they also note that aerosols can slightly enhance photolysis rates during noontime when UV scattering dominates absorption by aerosols (Li et al., 2011).

The composition of BB aerosols is highly variable between plumes but is an important factor for determining its impact on photolysis rates and ozone production. Collier et al. (2016) studied the regional and near-field influences of wildfire emissions on ambient aerosol concentrations and chemical properties at the MBO. Using two high-resolution time-of-flight aerosol mass spectrometers (HR-AMS), they found that organic aerosols (OA) account for >94% of the non-refractory submicrometer aerosol mass (NR-PM_1) (Collier et al., 2016). The brown carbon (BrC) component in OA absorbs mostly in the near-UV, as opposed to black carbon (BC) which absorbs light throughout the UV-visible spectrum (Andreae and Gelencser, 2006). In one study, the combined optical properties of BC and BrC have been shown to slow the net ozone production rate by up to 18% (Mok et al., 2016). However, the composition of BB aerosols is highly variable (Collier et al., 2016; Zhou et al., 2017).

Another important factor is the vertical location of the aerosols with respect to the point of observation. Model simulations near Mexico City during the MILAGRO campaign suggest that aerosols enhance actinic flux, and therefore photolysis rates, above the BL and reduce actinic flux near the surface (Palancar et al., 2013). Alvarado et al. (2015) looked at model simulations over the Williams fire in California and found that $j(NO_2)$ is lowest in the bottom of the plume, reduced in the middle of the plume, and enhanced above the plume.

Clouds can also affect the photolysis rates and ozone. They have been shown to reduce actinic flux and therefore photolysis rates below them (Liao et al., 1999; Madronich, 1987). Using a regional-scale photochemical model, Matthijsen et al. (1997) found that clouds lead to ozone reductions in the BL in Europe by as much as 22%. But model simulations have shown that in the upper parts of clouds, backscattering by cloud droplets can increase the actinic flux and therefore the photolysis rates as well (Liao et al., 1999; Madronich, 1987; Voulgarakis et al., 2009). Using a 3D chemical transport model over East Asia-West Pacific, Tang et al. (2003) showed that photolysis rates decrease by 20% below clouds and are enhanced by 30% above cloud layers during the observation period. In reality, however, clouds and aerosols together impact photolysis rates. In a polluted urban environment in Houston, TX, model results show that aerosols alone reduced $j(NO_2)$ by 3% on six clear days. The combined effect of clouds and aerosols reduced $j(NO_2)$ by 17%, and subsequently ozone production was reduced by approximately 8 ppbv/hr (Flynn et al., 2010).

Most of these studies rely on model simulations of photochemistry in BB plumes. Very few were based on in-situ measurements aimed at exploring the photochemical environment in BB plumes. This study aims to fill this knowledge gap. Our goal is to understand the photochemistry in biomass burning plumes by looking at field measurements of actinic flux, aerosols, and NOx at MBO, a mountaintop research station located on the summit of a dormant volcano in central Oregon (Jaffe et al., 2005).

Data from MBO have previously been used to explore the impact of fires on ozone formation (Wigder et al., 2013). In a recent study by Baylon et al. (2015), the average NO/NO_2 ratio in fire plumes was higher than outside the fire plumes. Because VOCs are presumably higher in fire plumes than in non-fire-influenced air, it was suggested that $j(NO_2)$ may be higher

in fire plumes. This is possible if the decreases in photolysis rates due to absorption are compensated for by scattering of aerosols.

This study aims to answer the following questions:

a. Can we identify variations in $j(NO_2)$, $j(O^1D)$, and NO/NO_2 ratios due solely to BB smoke?

b. What is the level of agreement between observed and modeled $j(NO_2)$ and $j(O^1D)$ for clear-sky conditions?

c. What are the calculated instantaneous O_3 production rates and $HO_2 + RO_2$ concentrations in P/NP?

To compute the HO_2 and RO_2 concentrations, we use the extended Leighton relationship:

$$\frac{(NO)}{(NO_2)} = \frac{j(NO_2)}{k_O[O_3]+k_H[HO_2]+k_R[RO_2]}, \quad (7)$$

where k_O is the rate constant for the reaction of NO with O_3, and k_H and k_R are the rate constants for Eq. 4. To calculate the rate of O_3 production, $P(O_3)$, we use the equation:

$$P(O_3) = (k_H[HO_2] + k_R[RO_2])[NO] \quad (8)$$

3.2 MATERIALS AND METHODS

The MBO (43.98°N, 121.69°W; 2.8 km a.s.l.) is a high-elevation mountaintop site in central Oregon established in 2004 (Jaffe et al., 2005). Routine measurements of the scattering coefficient (σ_{sp}) (TSI Model 3563), O_3 (Dasibi 1008 RS), and CO (May 2012 onwards: Picarro

G2302), along with measurements of basic meteorology, such as temperature, humidity and wind speed, have been on-going at MBO since 2004. We typically add a suite of measurements during intensive field campaigns. For example, during Summer 2012, we added NOx and NOy (Baylon et al., 2015). During Summer 2013, we added PAN (Briggs et al., 2016). During Summer 2015, we re-installed the NOx and PAN instruments, and added the Scanning Mobility Particle Sizer (SMPS) (Laing et al., 2016), and a METCON GmbH diode array actinic flux spectroradiometer (DAFS) to determine photolysis frequencies.

3.2.1 NOx

We measured NOx during the summer of 2015 using a chemiluminescence detector manufactured by Air Quality Design (AQD), Inc. The instrument was used at MBO previously (Baylon et al., 2015; Reidmiller et al., 2010). When NO is reacted with a high concentration of O_3, excited state NO_2 (i.e., NO_2*) and O_2 are produced. The NO_2* either decays to ground state (by emitting a photon) or is deactivated via collisions. A photomultiplier tube (red-IR) detects the photons and the signal is proportional to the initial NO concentration in the sampled air. NO_2 is detected as NO after UV photolysis at wavelengths between 385 and 405 nm using a Blue Light Converter (Air Quality Design Inc, Boulder, CO). We used a gas-phase titration system, where a known amount of NO is reacted with O_3 (which was formed by exposing ultra zero air to a Hg-Pen Ray lamp) to form NO_2, for calibration.

A typical operating cycle for the NOx instrument includes a 3-min measure mode and a 2-min zero mode. During measure mode, we added O_3 to the ambient airflow in the reaction chamber, causing the chemiluminescent reaction between NO and O_3 that takes place in front of the PMT. During zero mode, ozone reacts upstream of the reaction chamber, and hence the chemiluminescent reaction takes place out of view of the PMT, thereby preventing any photon

detection due to NO. We could subtract the counts detected during the zero mode from the counts detected during the measure mode to derive the signal from the NO_2* chemiluminescence alone. This alternation between measure and zero modes continues for 11 hours, after which an automated one-hour standard addition calibration takes place. We obtained a total of 2 calibrations (and hence 2 sets of sensitivity values) each day. For 2015, our 5-min NO and NO_2 detection limits (3–σ) were 10 pptv and 35 pptv, respectively.

3.2.2 Photolysis rates

Actinic flux was measured at MBO using a METCON GmbH diode array actinic flux spectroradiometer (DAFS). The DAFS collects spectrally resolved radiation from 273 to 700 nm (Edwards and Monks, 2003; Jäkel et al., 2005). The instrument consists of a 2π sr actinic flux entrance optic, a 512-pixel diode array detection system, and a computer for data acquisition. Wavelengths between 282 and 288 nm were used to estimate the background noise since no photons with wavelengths shorter than 290 nm can penetrate the atmosphere. A spectral calibration was performed at the National Center for Atmospheric Research calibration facility using 1000-W NIST traceable QTH lamps. The absolute uncertainty of the actinic flux measurements is estimated to be 6% in the UV-B band. The relative uncertainty for comparing two different observations of $j(NO_2)$ was 0.10%. This was estimated by calculating the relative standard deviation of the actinic flux measurements at high solar noon over a 30-minute time window on a cloud-free day at MBO.

The photolysis frequency j is dependent on local actinic flux, F, the absorption cross section, σ, and quantum yield, ϕ, for molecule A (Edwards and Monks, 2003; Madronich, 1987; Madronich and Weller, 1990). These molecular parameters are functions of wavelength, λ, and

temperature, *T*. Therefore, a photolysis frequency can be defined as the integral of the product of solar actinic flux, absorption cross section, and quantum yield with respect to wavelength:

$$j = \int_{\lambda_1}^{\lambda_2} F(\lambda)\sigma\,(\lambda, T)\phi(\lambda, T)d\lambda \qquad (9)$$

For ground-based instruments, the limit λ_1 is typically set to 290 nm, the so-called atmospheric cut-off where minimal solar actinic flux reaches the ground because of absorption of shorter wavelengths by stratospheric ozone. On the other hand, λ_2 is the upper bound of the quantum yields for molecule A. Typically, λ_2 = 420 nm for $j(NO_2)$ and λ_2 = 340 nm for $j(O^1D)$ (Eq. 5 and Eq. 1, respectively). Absorption cross-section and quantum yield data for $j(NO_2)$ and $j(O^1D)$ are obtained from the Jet Propulsion Laboratory (JPL) kinetics/photochemical recommendation (https://jpldataeval.jpl.nasa.gov/index.html). Uncertainties in these molecular data are typically ±5-10% for cross-sections and greater than ±10% for quantum yields. The overall uncertainty for $j(NO_2)$ is ±14% (Edwards and Monks, 2003, Shetter et al., 2003). However, because the DAFS is an instrument with a high straylight and significant instability in the dark current, it has been shown to impact the deep UV-B where ozone absorption is very strong. Using a neighboring scanning instrument, Edwards and Monks (2003) computed a diode array $j(O^1D)$ uncertainty of ±20% for data where the solar zenith angles are smaller than 70°. Without proper parameterization, uncertainties can be as high as ±60% (Jäkel et al., 2005). Jäkel et al. (2006) provided parameterization methods to improve $j(O^1D)$ but only for solar zenith angles smaller than 70°. In this paper, we estimate the overall uncertainty for $j(O^1D)$ to be ±40%. For this reason, we report the measured $j(O^1D)$ values, but treat the results qualitatively.

Note that we measured only downwelling actinic flux at MBO. However, given the mostly rocky terrain of the surroundings, we assume a very small upwelling component (5%).

Therefore, we approximate the total photolysis rates to be 1.05 times the calculated downwelling rates.

3.2.3 Radiative Transfer Model

Simulations of the ultraviolet radiation field were performed for cloud-free conditions using the Tropospheric Ultraviolet-Visible (TUV) model v.5.2. A complete description of the model is given elsewhere (Madronich, 1987; Madronich and Flocke, 1998). Briefly, the model considers the propagation of solar irradiance through the Earth's atmosphere taking into account multiple scattering and absorption due to gases and particles. The atmosphere is divided into 80 equally spaced layers, each 1 km thick, with homogenous composition and properties according to the United States Standard Atmosphere (USSA, 1976). In this study, the photolysis rates $j(NO_2)$ and $j(O^1D)$ are calculated using TUV v.5.2 to simulate clear-sky conditions at MBO. It was run in pseudo-spherical discrete ordinate 4-stream mode. These simulations are compared with DAFS-measured values.

3.2.4 BB Event Identification

There are various ways of identifying BB plumes. For example, Weiss-Penzias, et al. (2007) used a series of criteria to identify pollution events: CO enhancement of >15% above the monthly mean for at least 12 hours, enhancements in at least one other species (total airborne mercury, PM, O_3, NOy), and an ensemble of backtrajectories that show a consistent pattern of transport from one of several pre-determined source regions. Parrington, et al. (2013) used acetonitrile (CH_3CN) as tracer. When the value of CH_3CN is below a certain threshold (180 pptv), the event is considered non-plume while it is considered a fire event if it is above the threshold.

To identify BB events, we employed the same criteria used by Baylon et al. (2015):

- Five-minute ambient aerosol scattering $\sigma_{sp} \geq 20$ Mm^{-1} for at least two hours.
- Five-minute CO $\geq$ 150 ppbv for at least two hours.
- Strong correlation ($r^2 \geq 0.70$) between σ_{sp} and CO.
- Consistent air mass back trajectories indicating transport over known fire locations.

For the fourth criterion, we used the Fire Information for Resource Management System (FIRMS) Web Fire Mapper to identify burning fires (https://firms.modaps.eosdis.nasa.gov/firemap/). Another important tool that we used was the AirNow Tech Navigator (http://www.airnowtech.org/navigator/index.cfm). It provides users with a graphical map of HYSPLIT (Hybrid Single Particle Lagrangian Integrated Trajectory Model) backtrajectories. We also calculated enhancement ratios ($\Delta Y/\Delta X$) by taking the linear regression (Reduced Major Axis, RMA) slope of multiple measurements of Y plotted against X.

3.3 DATA

The summer of 2015 was a very active fire season in the Pacific Northwest, with an area burned of approximately 2.4 million acres, the third-largest August burned area on record (www.nifc.gov/). Fires burned in Washington, Oregon, Idaho, Montana, and Northern California. The most significant fires were from north-central Washington, which burned more than 300,000 acres and destroyed 176 homes. At MBO, aerosol scattering exceeded 20 Mm^{-1} for a large part of August (~50% of the 5-minute dataset). Figure 3.1 shows a time series of σ_{sp}, O_3, $j(NO_2)$, and $j(O^1D)$ at MBO. Using the criteria enumerated by Baylon et al. (2015), 19 fire

events were identified. A detailed discussion about the location of these fires and the optical properties of the BB aerosols observed at MBO is presented elsewhere (Laing et al., 2016; Gao et al., submitted). Briefly, these fire events ranged from 1.5 to 45 hours in duration, and come from a mix of both regional (Northern California and Southwestern Oregon) and Siberian BB smoke. Laing et al. (2016) noted that the regional BB events were influenced by multiple fires with various transport times ranging from 3 to 35 hours. On the other hand, Siberian events were transported to MBO with transport times of 4 to 10 days.

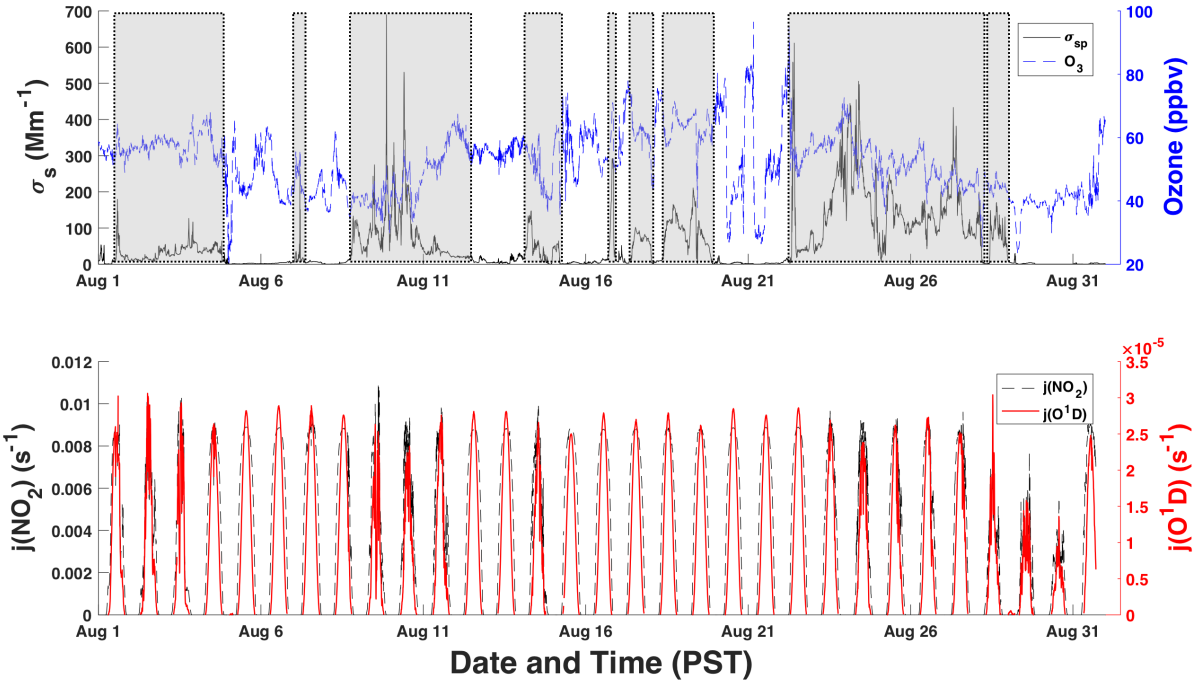

Figure 3.1. Time series of σ_{sp}, O_3, $j(NO_2)$, and $j(O^1D)$ during August 2015. Shading represents smoky days.

3.4 RESULTS

We divided our 5-minute local noontime (11:00-14:00) dataset into three categories based on σ_{sp} levels: clean ($\sigma_{sp} < 10$ Mm^{-1}), moderate smoke (10 Mm^{-1} $< \sigma_{sp} <$ 40 Mm^{-1}), and heavy smoke ($\sigma_{sp} > 40$ Mm^{-1}). Table 3.1 summarizes the statistics. Local mid-day O_3 for moderate smoke conditions is 7.3 ppbv higher than for clean air. Average O_3 for heavy smoke is not very different from moderate smoke. The average water vapor for all categories is relatively high, which is indicative of boundary layer transport. This is common for mid-day at MBO (McClure et al., 2016).

For mid-day, the NO/NO_2 ratio in 2015 is highest for heavy smoke, which is consistent with a similar study conducted at MBO during Summer 2012 and 2013 (Baylon et al., 2015). The NO_2 photolysis rates, $j(NO_2)$, are higher on average during heavy- and moderate-smoke conditions versus non-smoke conditions. In particular, the heavy smoke $j(NO_2)$ values are statistically different from the clean air whereas the moderate- and heavy-smoke datasets are not statistically different. On the other hand, there is no clear pattern for $j(O^1D)$. We should note that Table 1 represents local noontime averages, without taking into account the effect of clouds which can interact with BB aerosols to produce the variations that we observe in the photolysis rates. Therefore, we further segregate our data into cloud-free periods which we describe next.

Table 3.1. Statistics for Summer 2015 local mid-day (11:00-14:00) data segregated based on σ_{sp} levels. N represents the number of 5-minute data points.

		Clean ($\sigma_{sp} < 10$ Mm^{-1})	Moderate smoke (10 Mm$^{-1} < \sigma_{sp} < 40$ Mm^{-1})	Heavy smoke ($\sigma_{sp} > 40$ Mm^{-1})
σ_{sp} (Mm^{-1})	Mean	3.41	22.9	124
	N	440	197	510
	S.D.	2.25	9.57	63.9
	Median	3.19	21.5	111
CO (ppbv)	Mean	97.0	137	308
	N	272	110	444
	S.D.	13.4	17.7	100.4
	Median	94.8	136	284
O_3 (ppbv)	Mean	45.6	52.9	52.1
	N	435	197	510
	S.D.	7.30	3.96	6.85
	Median	43.5	53.0	52.6
Water vapor (g/kg)	Mean	4.41	4.42	5.27
	N	436	197	510
	S.D.	1.38	1.55	1.03
	Median	4.44	4.34	5.33
NO/NO_2	Mean	0.16	0.15	0.20
	N	129	102	331
	S.D.	0.10	0.13	0.17
	Median	0.14	0.14	0.19
$j(O^1D)$ (s^{-1})	Mean	$2.27(10^{-5})$	$2.39(10^{-5})$	$2.25(10^{-5})$
	N	440	197	510
	S.D.	$6.71(10^{-6})$	$4.98(10^{-6})$	$4.44(10^{-6})$
	Median	$2.49(10^{-5})$	$2.56(10^{-5})$	$2.37(10^{-5})$
$j(NO_2)$ (s^{-1})	Mean	$7.89(10^{-3})$	$8.15(10^{-3})$	$8.13(10^{-3})$
	N	440	197	510
	S.D.	$2.00(10^{-3})$	$1.51(10^{-3})$	$1.45(10^{-3})$
	Median	$8.79(10^{-3})$	$8.74(10^{-3})$	$8.71(10^{-3})$

3.4.1 Photolysis rates in BB plumes versus clean air

We are interested in examining the impact of only BB aerosols on photolysis rates. However, because clouds impact photolysis rates as well, we carefully selected three mostly-cloud-free days at MBO. To do this, we looked at GOES-WEST visible images from the NOAA

Comprehensive Large Array-Data Stewardship System (www.class.ncdc.noaa.gov). We identified August 6th, 18th, and 25th as cloud-free days at MBO. Figure 3.2 shows a time series of σ_{sp}, $j(O^1D)$, and $j(NO_2)$ on these days. August 6th is a clean day at MBO, with noontime $\sigma_{sp} < 5$ Mm^{-1}. August 18th and 25th are smoky days at MBO, with noontime σ_{sp} ~120 and 160 Mm^{-1}, respectively. The smoke on Aug 18th is coming from fires burning in California. CALIPSO images (www.calipso.larc.nasa.gov) suggest a smoke plume at MBO, with plume top at ~3 km a.s.l. (Figure S1). Similarly, the smoke event on Aug 25th is likely from fires originating in California and Oregon. CALIPSO suggests a plume top of closer to 5 km a.s.l. (Figure 3.3). However, at ~14:00 LT, clouds disrupt the diurnal photolysis profiles.

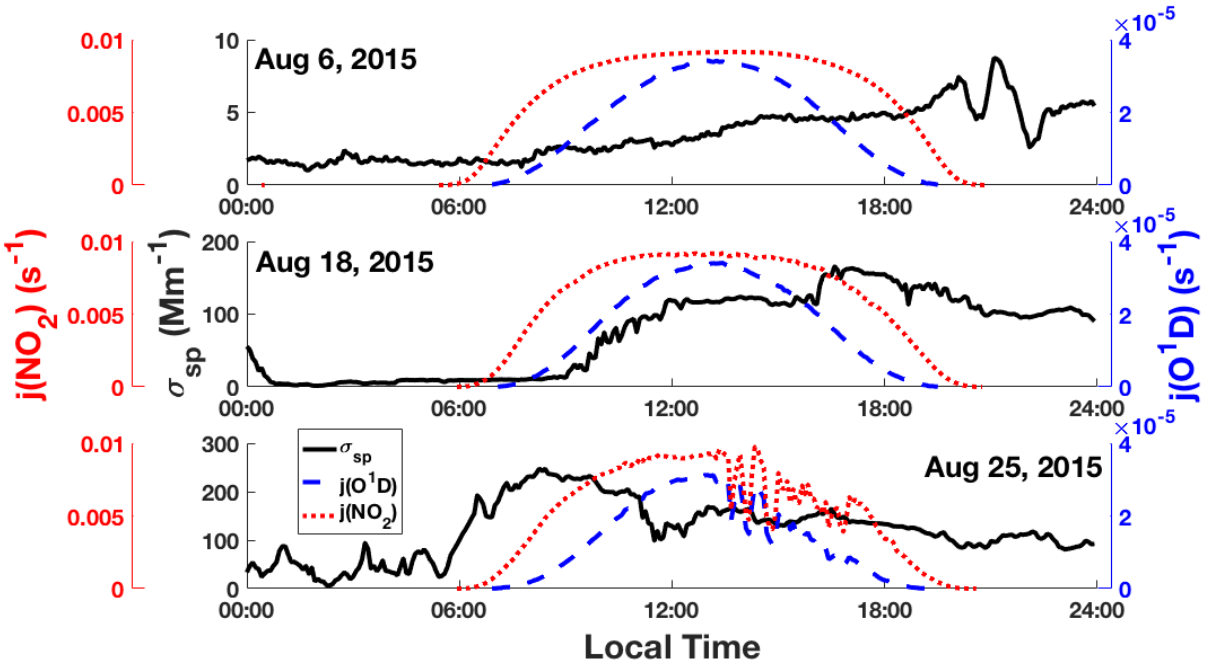

Figure 3.2. Time series of σ_{sp}, $j(O^1D)$, and $j(NO_2)$ on selected pollution-free (Aug 6th) and polluted days (Aug 18th and 25th). All three days are cloud-free until 14:00 LT (LT = UTC – 7).

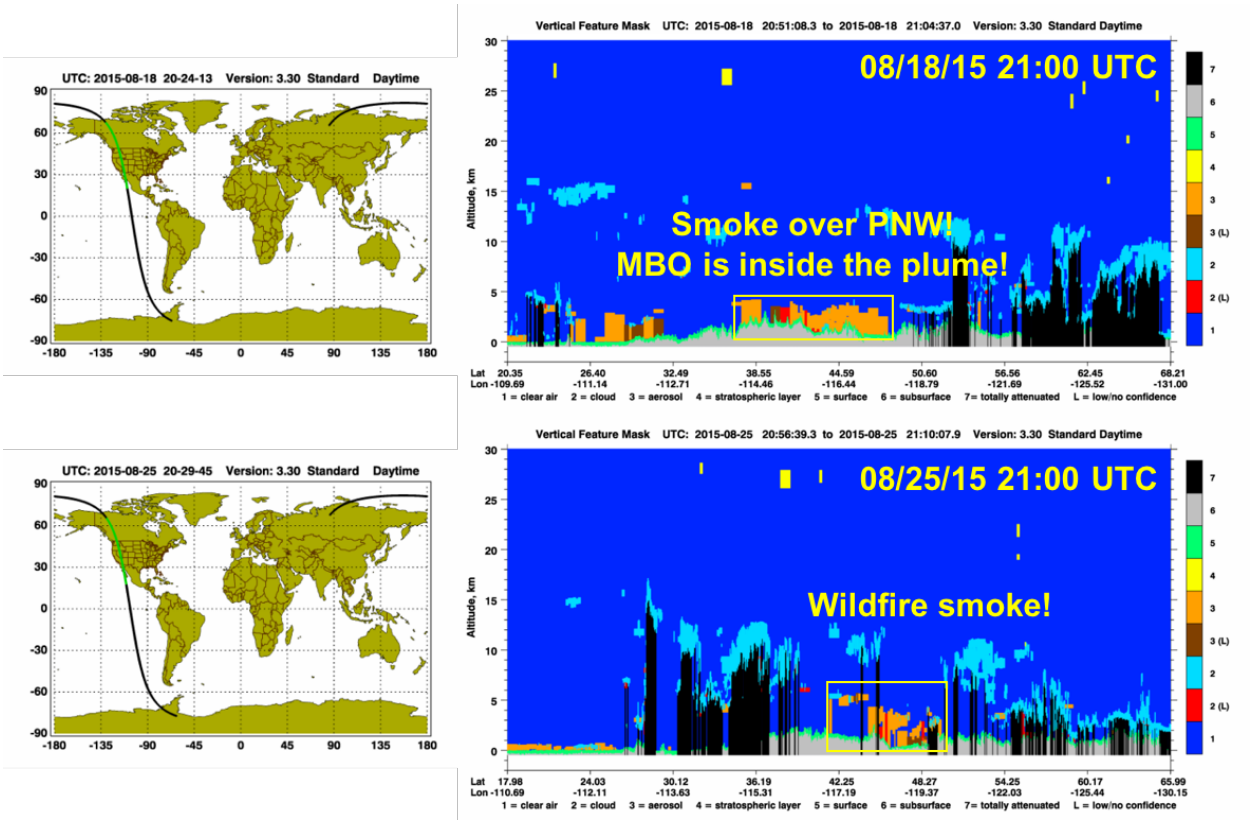

Figure 3.3. CALIPSO images over the Pacific Northwest on Aug 18th and 25th 2015.

Another interesting feature from Figure 3.2 is that $j(NO_2)$ and $j(O^1D)$ have different shapes. $j(NO_2)$ is broader than $j(O^1D)$ because the dissociation spectra for NO_2 reaches to longer wavelengths. On the other hand, $j(O^1D)$ has a narrower diurnal profile because it is increasingly absorbed by atmospheric O_3 at higher solar zenith angles (early morning and late afternoon). $j(NO_2)$ is not very sensitive to atmospheric O_3 column (see later discussion on sensitivity tests conducted using TUV5.2).

We then compare the photolysis rates during the smoky days with respect to the clean day (Figure 3.4a). Given the ±40% uncertainty in our $j(O^1D)$ measurements, we perform the day-to-day comparison only for the $j(NO_2)$ values. At 13:00 LT, the Aug 18th and Aug 25th $j(NO_2)$ values were 0.34% and 1.21% higher, respectively, compared with the data on Aug 6th.

These results suggest a small enhancement in mid-day $j(NO_2)$. At 08:00 LT, BB aerosols decrease $j(NO_2)$ by 14.2% and 33.4% on Aug 18th and Aug 25th, respectively. Table 3.2 summarizes these numbers. We also plot $j(NO_2)$ versus solar zenith angle (SZA) (Figure 3.4b) instead of local time to normalize for SZA differences between the days. Because of no aerosols in the morning of Aug 18th (Figure 3.2), we show only afternoon data in Figure 3.4b. Similarly, because of clouds in the afternoon of Aug 25th (Figure 3.2), we show only morning data in Figure 3.4b. While $j(NO_2)$ shows lower values (reduction of 13.5% and 20.5% on Aug 18th and 25th, respectively) in the smoky days compared to the clean day at high SZA (70^{o}), the photolysis rates are slightly higher (enhancement of 1.84% and 0.18% on Aug 18th and 25th, respectively) at lower SZA (35^{o}).

We also investigate the behavior of actinic flux at UV wavelengths (Figure 3.5). We calculate the % difference in the actinic flux on the polluted days (Aug 18 and 25) with respect to the clean day (Aug 6), and find that at SZA = 70^{o} (Figure 3.5a), there is a 15-25% decrease in actinic flux in the shorter wavelengths (310-350 nm). Note that the total ozone column varies between the days affecting the actinic flux ratios below 340 nm. The reduction is stronger for heavier smoke (Aug 25th). We hypothesize that this reduction in actinic flux is due to excess extinction from BrC in the smoke. At mid-day (SZA = 35^{o}), the reduction in actinic flux is from 1-4% (Figure 3.5b), with the largest reductions at the smallest wavelengths. From 360-420 nm, there is an enhancement in actinic flux with respect to the non-smoky day, consistent with the higher calculated $j(NO_2)$ values at SZA = 35^{o} in Table 3.2. The relative uncertainty in the actinic flux observations is 0.10% for $j(NO_2)$. Thus, the changes in $j(NO_2)$ (greater at solar noon, lower at high SZA) are significant.

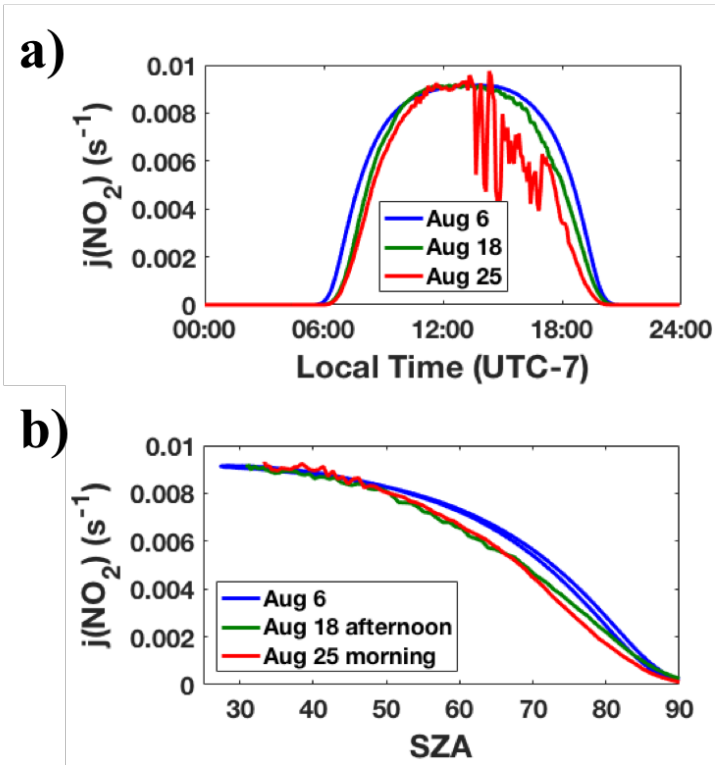

Figure 3.4. Comparison of DAFS-measured $j(NO_2)$ on clean (Aug 6th) and polluted days (Aug 18th and 25th) at MBO, versus (a) local time and (b) SZA. Because of no aerosols in the morning of Aug 18th, we show only the afternoon data in (b). Because of clouds in the afternoon of Aug 25th, we show only the morning data in (b).

Table 3.2. % change in photolysis rates during cloud-free and smoky days (Aug 18th and 25th) with respect to a smoke-free day (Aug 6th) at MBO, at 13:00 and 08:00 LT and for SZA = 35^{o} and 70^{o}.

	13:00 LT	08:00 LT
Aug 18th	0.34%	-14.2%
Aug 25th	1.21%	-33.4%
	SZA = 35^{o}	SZA = 70^{o}
Aug 18th	1.84%	-13.5% (afternoon only)
Aug 25th	0.18%	-20.5% (morning only)

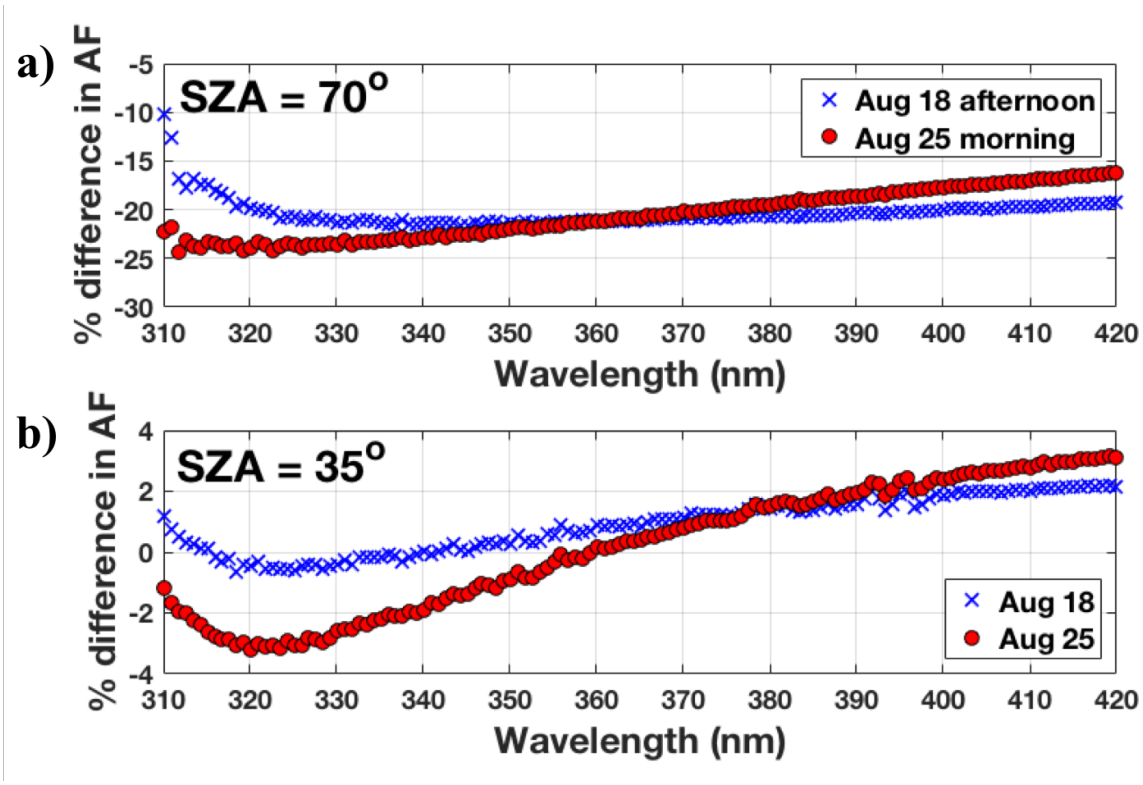

Figure 3.5. Change in actinic flux on Aug 18th and 25th with respect to Aug 6th at (a) SZA = 70° and (b) SZA = 35°. Positive values refer to greater actinic flux values on Aug 18th or 25th.

3.4.2 Measured and modeled photolysis rates

We then compare our measured photolysis rates to the modeled concentrations using TUV5.2. We use AOD at 550 nm from MODIS (0.15, 0.50, and 0.64 on Aug 6, 18, and 25, respectively) and O_3 column from OMI (327, 304, and 295 Dobson units, respectively) as inputs. The results are shown in Figure 3.6. Some of the differences on Aug 6 between the measurement and model may be attributed to uncertainties in angular response of the optical collector. Overall, results show that there is a fairly good level of agreement between DAFS-measured and TUV-modeled $j(NO_2)$.

We perform sensitivity runs as well by toggling between different SSA, O_3 column, and AOD values (Figure 3.7). Results show that $j(NO_2)$ is not sensitive to O_3 column input. Keeping SSA and AOD constant, increasing total ozone from 280 to 400 DU leads to only a 0.8% decrease in $j(NO_2)$. If SSA were increased from 0.8 to 1.0 (more absorbing to more scattering), $j(NO_2)$ increases by 11% (keeping AOD and O_3 column constant). Keeping SSA and O_3 column constant, $j(NO_2)$ shows a 30% increase as AOD is increased to 1. Moreover, $j(NO_2)$ is not sensitive to AOD for high SSA (highly scattering aerosols) but are both sensitive for low SSA (more loss due to absorption).

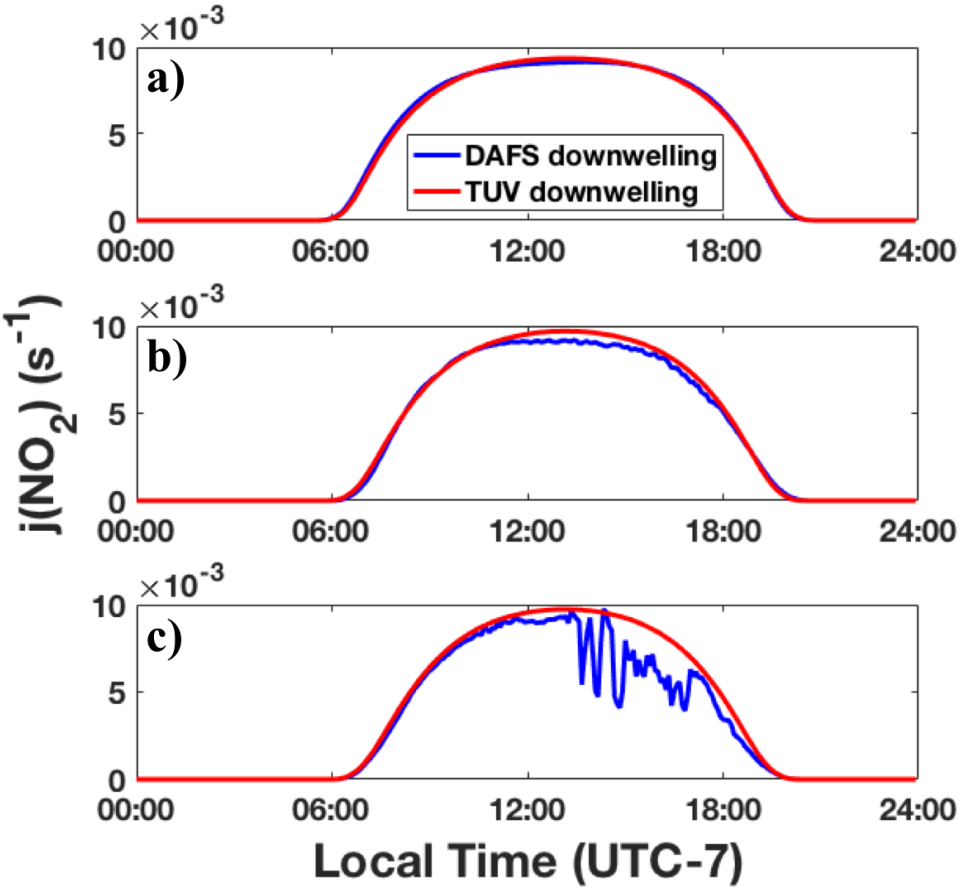

Figure 3.6. Comparison between measured (DAFS) and modeled (TUV5.2) downwelling $j(NO_2)$ on (a) clean (Aug 6th) and (b and c) polluted days (Aug 18th and 25th).

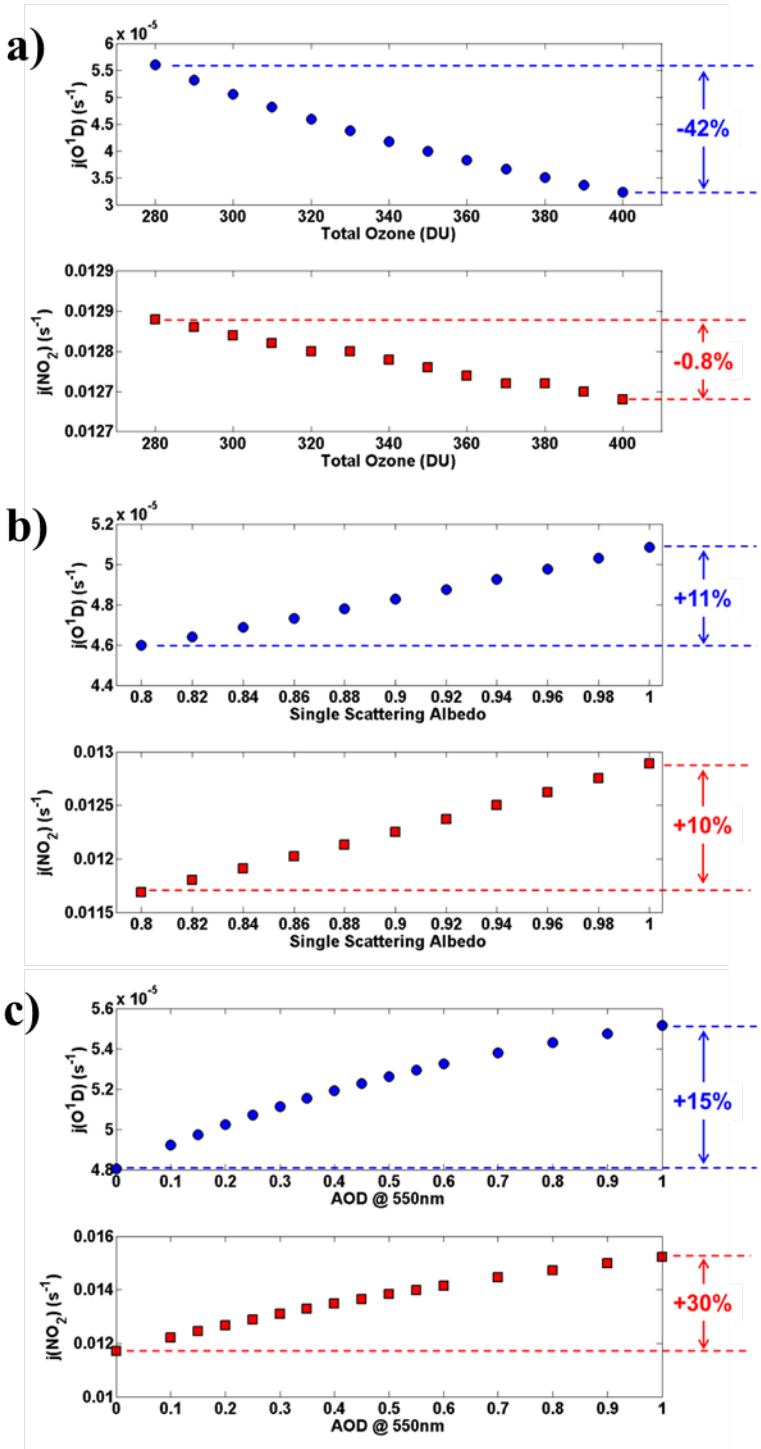

Figure 3.7. Sensitivity of $j(NO_2)$ and $j(O^1D)$ to (a) total ozone, (b) single scattering albedo (SSA), and (c) aerosol optical depth (AOD). For each variable not plotted, the base comparison holds. Total ozone, SSA, and AOD fixed at 300 DU, 0.99, and 0.235.

3.4.3 Estimating HO_2, RO_2, and $P(O_3)$ using the Extended Leighton relationship

Finally, we approximate the HO_2 and RO_2 concentrations using the extended Leighton relationship (Eq. 7). For RO_2, we consider both CH_3O_2 and $CH_2C(O)O_2$. Noontime (11:00–14:00 PST) average values of temperature, water vapor, ambient pressure, ozone, CO, aerosol scattering, NOx, and photolysis rates are summarized in Table 3.3. For the Leighton relationship, we consider the following reactions:

$$\boldsymbol{HO_2 + NO \rightarrow NO_2 + OH} \quad (10)$$

$$\boldsymbol{CH_3O_2 + NO \rightarrow CH_3O + NO_2} \quad (11)$$

$$\boldsymbol{CH_2C(O)O_2 + NO \rightarrow CH_3C(O)O + NO_2} \quad (12)$$

Rate constant (cm^3 $molecule^{-1}$ s^{-1}) is expressed by $k = A \exp(-E_a/RT)$, where A, the pre-exponential factor, is given in cm^3 $molecule^{-1}$ s^{-1}, and E_a/R (activation energy of the reaction divided by the gas constant) is given in degrees Kelvin (Brasseur, 1999). Table 3.4 summarizes the A factor and the E_a/R constant for reactions 10-12.

We calculate HO_2, CH_3O_2, and $CH_2C(O)O_2$ separately, assuming zero concentrations of the other components. We find that HO_2 and RO_2 concentrations were higher in the cleaner air versus the polluted air. This pattern is mostly driven by the higher NO/NO_2 ratios. This seems counterintuitive but is possible if the hydroxyl radical (OH) concentrations in the fire plume were lower than outside. OH is the primary oxidant in the troposphere (Seinfeld and Pandis, 1998) and reacts efficiently with CO and VOCs, which are much higher in the fire plumes. We also estimate the mid-day rate of O_3 production using Eq. (8) and find values of 2.37, 3.12, and 1.99 ppbv/hour on Aug 6^{th}, 18^{th}, and 25^{th}, respectively, consistent with other reported values in BB plumes (Cantrell et al., 1997; Griffin et al., 2007; Ridley et al., 1992; Shon et al., 2008).

Table 3.3. Local noontime (11:00–14:00) average values on Aug 6, 18, and 25 at MBO. HO_2, ROx, and $P(O_3)$ are estimated from the extended Leighton relationship. *CO data was unavailable on Aug 6; therefore, the local noontime median value for August 2015 is used. **Uncertainty: ±33%.

Local noontime average	Units	Aug 6	Aug 18	Aug 25
Temperature	^{O}C	12.3	18.6	13.3
Water vapor	g/kg	3.76	4.61	5.70
Pressure	mbar	735.4	738.4	736.3
Ozone	ppbv	44.1	58.2	50.2
CO	ppbv	194*	270	350
Scattering Coefficient	Mm^{-1}	3.33	112	145
NO	pptv	20.1	39.0	34.9
NO_2	pptv	95.4	162	115
NOx	pptv	116	201	150
NO/NO_2 ratio	unitless	0.21	0.24	0.32
$j(NO_2)$	s^{-1}	9.05E-03	9.09E-03	8.87E-03
$j(O^1D)$	s^{-1}	3.20E-05	3.18E-05	2.84E-05
HO_2**	pptv	299	174	109
CH_3O_2**	pptv	318	185	116
$CH_2C(O)O_2$**	pptv	134	79.0	49.0
$P(O_3)$	ppbv/hour	2.37	3.12	1.99

Table 3.4. A Factor and Ea/R constant for reactions 9-11 (values obtained from Brasseur, 1999).

Equation	A Factor cm^3 $molecule^{-1}$ s^{-1}	E_a/R
10	3.5 x 10^{-12}	-250
11	4.2 x 10^{-12}	-180
12	5.3 x 10^{-12}	-360

For comparison, we compiled Leighton relationship-derived (or photostationary state-derived, PSS) calculations and measurements of $HO_2 + RO_2$ from similar studies. Results are summarized in Table 3.5. Our estimates of HO_2 and RO_2 (49-185 pptv) are in the same order of

magnitude as these studies, although the PSS-derived values tend to be higher than observed values. This points out that our understanding of these photochemical processes remains incomplete.

Table 3.5. Photostationary state-derived (PSS-derived) and measured HO_2 + RO_2 concentrations from field campaigns.

Field campaign	Location	PSS-derived HO_2 and RO_2 (pptv)	Measured HO_2+RO_2 (pptv)
MLOPEX	Mauna Loa	60	-
MLOPEX 2	Mauna Loa	100	25
Trop OH Expt	UNH	66	33
ICARTT	Boulder	50-200	30
MIRAGE-Mex	Mexico City	220	217 (BB)
			131 (BL)
			88 (FT continental)
This study	MBO	49-185	-

3.5 SUMMARY

We looked at wildfire events that we observed at the Mt. Bachelor Observatory (MBO) during summer 2015, a huge fire season in the Pacific Northwest. These smoke events were generally associated with ozone enhancements at MBO. The photochemical environment in biomass burning (BB) plumes remains poorly understood, and our study aims to fill this knowledge gap.

We are interested in understanding the effect of aerosols only on photolysis rates (as opposed to the combined effect of aerosols and clouds). To do this, we carefully selected cloud-

free days (one clean and two smoky days) and investigated the photochemistry in these plumes. We note that $j(NO_2)$ has a broader profile than $j(O^1D)$ because the dissociation spectra for NO_2 reaches to longer wavelengths. At local noontime (SZA fixed to 35^o), $j(NO_2)$ values were slightly higher (0.2-1.8%) in the smoky days compared to the clean day. At higher SZA (70^o), BB aerosols decrease $j(NO_2)$ at much larger magnitudes (14-21% decrease). We also observe a 15-25% decrease in actinic flux at UV wavelengths, presumably due to BrC absorption. We compare our measurements with results from the TUV5.2 model and find a good agreement during cloud-free conditions. We also perform sensitivity runs and find that $j(NO_2)$ is only weakly sensitive to O_3 column input. If we keep single scattering albedo (SSA) and aerosol optical depth (AOD) constant, an increase in the total ozone from 280 to 400 DU leads to only a 0.8% decrease in $j(NO_2)$. Thus, the observed changes in $j(NO_2)$ were not driven by changes in the ozone column. $j(NO_2)$ is less sensitive to AOD for high SSA (highly scattering aerosols) but more sensitive to AOD for low SSA (more loss due to absorption). Hence the strong reductions in $j(NO_2)$ at high SZA. The noontime values may be enhanced by scattering.

Finally, we used the extended Leighton relationship to estimate HO_2 and RO_2 concentrations and $P(O_3)$ in the fire plumes. We calculate lower HO_2 and RO_2 values in the fire plumes, from 49-185 pptv which is in the same range as other studies. This is likely due to enhanced CO and VOCs acting as a sink for HO_2 and RO_2 radicals. We also compute ozone production rates of 2.0-3.1 ppbv/hour. Future work can examine these plumes using a detailed chemical model to shed more light on the complex photochemistry in biomass burning plumes.

CHAPTER 4

INFLUENCE OF LONG-RANGE TRANSPORT OF SIBERIAN BIOMASS BURNING AT THE MT. BACHELOR OBSERVATORY DURING THE SPRING OF 2015

(adapted from Baylon et al., submitted to Aerosol and Air Quality Research)

4.1 INTRODUCTION

Biomass burning (BB) is a significant source of trace gases (ie, CO, NOx, VOCs) and particulate matter (PM) in the atmosphere (Andreae, 1991; Andreae and Merlet, 2001; Crutzen and Andreae, 1990; Martins et al., 2012; Real et al., 2007). These emissions lead to the formation of secondary pollutants with consequences ranging from local to global in scale. One of these secondary pollutants is ozone, which forms in the troposphere from the interaction of nitrogen oxides (NOx = NO + NO_2) and volatile organic compounds (VOCs) in the presence of sunlight (Finlayson-Pitts and Pitts, 2000). Ozone is a health hazard to sensitive individuals (Bell et al., 2006), is the third strongest anthropogenic greenhouse gas (Henderson et al., 2012), and is the main source of hydroxyl radicals that drive the oxidizing capacity of the atmosphere (Monks et al., 2009; Seinfeld and Pandis, 1998). Moreover, it damages food crops, forests, and other ecosystems (Fiscus et al., 2005).

The rate of ozone formation in wildfire plumes is complicated by various factors (Akagi et al., 2011). While Jaffe and Wigder (2012) broadly showed in their review paper that the $\Delta O_3/\Delta CO$ enhancement ratio, which was used as a measure of ozone production, generally increases with plume age, they note that there is a lot of variability. Uncertainties such as fire emissions, combustion efficiency, meteorological patterns, chemical and photochemical

reactions, aerosol effects on chemistry, and solar radiation complicate quantifying ozone production from wildfires. More studies are needed to investigate the impact of fires on downwind air quality for long-range transport (LRT) events.

It is well established that Asian long-range transport (ALRT) episodes, which can be natural (i.e., biomass burning) or anthropogenic (i.e., fossil fuel burning, biofuel burning, human-caused fires), contain trace gases and particulates such as ozone, CO, NOx, VOCs, and dust that can be transported across the Pacific under certain meteorological conditions (Jaffe et al., 1999; Liang et al., 2004; Teakles et al., 2017). Siberian BB events during the summer of 2003 resulted in ozone and CO enhancements from the background of 5-9 ppbv and 23-37 ppbv, respectively, at 10 surface stations in Alaska, Canada and the Pacific Northwest, contributing to exceedances in the national air quality standards (Jaffe et al., 2004). In another large event, ozone and CO exceeded 100 ppbv and 220 ppbv, respectively (Bertschi and Jaffe, 2005). Similarly, the Siberian fires in July 2012 resulted in trans-Pacific transport of a large smoke plume which affected air quality in British Columbia and Washington State (Teakles et al., 2017). Ozone and $PM_{2.5}$ enhancements of 34-44 ppbv and 10-32 $\mu g/m^3$, respectively, were observed. Smaller ozone and $PM_{2.5}$ enhancements of 10 ppbv and 4-9 $\mu g/m^3$ were observed at sites with stable atmospheric conditions, leading to stagnant conditions which limited the entrainment of the fire plume into the BL (Teakles et al., 2017). $\Delta O_3/\Delta CO$ enhancement ratios for the Siberian 2012 BB events observed at Whistler high-elevation site had a mean value of 0.26 ppbv/ppbv, comparable to other similarly aged Siberian wildfire plumes with ratios of 0.22–0.36 ppbv/ppbv (Bertschi et al., 2005) and 0.15–0.84 ppbv/ppbv (Bertschi and Jaffe, 2005).

These studies suggest that long-range transport of Siberian BB emissions has far-reaching impacts on surface air quality downwind. However, air quality impacts can vary with downwind

meteorology and entrainment pathways. Smaller ozone and PM enhancements at the surface are associated with stable atmospheric conditions and BL transport. On the other hand, higher enhancements are linked to FT transport, strong source, and favorable transport.

The Mt. Bachelor Observatory (MBO; 2.8 km a.s.l.) is a mountaintop site established by the University of Washington Atmospheric Chemistry group in 2004 (Jaffe et al., 2005). Data from MBO has been extensively used to study the LRT of natural and anthropogenic pollution from Siberia and Asia to North America. Year-to-year variability of ALRT events observed at MBO can be traced to variability in both emission source and transport (Reidmiller et al., 2009).

In this paper, we examine an episodic LRT of Siberian wildfire smoke to the western U.S. on April 2015. We use free tropospheric (FT) data from MBO and from the NOAA WP-3D research aircraft during the Shale Oil and Natural Gas Nexus (SONGNEX) campaign, as one of these flights intercepted the Siberian plume. We also look at boundary (BL) sites in the western U.S. We are interested in answering the following questions:

- Were the MBO and aircraft observations consistent with respect to the enhancement ratios?
- What caused the relatively high $\Delta O_3/\Delta CO$ and $\Delta\sigma_{sp}/\Delta CO$ ratios for the Siberian 2015 fires?
- Was there O_3 production and if so, was this O_3 mixed into the boundary layer? Was there entrainment from the upper troposphere/lower stratosphere (UT/LS)?
- How does the reactive nitrogen speciation of the plume relate to O_3 production and $\Delta NOy/\Delta CO$?

4.2 METHODS

Mt. Bachelor Observatory (MBO) is a mountaintop site established in 2004 (Jaffe et al., 2005). It is located on the summit of Mt. Bachelor in the Cascades Mountains of central Oregon. Mt. Bachelor is located in the Deschutes National Forest and is home to a ski resort. Measurements of σ_{sp} (TSI Model 3563), O_3 (Dasibi 1008 RS) and CO (May 2012 onwards: Picarro G2302), along with measurements of basic meteorology, such as temperature, humidity and wind speed, have been on-going at MBO since 2004 (see Ambrose et al., 2011 and Gratz et al., 2014 and references therein for details on σ_{sp}, O_3 and CO instrumentation).

We also used measurements from the NOAA WP-3D Orion research aircraft during the Shale Oil and Natural Gas Nexus (SONGNEX) campaign in Spring 2015. The mission of SONGNEX was to quantify atmospheric emissions from various U.S. energy infrastructures and to study how these emissions transform chemically in the atmosphere and how they contribute to ozone and PM formation (https://esrl.noaa.gov/csd/projects/songnex/). The NOAA WP-3D aircraft was based in Broomfield, CO, and Austin, TX. Twenty research flights were conducted between March 19 and April 27, 2015 over oil and gas production regions in the western U.S. The aircraft was equipped with an extensive set of gas-phase measurements, including instruments for methane, CO, canister samples for VOCs, NOx, NOy, PAN, and ozone (Lerner et al., 2017). One of the SONGNEX flights sampled the Siberian plume. This gives us an opportunity to study a similar, possibly the same, plume at both MBO and via the aircraft.

Observations of O_3 in Boise City, ID (AQS ID: 16-001-0010); Idaho Falls, ID (16-023-0101); and Portland, OR (41-067-0005) were obtained from the U.S. EPA AirData archive (www.epa.gov/airdata). Figure 4.1 shows a map of the surface sites and the aircraft flight track.

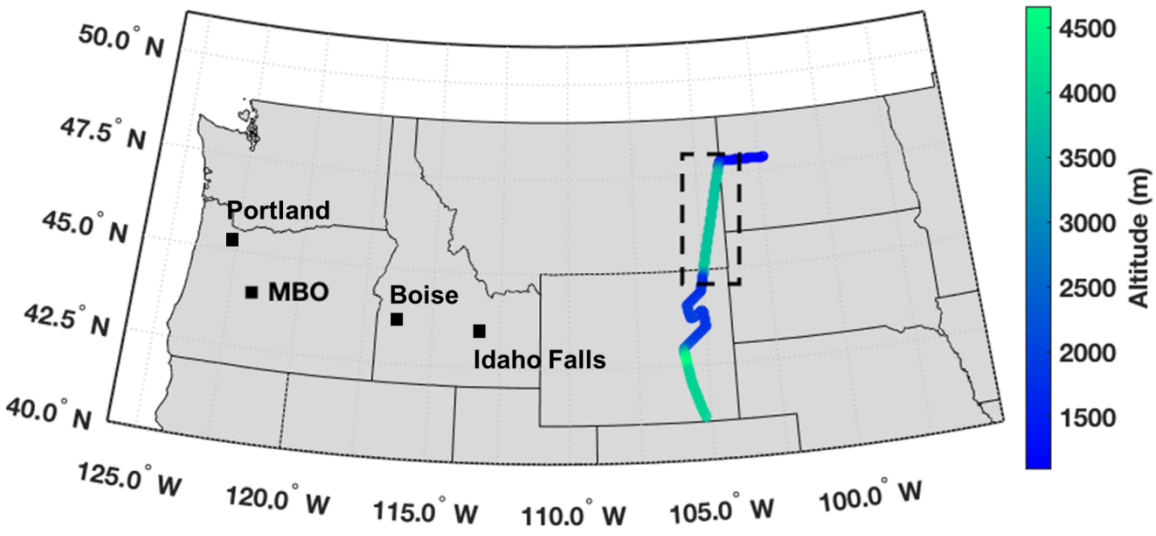

Figure 4.1. Location of air quality sites used in this study and track of SONGNEX Flight 20150421. Only four stations in Oregon and Idaho have MDA8 O_3 data on April 2015.

We also used Lidar data from CALIPSO to examine plume height (https://www-calipso.larc.nasa.gov). We ran the HYSPLIT (Hybrid Single Particle Lagrangian Integrated Trajectory Model) backtrajectories and forward dispersion to identify the transport time and mechanisms (http://ready.arl.noaa.gov/HYSPLIT.php). We also used the Navy Aerosol Analysis and Prediction System (NAAPS) Global Aerosol Model (https://www.nrlmry.navy.mil/aerosol/) to look at the forecast total optical depth and smoke surface concentrations.

4.3 DATA AND RESULTS

4.3.1 Siberian 2015 smoke event overview

In April 2015, huge agricultural fires burned in the steppes of southern Russia. These fires are routinely set to fertilize the soil for the coming year, but abnormally warm temperatures and strong winds in April 2015 led to devastating fires that burned several villages and killed dozens of people. Figure 4.2 shows a true-color image of the Zabaikalsky Territory on April 14, 2015 from the Moderate Resolution Imaging Spectroradiometer (MODIS) aboard NASA's Terra satellite (NASA image courtesy of Jeff Schmaltz). Burning sources are outlined in red. Smoky air is evident throughout the region. Typically, these fires remain in the boundary layer (BL). However, because of unusually warm temperatures and a baroclinic cyclone that developed near Chita, Russia, they were lofted high up into the upper troposphere where strong upper-level winds dispersed them widely. Figure 4.3 shows shows both a MODIS infrared (IR) image from NASA's Aqua satellite (top) and a Lidar image from the Cloud-Aerosol Lidar with Orthogonal Polarization (CALIOP) instrument on the CALIPSO satellite (bottom) (NASA Earth Observatory image by Jesse Allen, using expediated data provided by the CALIPSO team). Both were taken overnight on April 15, 2015. The Lidar image in the bottom shows the vertical profile for the red line in the top figure which represents the north-south flight of the CALIPSO satellite (overpass at the Sea of Okhotsk). CALIOP detected smoke between 4–10 kilometers (2–6 miles). This height indicates that the smoke plumes were injected relatively high in the atmosphere.

It is well-established that Asian dust can be transported across the Pacific during springtime (Fischer et al., 2010; Jaffe et al., 2003). Therefore, it is possible that the Siberian BB plume is mixed with dust.

After the Siberian smoke was lofted high in the atmosphere, strong upper-level winds carried it over the Sea of Okhotsk and eventually across the Pacific Ocean. Figure 4.4 shows a true-color MODIS image of the smoke moving across the Pacific into the west coast of North America on April 18, 2015 (NASA image courtesy of Jeff Schmaltz).

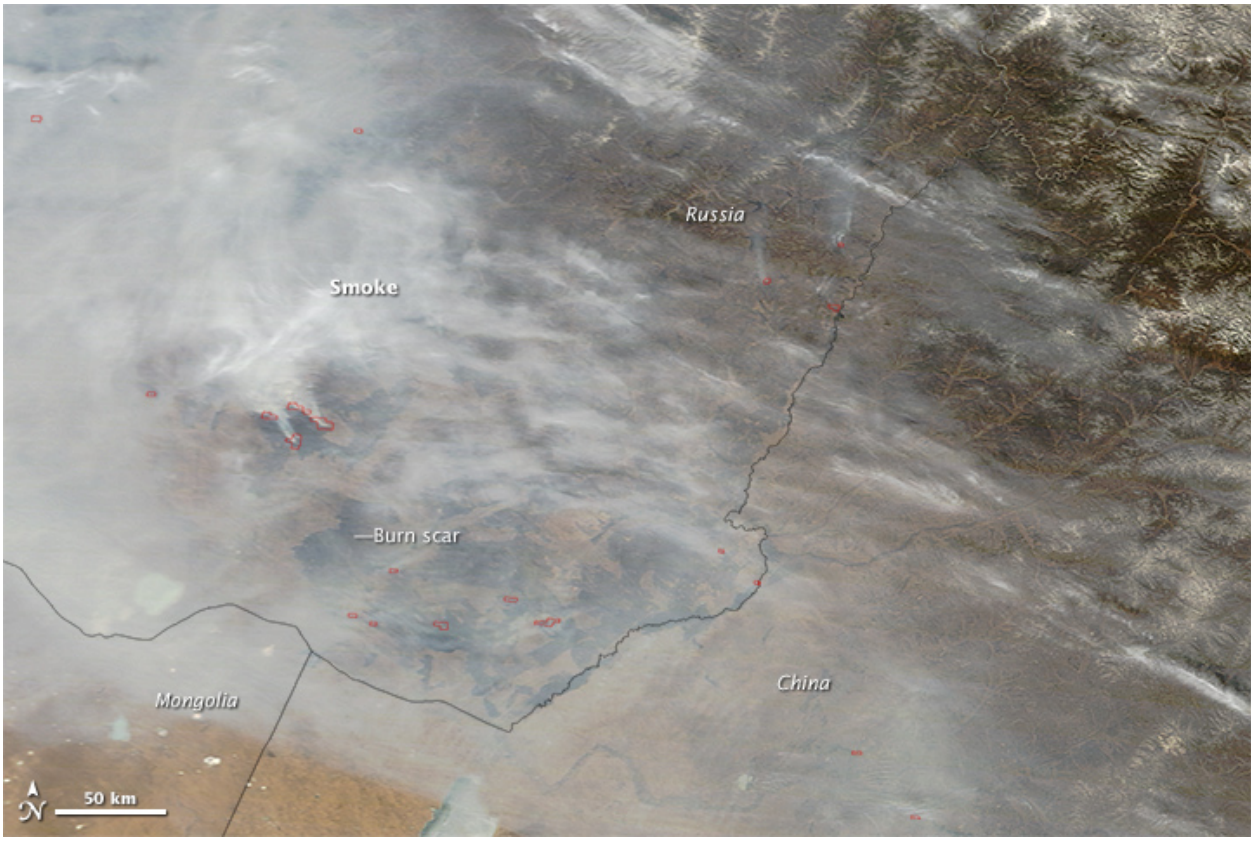

Figure 4.2. True-color image of the Zabaikalsky Territory obtained from MODIS aboard NASA's Terra satellite on April 14, 2015, 10:30 local time (NASA image courtesy of Jeff Schmaltz).

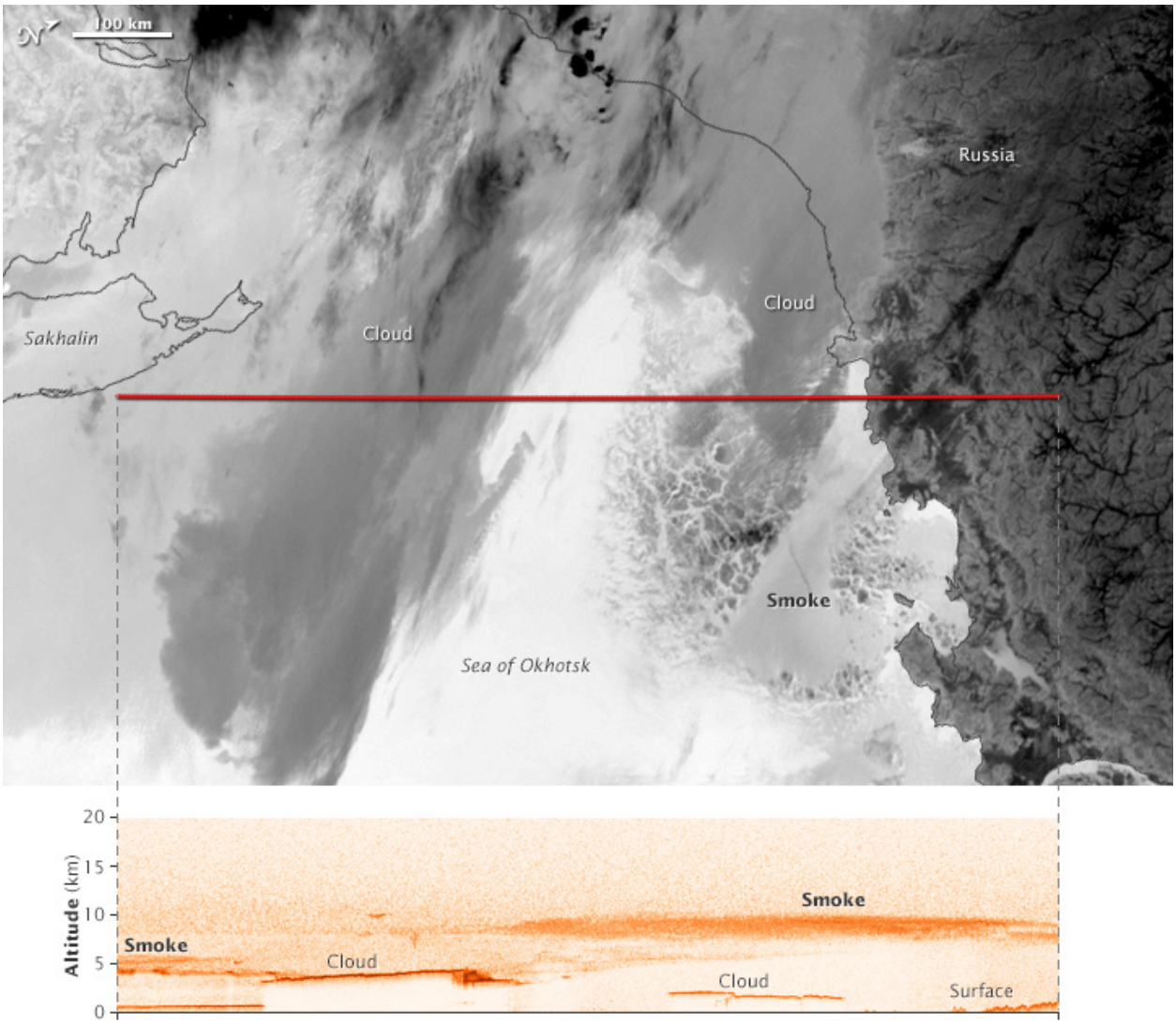

Figure 4.3. Aqua MODIS IR image (top) and Lidar retrieval from the CALIOP instrument aboard the CALIPSO satellite (bottom) overnight on April 15, 2015 (NASA Earth Observatory image by Jesse Allen, using data provided by the CALIPSO team).

Figure 4.5 shows Aqua MODIS images over the Pacific Northwest from April 17-19, 2015. Figure 4.6 shows the Lidar image from CALIPSO on April 19, 2015. At this time, Siberian fires are observed at an elevation of 4-8 kilometers, consistent with the initial observed heights at the source described in Figure 4.3.

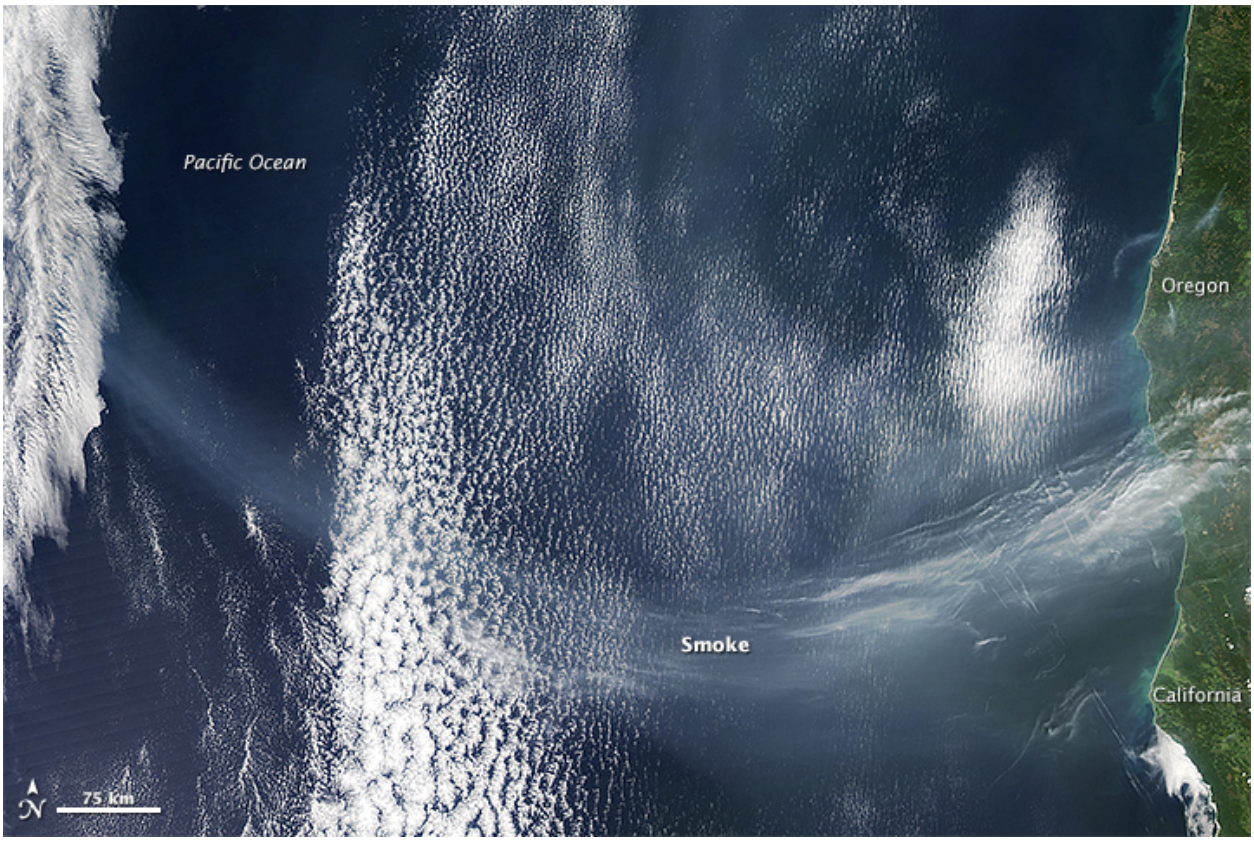

Figure 4.4. Aqua MODIS image of the Siberian smoke moving across the Pacific on April 18, 2015 (NASA image courtesy of Jeff Schmaltz).

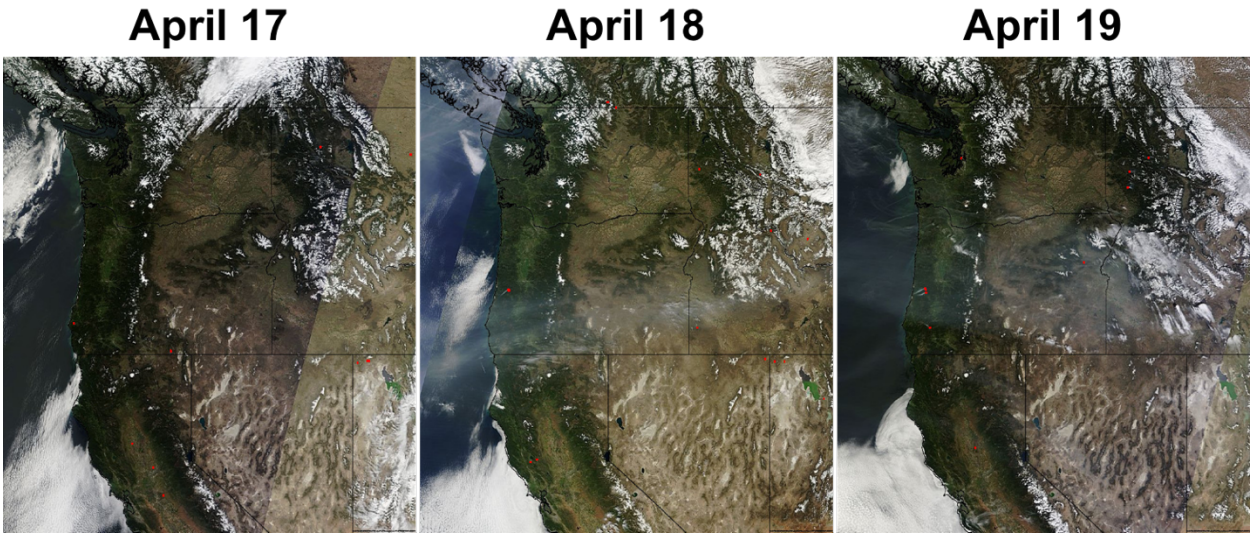

Figure 4.5. True-color Terra MODIS images of the Pacific Northwest from April 17-19, 2015, 10:30 local time.

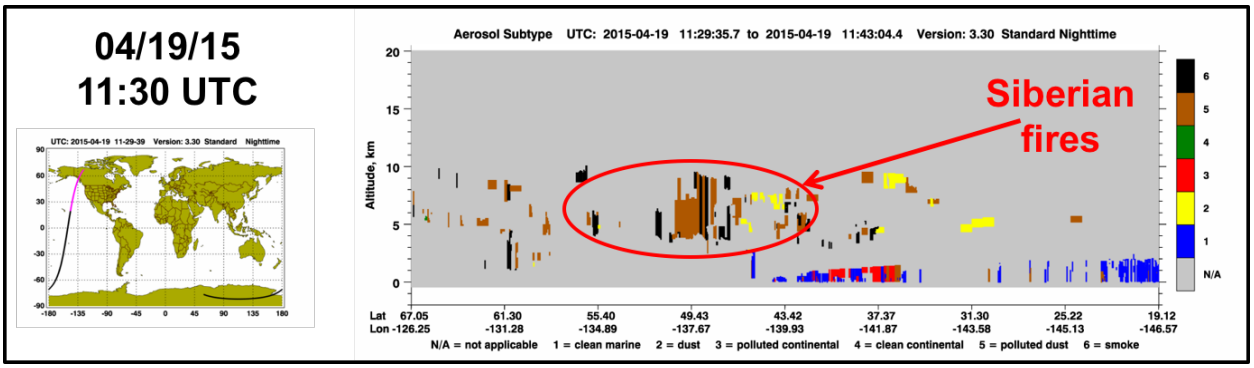

Figure 4.6. Lidar retrieval over NE Pacific obtained from CALIPSO on April 19, 2015.

4.3.2 Siberian plume observations in the FT at MBO

At MBO, we observed hourly aerosol scattering (550 nm) values of ~130 Mm^{-1} (PM_1 ~ 43 $\mu g/m^3$) and hourly ozone of ~85 ppbv on April 21, 2015 (Figure 4.7). Water vapor during these PM and O_3 peaks was ~0.9 g/kg, which is characteristic of dry FT air. Figure 4.8 shows plots of hourly ozone, water vapor, CO, and aerosol scattering (σ_{sp} at 550 nm) observed at MBO for the entire month of April 2015. The period from April 20-21 stands out because of the high ozone, CO, and σ_{sp} and low water vapor observed at MBO.

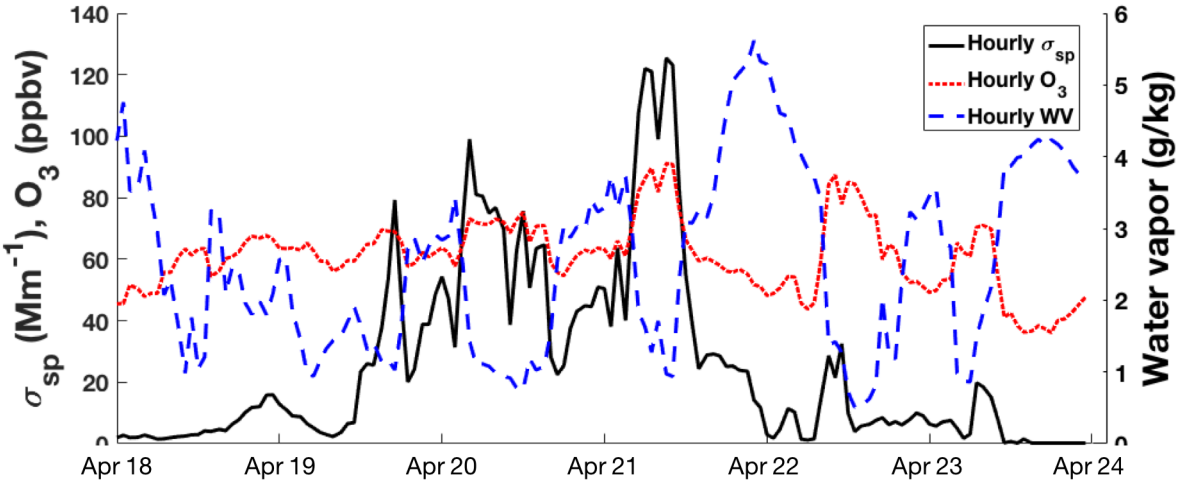

Figure 4.7. Time series of hourly σ_{sp}, O_3, and water vapor at MBO.

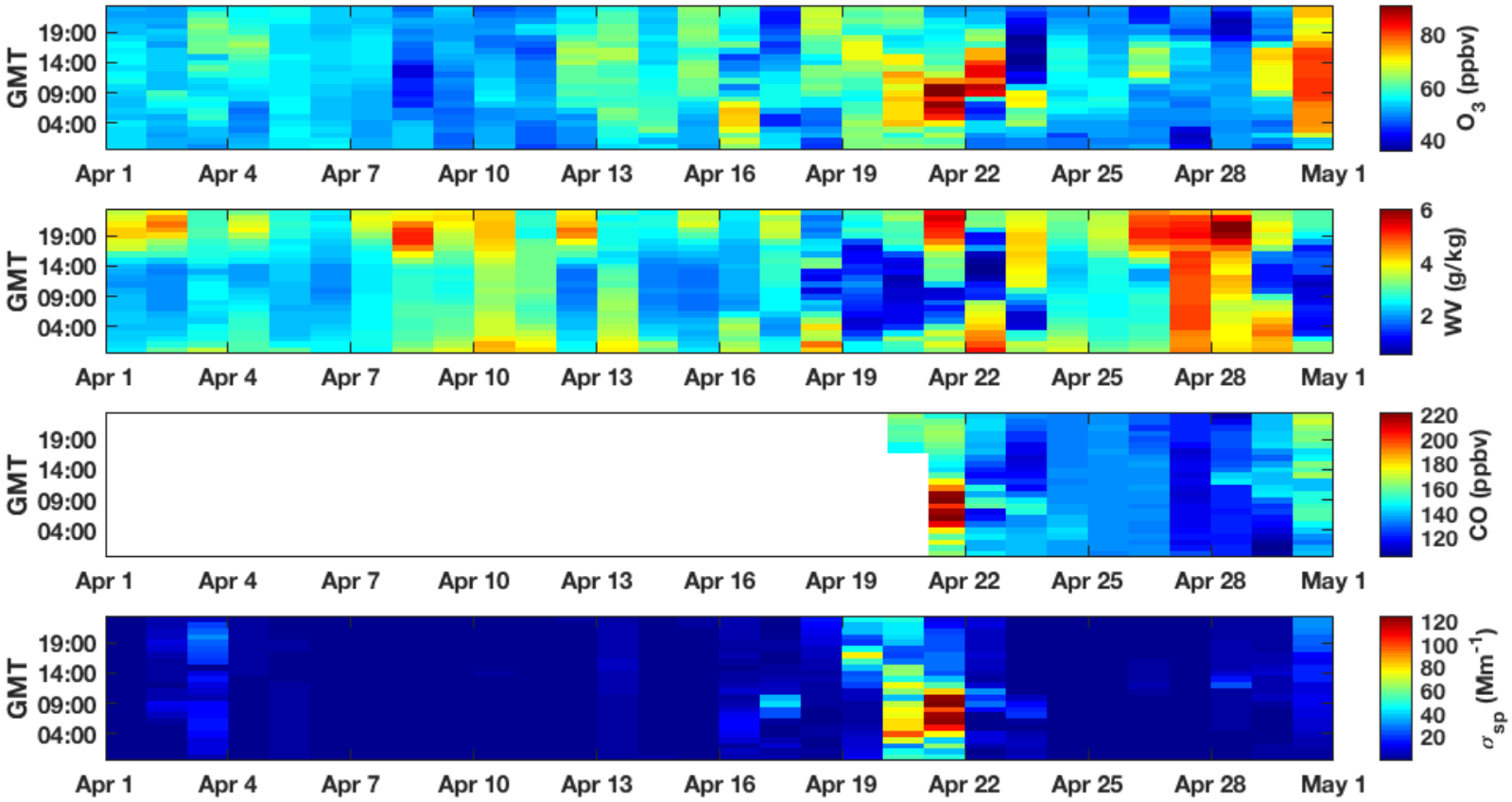

Figure 4.8. Plots of hourly O_3, water vapor, CO, and σ_{sp} observed at MBO on April 2015.

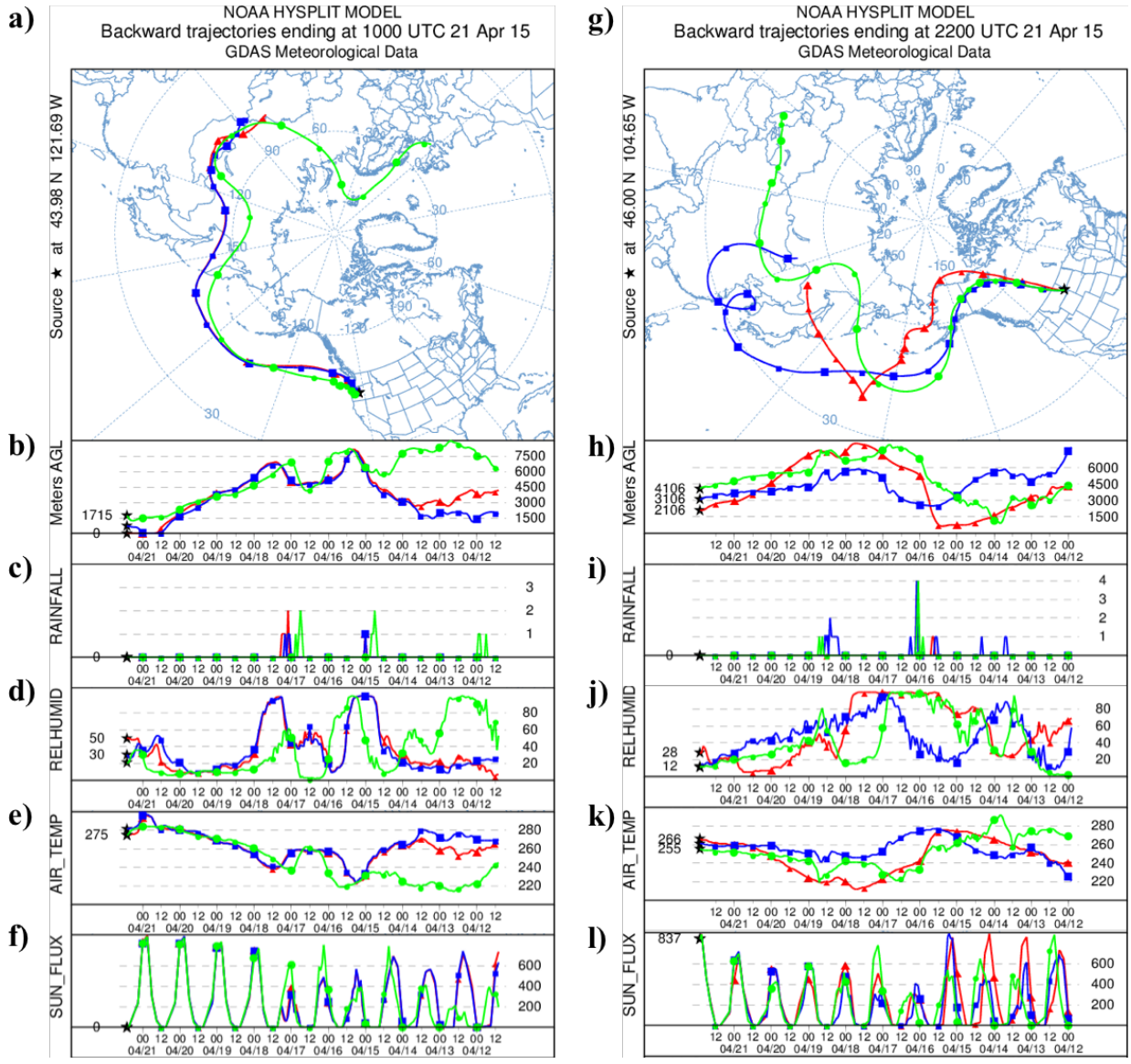

Figure 4.9. Ten-day HYSPLIT backtrajectories initiated (a-f) at MBO and (g-l) at the location of the aircraft. Also plotted are the rainfall (in mm/hr), relative humidity (%), air temperature (in K), and downward solar radiation (in W/m^2) values from the meteorological fields used for the trajectories

To verify the influence of Siberian smoke on our MBO observations, we perform a 10-day HYSPLIT backtrajectory (Fig. 4.9(a-f)). Results confirm that the pollution episode came from Siberia and that the plume stayed in the FT for the most part during its transport. Wet deposition was minimal as indicated by the negligible rainfall (Fig. 4.9(c)). Relative humidity was also low during transport (Fig. 4.9(d)). We now look at the observations from the NOAA WP-3D aircraft.

4.3.3 Siberian plume observations in the FT on the NOAA WP-3D research aircraft

One of the flights during the SONGNEX field campaign in 2015 intercepted the Siberian plume on April 21. Fig. 4.1 shows the location of the flight track with respect to the location of MBO. Fig. 4.10(a-b) shows a time series of the aircraft data. We divide the aircraft time series into three (AC plumes 1, 2, and 3) because the ozone-CO plots for these three plumes appear distinct from each other (discussed later on Fig. 4.13(a)). From 22:30–22:39 UTC (Fig. 4.10(c)), the aircraft intercepted a plume (AC plume 1) with elevated CO, σ_{sp}, and O_3 levels. From 22:39–22:42 UTC (Fig. 4.10(d)), a similar plume (AC plume 2) with higher O_3 levels was observed. However, from 22:42–22:52 UTC (Fig. 4.10(e)), the aircraft intercepted a plume that was rich in ozone but relatively lower in CO (AC plume 3).

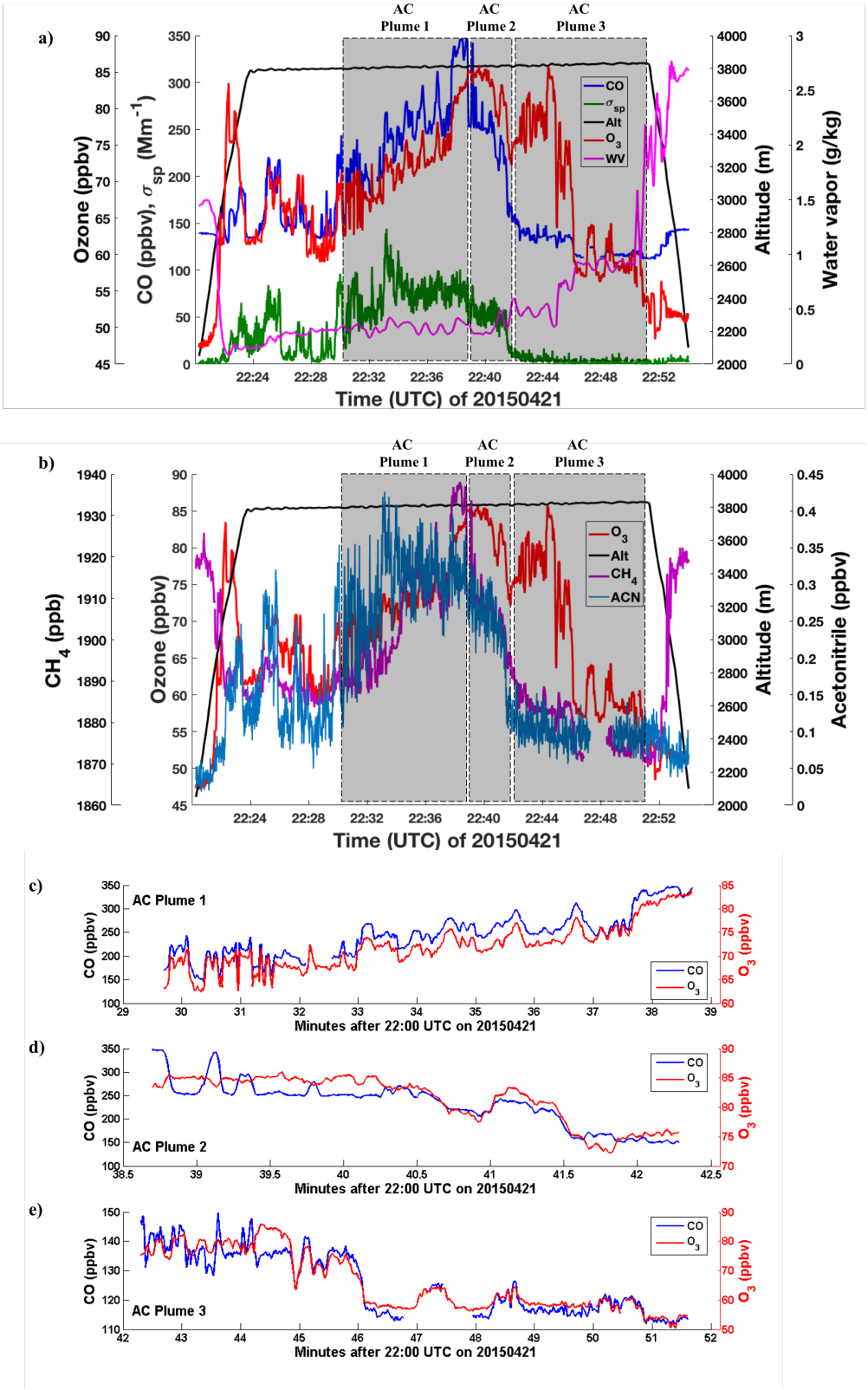

Figure 4.10. Aircraft data during the April 21st flight of SONGNEX.

Hourly CO and ozone at MBO on April 21 09:00 UTC were 223 ppbv and 91.1 ppbv, respectively. On the other hand, instantaneous CO and ozone measurements from the aircraft on April 21 during the plume intercept (~22:28-22:40 UTC) ranged from 200-300 ppbv and 70-85 ppbv, respectively. The CO observed by the aircraft is comparable to the measurements at MBO. However, the ozone observed by the aircraft is lower than that observed in MBO. The MBO and aircraft observations are 13 hours apart. We perform HYSPLIT forward dispersion runs initiated at MBO (April 21 09:00 UTC) and observe that it takes ~70 hours for a plume to be transported from MBO to the location of the aircraft. Fig. 4.11 shows the time-of-arrival plot. Given that the MBO and the SONGNEX aircraft observed this plume only 13 hours apart, this indicates that the Siberian plume observed at MBO on 09:00 UTC was not the same plume intercepted by the aircraft at ~22:28 UTC, but was of similar Siberian origin.

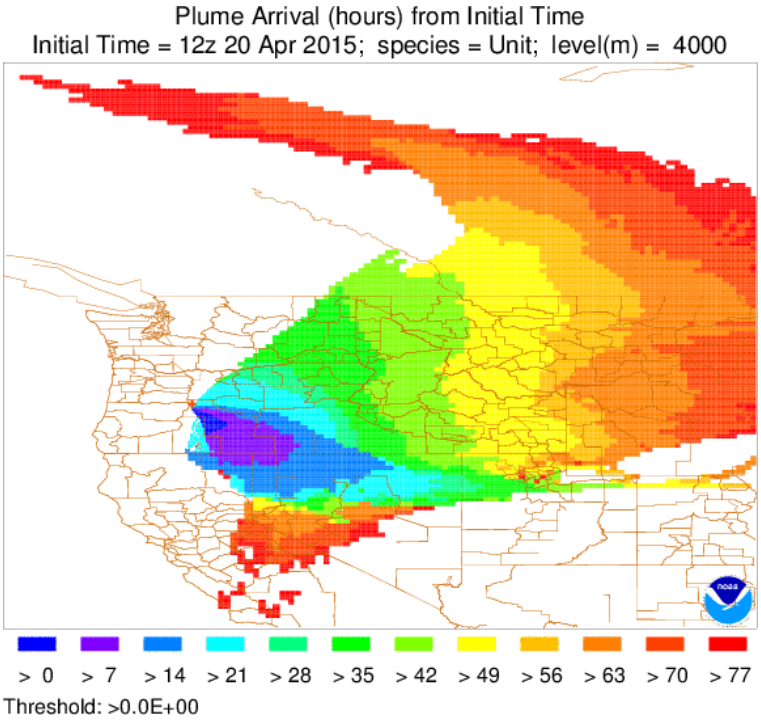

Figure 4.11. Time-of-arrival plot for a plume initiated at MBO on April 21 09:00 UTC. This shows that an air mass at MBO would take at least 70 hours to reach the SONGNEX aircraft.

To identify the origin of the plume intercepted by the aircraft, we look at the Global Aerosol Model from the Navy Aerosol Analysis and Prediction System (NAAPS) (Fig. 4.12 and Appendix D) and HYSPLIT backtrajectories (Fig. 4.9(g-l)). We find that as the Siberian plume crossed the eastern Pacific, it splits: one plume moves eastward and the other moves over Alaska and down to the U.S. mid-West (Fig. 4.12). MBO observed the former while the aircraft intercepted the latter. Both plumes are Siberian in origin but were transported through different pathways. Fig. 4.9 (g-l) show HYSPLIT backtrajectories initiated at the location of the aircraft. Compared to the backtrajectories initiated at MBO (Fig. 4.9(a-f)), the backtrajectories corresponding to the aircraft data suggest that the plume encountered more hours in rainfall (Fig. 4.9(i)) and higher relative humidity (Fig. 4.9(j)). This could lead to aerosol deposition, which could explain why the aircraft observed lower $\Delta\sigma_{sp}/\Delta CO$ ratios than at MBO (Table 4.1).

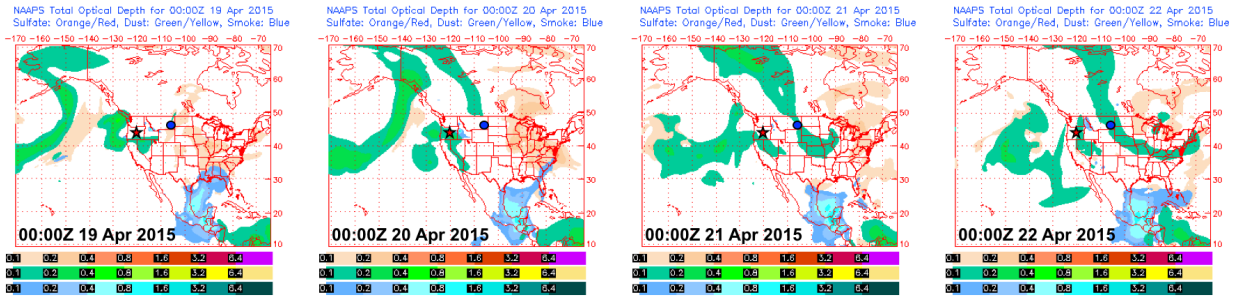

Figure 4.12. AOD forecast from the Global Aerosol Model of the Navy Aerosol Analysis and Prediction System (NAAPS). The location of MBO and the NOAA WP-3D aircraft are represented by the red star and blue circle, respectively.

4.3.4 Enhancement ratios for the Siberian plume

We now look at scatter plots of O_3, σ_{sp}, and NOy with respect to CO for both MBO and aircraft data (Fig. 4.13). From the scatter plots, we can calculate the enhancement ratio by taking

the slope of a Reduced Major Axis (RMA) linear regression. These enhancement ratios, along with results from similarly aged Siberian plumes observed in North America, are summarized in Table 4.1. Bertschi et al. (2004) reported plume heights from 1–4 km whereas Teakles et al. (2017) reported heights from 2–3.6 km. The Siberian 2015 fires were transported at higher elevations (4–10 km). Note that NOy was not measured at MBO during Spring 2015. Because CO data at MBO was available only on April 21, we calculate these ratios at MBO for this day only. All three parameters are well-correlated. $\Delta O_3/\Delta CO$ is 0.455 ppbv/ppbv ($R^2 = 0.90$) and $\Delta\sigma_{sp}/\Delta CO$ enhancement ratio is 1.83 Mm^{-1}/ppbv ($R^2 = 0.92$) at MBO.

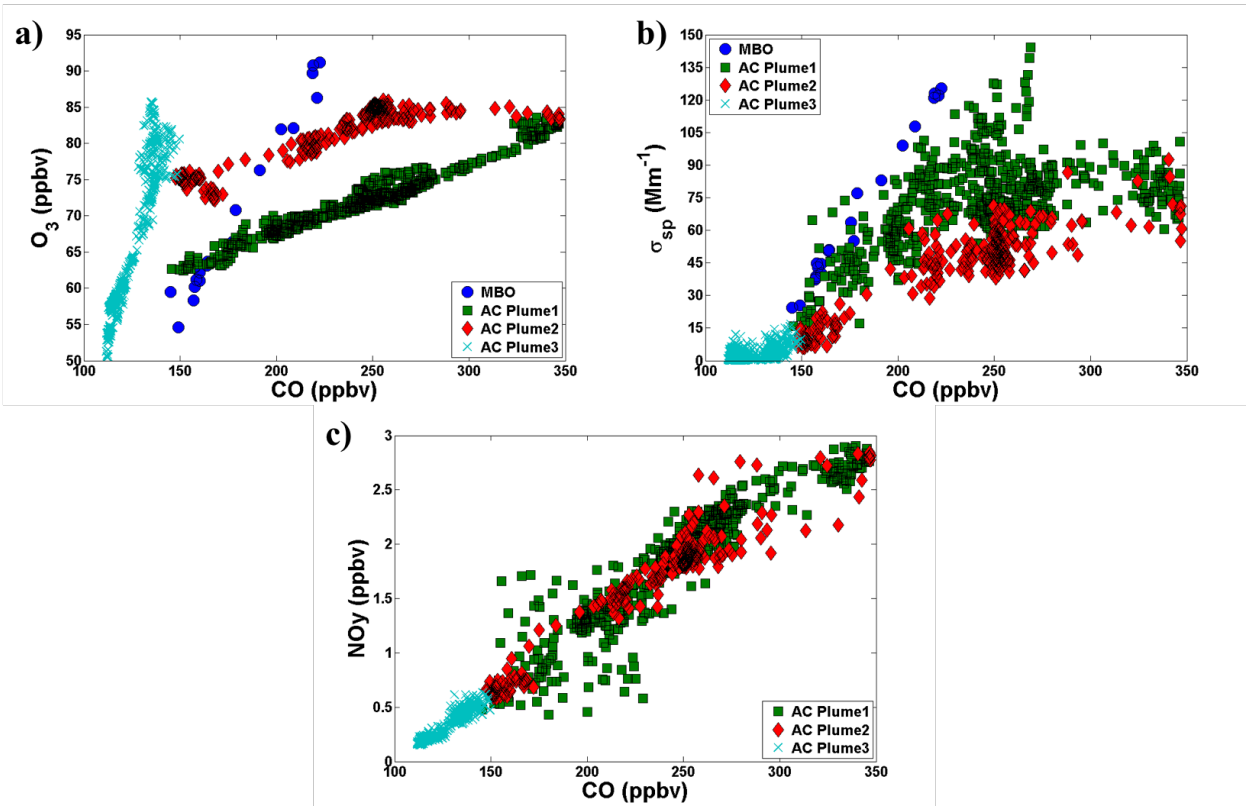

Fig. 4.13. Scatter plots of (a) O_3, (b) σ_{sp}, and (c) NOy with respect to CO for both aircraft and MBO data.

Table 4.1. $\Delta O_3/\Delta CO$, $\Delta\sigma_{sp}/\Delta CO$, and $\Delta NOy/\Delta CO$ ratios for similarly aged Siberian plumes observed in North America, and for the Siberian 2015 plume observed at MBO and on the NOAA WP-3D aircraft (AC) during the SONGNEX campaign.

	Reference	$\Delta O_3/\Delta CO$ (ppbv/ppbv)	$\Delta\sigma_{sp}/\Delta CO$ (Mm^{-1}/ppbv)	$\Delta NOy/\Delta CO$ (ppbv/ppbv)
Spring 2002	Bertschi et al. (2004)	0.22–0.42	0.27–0.88	
Summer 2003	Jaffe et al. (2004)	0.14–0.39		
Summer 2012	Teakles et al. (2017)	0.26	0.24	
Spring 2015 (This study)	MBO	0.46	1.83	
	AC Plume 1	0.10	0.67	0.0124
	AC Plume 2	0.084	0.63	0.0119
	AC Plume 3	0.97	0.48	0.0123

The aircraft intercepted plumes with three distinct O_3-CO profiles. The first two plumes (AC plumes 1 and 2) had $\Delta O_3/\Delta CO$ enhancement ratios of 0.10 and 0.084 ppbv/ppbv which are lower than, but within the bounds of, the values from other studies (Table 4.1). During the latter part of the plume crossing (AC plume 3), the aircraft intercepted an ozone-rich airmass that had lower CO levels (Fig. 10a), but still with a strong, positive O_3-CO correlation, with an $\Delta O_3/\Delta CO$ enhancement ratio of 0.97 ppbv/ppbv, much higher than AC plumes 1 and 2. This high value is mostly driven by the lower CO enhancement. We hypothesize that AC plume 3 could be mixed with non-BB air (low acetonitrile values in Fig. 10b; acetonitrile is a BB tracer), probably from a

local pollution source as evidenced by the increasing water vapor during the plume crossing (Fig. 4.10a). UT/LS air is not likely a dominant factor as this type of air is typically associated with negatively correlated O_3 and CO profiles (Ambrose et al., 2011). Fig. 4.10e shows that O_3 and CO are well-correlated for AC plume 3. However, the methane concentrations for AC plume 3 are low, which could suggest some UT/LS influence. Overall, it appears that AC plume 3 is likely a mix of sources.

The $\Delta O_3/\Delta CO$ ratio at MBO is higher than AC plumes 1 and 2 and this could be explained by more subsidence in the Siberian plume arriving at MBO (Fig. 4.9b) and less subsidence for the aircraft observations (Fig. 4.9h). The plume was warmer at MBO (275 K). At this temperature, PAN has a lifetime of 1.5 days. Given that the plume stayed at this temperature for 2 days prior to being sampled at MBO (Fig. 4.9e), PAN must have decomposed back to NOx which then led to ozone production, hence the higher $\Delta O_3/\Delta CO$ ratio at MBO. On the other hand, the aircraft observations were colder (255-260 K) (Fig. 4.9k). At these temperatures, PAN has a lifetime of 27–77 days. This suggests that NOx remained locked up as PAN during transport and did not lead to ozone production, hence the lower $\Delta O_3/\Delta CO$ ratios for the aircraft data.

For the $\Delta\sigma_{sp}/\Delta CO$ ratios summarized in Table 4.1, two things stand out. First, the $\Delta\sigma_{sp}/\Delta CO$ ratios at MBO are nearly three times larger than the ratios for all three AC plumes. This is because of the different transport mechanisms for both observation platforms. The plume observed at MBO was transported eastward with minimal washout. On the other hand, the plume observed by the aircraft moved over to the Arctic where the troposphere is lower. This suggests wet deposition of particulates which explains the lower $\Delta\sigma_{sp}/\Delta CO$ ratios observed by the aircraft.

Second, the $\Delta\sigma_{sp}/\Delta CO$ ratios for the Siberian 2015 fire plumes are on the higher end of the observed ratios in similarly aged plumes. In particular, the $\Delta\sigma_{sp}/\Delta CO$ ratio at MBO is the highest among any observed plumes. Based on emission factors for biomass burning reported by Akagi et al. (2011), boreal fires have a $\Delta PM/\Delta CO$ emission factor ratio of 0.14 $\mu g/m^3$. The corresponding $\Delta PM_{2.5}/\Delta CO$ ratios at MBO and AC plumes 1, 2, and 3 are 0.61, 0.22, 0.21, and 0.16 $\mu g/m^3$, respectively. The higher ratios for the Siberian 2015 fires suggest an additional source aside from the BB smoke. AOD forecasts from NAAPS (Fig. 4.12 and Appendix D) show that this additional PM comes from dust (green-yellow shade). The calculated scattering Angstrom exponent for this event at MBO (using the 450-700 nm pair) is 1.9, which is indicative of a smoke/dust mixture.

All other events enumerated in Table 4.1 reported effects on surface air quality via ozone exceedances. Later, we look at effects of the Siberian 2015 fires on surface air quality in the western U.S.

Fig. 4.14 shows a time series of the reactive nitrogen species in the Siberian plume as observed from the aircraft. Most of the NOy (~75%) is stored as PAN. NOx is insignificant. This suggests that most photochemical production of O_3 from the plume likely has not happened. However, if the plume warmed up (i.e., via descent), then PAN would decompose back to NOx and ozone formation can take place. For comparison, Briggs *et al*. (2016) looked at regional fires observed at MBO during summer 2012 and 2013 and found that PAN comprised 25-57% of the total reactive nitrogen.

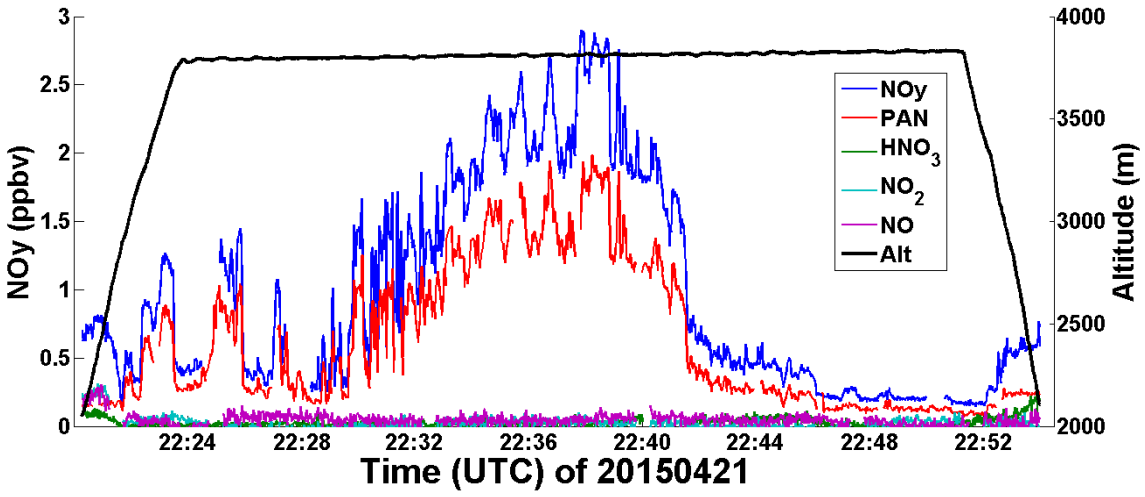

Figure 4.14. NOy speciation of the plume observed by the aircraft.

4.3.5 Siberian plume observations in the BL

Finally, we pick sites in the Pacific Northwest that have data on April 2015. We focus on Oregon and Idaho as these states are the most impacted by the Siberian plumes based on the MODIS images (Figs. 4.4 and 4.5). Aside from MBO, we selected Boise (826 m a.s.l.), Idaho Falls (1815 m), and Portland (53 m) (see Fig. 4.1). Fig. 4.15 shows a time series of the maximum daily average 8–hour (MDA8) ozone at these sites for April 2015. MBO has the highest MDA8 values (50-85 ppbv) compared to the other sites. Idaho Falls showed a small enhancement but no other sites showed a similar trend. This supports the satellite and Lidar observations that most of the Siberian smoke has stayed aloft.

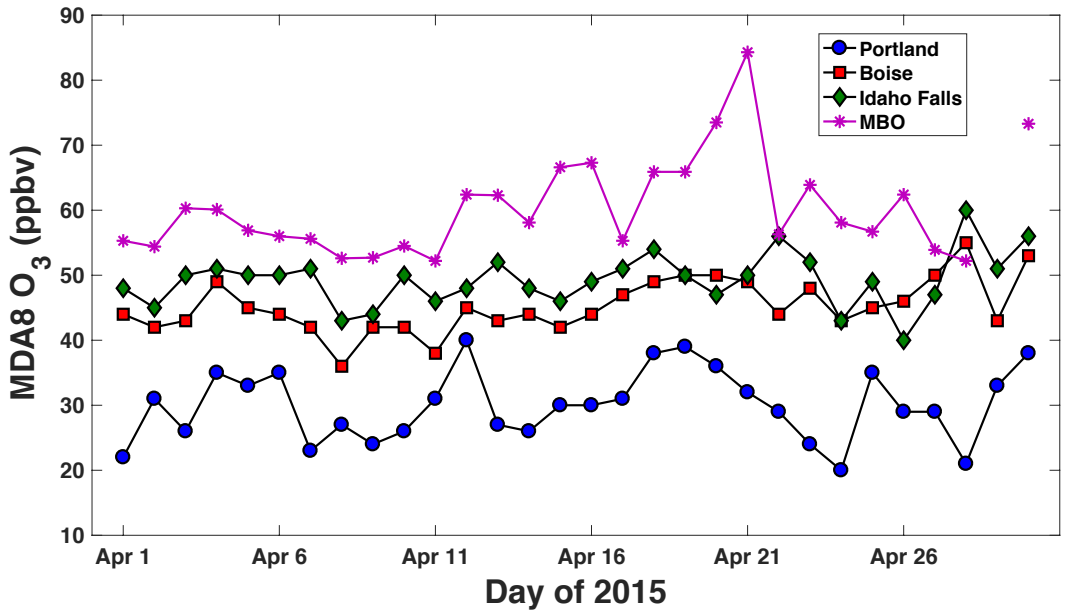

Figure 4.15. MDA8 O_3 time series at Portland, Boise, Idaho Falls, and MBO on April 2015.

4.4 SUMMARY

In April 2015, huge agricultural fires burned in the steppes of Southern Russia. Due to strong winds, the fires burned out of control and likely mobilized large amounts of mineral dust as well. The smoke and dust were injected relatively high in the atmosphere where strong upper-level winds dispersed them widely. We used data at Mt. Bachelor Observatory in central Oregon (MBO; 2.8 km a.s.l.) and from the NOAA WP-3D aircraft during the Shale Oil and Natural Gas Nexus (SONGNEX) campaign (SONGNEX) to examine the plume chemistry downwind of the fire source. We find that both platforms observed a plume of Siberian origin but not the same exact plume.

We find that $\Delta O_3/\Delta CO$ enhancement ratio at MBO is higher than for the plume intercepted by the aircraft. This is due to the warmer plume observed at MBO which led to

thermal decomposition of PAN to NOx. The colder plume observed by the aircraft allowed PAN to be locked up and therefore less ozone production. We also find that the $\Delta\sigma_{sp}/\Delta CO$ enhancement ratios at MBO and on the aircraft were much higher than the ratios for similarly aged Siberian fires that were observed previously in the western U.S. We observe that this is because of dust transport in addition to the smoke. We also hypothesize minimal wet scavenging of aerosols en route to MBO because of the relatively intact nature of the Siberian plume. For the aircraft, greater plume encounter with clouds reduced the aerosol loading. We also observe that 75% of the reactive nitrogen in the Siberian plume intercepted by the aircraft is in the form of PAN and that NOx was a minor component of the plume. This suggests that most photochemical production of ozone from this part of the plume has not happened, but can occur once the plume warms up during descent. The Siberian 2015 fires that we studied did not lead to air quality enhancements at the surface in North America. This is because the Siberian fires were lofted at 4-10 kilometers a.s.l. in Russia, and while the plumes were efficiently transported across the Pacific, there was no significant high-pressure system to cause subsidence and mixing into the boundary layer.

CHAPTER 5

CONCLUSIONS AND FUTURE WORK

This dissertation focused on three types of high-ozone events that we typically observe at Mount Bachelor Observatory (MBO) and in the western United States during spring and summer: (1) upper troposphere/lower stratosphere (UT/LS) episodes; (2) biomass burning (BB) plumes; and (3) long-range transport (LRT) of pollution.

In Chapter 2, I described a UT/LS event that affected air quality in the western U.S. in Spring 2012. We observed an O_3 increase of 2.0–8.5 ppbv in monthly average maximum daily 8–hour average O_3 mixing ratio (MDA8 O_3) at MBO and numerous other sites in the western U.S. compared to previous years. This shift in the O_3 distribution had a strong effect on the number of exceedance days at surface sites in the western U.S. We also observed a good correlation between daily MDA8 variations at MBO and at downwind sites. This suggests that under specific meteorological conditions, synoptic variation in O_3 at MBO can be observed at other surface sites in the western U.S. At MBO, the elevated O_3 concentrations in May 2012 are associated with low CO values and low water vapor values, consistent with transport from the upper troposphere/lower stratosphere (UT/LS). Furthermore, the Real-time Air Quality Modeling System (RAQMS) analyses indicate that a large flux of O_3 from the UT/LS in May 2012 contributed to the observed enhanced O_3 across the western U.S. Our results suggest that a network of mountaintop observations, LiDAR and satellite observations of O_3 could provide key data on daily and interannual variations in baseline O_3.

In Chapter 3, I looked at regional BB events during Summer 2015. The photochemical environment in biomass burning (BB) plumes remains poorly understood, and our study aims to fill this knowledge gap. I selected cloud-free days at MBO and investigated the photochemistry in these plumes. At local noontime (lower solar zenith angle), $j(NO_2)$ values were slightly higher (0.2-1.8%) in the smoky days compared to the clean day. At higher SZA (70^o), BB aerosols decrease $j(NO_2)$ at much larger magnitudes (14-21% decrease). We also observe a 15-25% decrease in actinic flux at UV wavelengths, presumably due to BrC absorption. We compare our measurements with results from the TUV5.2 model and find a good agreement during cloud-free conditions. Finally, I used the extended Leighton relationship to estimate HO_2 and RO_2 concentrations and $P(O_3)$ in the fire plumes. I calculate HO_2 and RO_2 values from 49-185 pptv, which is in the same range as other studies. I also compute ozone production rates of 2.0-3.1 ppbv/hour. Results of this work need to be verified with a photochemical model. In particular, the calculated HO_2 and RO_2 radicals need to be examined. Future work can examine these plumes using a detailed chemical model to shed more light on the complex photochemistry in biomass burning plumes.

In Chapter 4, I described a Siberian BB event that was observed at high elevation in the western U.S. but not at low elevations. I used data from MBO and from the NOAA WP-3D Orion research aircraft during the Shale Oil and Natural Gas Nexus (SONGNEX) campaign in Spring 2015 to gain insights about the plume chemistry. Using satellite data and model forecasts from NAAPS, we find that MBO and the aircraft did not observe the same exact plume although both have similar Siberian origin. We also find that the $\Delta O_3/\Delta CO$ and $\Delta\sigma_{sp}/\Delta CO$ enhancement ratios at MBO were much higher than the ratios for similarly aged Siberian fires that were observed in the western U.S. We find that the smoke was mixed with dust, generating $\Delta\sigma_{sp}/\Delta CO$

ratios that were much higher than BB alone. The plume observed at MBO was warmer hence allowing PAN to thermally decompose to NOx, thus we see higher $\Delta O_3/\Delta CO$ at MBO. On the other hand, the plume observed by the aircraft was colder, hence PAN remained locked up. This is consistent with the aircraft observations that 75% of the reactive nitrogen is in the form of PAN and that NOx is insignificant. Model simulations of the Siberian event would help in verifying both mountaintop and aircraft observations. In particular, it would be interesting to quantify how much ozone was produced downwind from the fires, how much ozone was produced from PAN decomposition, and how much ozone was mixed from the UT/LS, if there was any.

CHAPTER 6

REFERENCES

Akagi, S. K., Yokelson, R. J., Wiedinmyer, C., Alvarado, M. J., Reid, J. S., Karl, T., Crounse, J. D., and Wennberg, P. O. (2011), Emission factors for open and domestic biomass burning for use in atmospheric models, *Atmos. Chem. Phys*., 11, 4039-4072, doi:10.5194/acp-11-4039-2011.

Akagi, S. K., Yokelson, R. J., Burling, I. R., Meinardi, S., Simpson, I., Blake, D. R., McMeeking, G. R., Sullivan, A., Lee, T., Kreidenweis, S., Urbanski, S., Reardon, J., Griffith, D. W. T., Johnson, T. J., and Weise, D. R. (2013), Measurements of reactive trace gases and variable O_3 formation rates in some South Carolina biomass burning plumes, *Atmos. Chem. Phys*., 13, 1141-1165, doi:10.5194/acp-13-1141-2013.

Alvarado, M.J., Wang, C., Prinn, R.G., (2009), Formation of ozone and growth of aerosols in young smoke plumes from biomass burning: 2. Three-dimensional Eulerian studies. *Journal of Geophysical Research-Atmospheres* 114, D09307.

Alvarado, M.J., J. A. Logan, J. Mao, E. Apel, D. Riemer, D. Blake, R. C. Cohen, K.-E. Min, A. E. Perring, E. C. Browne, P. J. Wooldridge, G. S. Diskin, G. W. Sachse, H. Fuelberg, W. R. Sessions, D. L. Harrigan, G. Huey, J. Liao, A. Case-Hanks, J. L. Jimenez, M. J. Cubison, S. A. Vay, A. J. Weinheimer, D. J. Knapp, D. D. Montzka, F. M. Flocke, I. B. Pollack, P. O. Wennberg, A. Kurten, J. Crounse, J. M. St. Clair, A. Wisthaler, T. Mikoviny, R. M. Yantosca, C. C. Carouge, and P. Le Sager (2010), Nitrogen oxides and PAN in plumes from boreal fires during ARCTAS-B and their impact on ozone: An integrated analysis of aircraft and satellite observations, *Atmos. Chem. Phys*. 10, 9739-9760.

Alvarado, M. J., C. R. Lonsdale, R. J. Yokelson, S. K. Akagi, H. Coe, J. S. Craven, E. V. Fischer, G. R. McMeeking, J. H. Seinfeld, T. Soni, J. W. Taylor, D. R. Weise, and C. E. Wold (2015), Investigating the links between ozone and organic aerosol chemistry in a biomass burning plume from a prescribed fire in California chaparral, *Atmos. Chem. Phys*., 15, 6667-6688, doi:10.5194/acp-15-6667-2015.

Ambrose, J.L., Reidmiller, D.R., Jaffe, D.A. (2011), Causes of high O_3 in the lower free troposphere over the Pacific Northwest as observed at the Mt. Bachelor Observatory. *Atmos. Environ.* 45, 5302-5315.

Andreae, M. O. (1991), Biomass burning: Its history, use, and distribution and its impact on environmental quality and global climate, p. 3-21, In J.S. Levine (ed.) Global biomass burning: Atmospheric, climatic, and biospheric implications, The MIT Press, Cambridge, MA.

Andreae, M. O., and P. Merlet (2001), Emission of trace gases and aerosols from biomass burning, *Global Biogeochem. Cycles*, 15(4), 955–966, doi:10.1029/2000GB001382.

Andreae, M. O. and Gelencser, A. (2006), Black carbon or brown carbon? The nature of light-absorbing carbonaceous aerosols. *Atmos. Chem. Phys*. 6, 3131−3148.

Baker, K. R., M. C. Woody, G. S. Tonnese, W. Hutzelle, H. O. T. Pye, M. R. Beaver, G. Pouliot, and T. Pierce (2016), Contribution of regional-scale fire events to ozone and $PM_{2.5}$ air quality estimated by photochemical modeling approaches, *Atmos. Environ.* 140, 539-554, doi:10.1016/j.atmosenv.2016.06.032.

Baylon, P.M., Jaffe, D.A., Wigder, N.L., Gao, H., Hee, J. (2015), Ozone enhancement in western US wildfire plumes at the Mt. Bachelor Observatory: The role of NOx. *Atmos. Environ*., 109, 297-304, DOI: 10.1016/j.atmosenv.2014.09.013.

Baylon, P.M., Jaffe, D.A., Pierce, R.B., and Gustin, M.S., (2016), Interannual variability in baseline ozone and its relationship to surface ozone in the western U.S. *Environmental Science & Technology*, 50, 2994–3001, doi: 10.1021/acs.est.6b00219.

Baylon, P.M., Jaffe, D.A., de Gouw, J., Warneke, C., and Veres, P., Influence of Long-Range Transport of Siberian biomass burning at the Mt. Bachelor Observatory during the Spring of 2015, *submitted to Aerosol and Air Quality Research*.

Baylon, P.M., Jaffe, D.A., Hall, S.R., Ullmann, K., and Lefer, B.L., Impact of biomass burning plumes on photolysis rates and ozone formation at the Mount Bachelor Observatory, *submitted to J. Geophys. Res.*

Beine, H. J. (1996), NO_x photochemistry in High Northern Latitudes during spring, a PhD dissertation.

Bell, M.L., Peng, R.D., Dominici, F. (2006), The exposure-response curve for ozone and risk of mortality and the adequacy of current ozone regulations, *Environmental Health Perspectives* 114:523-536.

Bertschi, I.T., and Jaffe, D.A. (2005), Long-range transport of ozone, carbon monoxide and aerosols to the NE Pacific troposphere during the summer of 2003: Observations of smoke plumes from Asian boreal fires. *Journal of Geophysical Research* 110, D05303, doi: 10.1029/2004JD005135.

Brasseur, G. P., J. J. Orlando, G. S. Tyndall (1999), *Atmospheric Chemistry and Global Change*, Oxford, 654 pp.

Briggs, N.L., Jaffe, D.A., Gao, H., Hee, J.R., Baylon, P.M., Zhang, Q., Zhou, S., Collier, S.C., Sampson, P.D., and Cary, R.A. (2016), Particulate matter, ozone, and nitrogen species in aged wildfire plumes observed at the Mount Bachelor Observatory. *Aerosol and Air Quality Research* 16, 3075–3087, doi: 10.4209/aaqr.2016.03.0120.

Brown-Steiner, B., Hess, P. G., and Lin, M. Y. (2015), On the capabilities and limitations of GCCM simulations of summertime regional air quality: A diagnostic analysis of ozone and temperature simulations in the US using CESM CAM-Chem, *Atmos. Environ*., 101, 134–148, doi:10.1016/j.atmosenv.2014.11.001.

Cantrell, C. A., R. E. Shetter, J. G. Calvert, F. L. Eisele, E. Williams, K. Baumann, W. H. Brune, P. S. Stevens, and J. H. Mather (1997), Peroxy radicals from photostationary state deviations and stead state calculations during the Tropospheric OH Photochemistry Experiment at Idaho Hill, Colorado, 1993, *J. Geophys. Res*., 102, 6369 – 6378.

Castro, T., S. Madronich, S. Rivale, A. Muhlia, and B. Mar (2001), The influence of aerosols on photochemical smog in Mexico City, *Atmos. Environ*., 35, 1765–1772, doi:10.1016/S1352-2310(00)00449-0.

Collier, S., Zhou, S., Onasch, T.B., Jaffe, D.A., Kleinman, L., Sedlacek, A.J., III, Briggs, N.L., Hee, J., Fortner, E., Shilling, J.E., Worsnop, D., Yokelson, R.J., Parworth, C., Ge, X., Xu, J., Butterfeld, Z., Chand, D., Dubey, M.K., Pekour, M.S., Springston, S., and Zhang, Q. (2016), Regional influence of aerosol emissions from wildfires driven by combustion efficiency: Insights from the BBOP campaign. *Environmental Science & Technology* 50, 8613–8622, doi: 10.1021/acs.est.6b01617.

Cooper, O.R.; Parrish, D.D.; Stohl, A.; Trainer, M.; Nedelec, P.; Thouret, V.; Cammas, J.P.; Oltmans, S.J.; Johnson, B.J.; Tarasick, D.; Leblanc, T.; McDermid, I.S.; Jaffe, D.A.; Gao, R.; Stith, J.; Ryerson, T.; Aikin, K.; Campos, T.; Weinheimer, A.; Avery, M.A (2010), Increasing springtime ozone mixing ratios in the free troposphere over western North America. *Nature* 463, 344-348.

Cooper, O.R.; Gao, R.; Tarasick, D.; Leblanc, T.; Sweeny, C. (2012), Long-term ozone trends at rural ozone monitoring sites across the United States. *J. Geophys. Res*. *117* (D22), D22307, DOI:10.1029/2012JD018261.

Crawford, J., D. Davis, G. Chen, R. Shetter, M. Müller, J. Barrick, and J. Olson (1999), An assessment of cloud effects on photolysis rate coefficients: Comparison of experimental and theoretical values, *J. Geophys. Res*., 104(D5), 5725–5734, doi:10.1029/98JD01724.

Crutzen, P. J. (1995), Ozone in the troposphere. *Composition, chemistry, and climate of the atmosphere*, H. B. Singh, Ed., Van Nostrand Reinhold, 527.

Crutzen, P. J. and M. O. Andreae (1990), Biomass burning in the tropics: impact on atmospheric chemistry and biogeochemical cycles, *Science*, 250(4988), 1669-1678.

DeMore, W. B., M. J. Molina, S. P. Sander, D. M. Goldan, C. E. Kolb, R. F. Hampson, M. J. Kurylo, C. J. Howard, and A. R. Ravishankara (1997), Chemical kinetics and photochemical data for use in stratospheric modeling, *JPL Publ*., 97-4.

Dentener, F.; Keating, T.; Akimoto, H., Eds. (2011), *Hemispheric Transport of Air Pollution 2010: Part A: Ozone and Particulate Matter*, vol. 17; United Nations: New York.

Dickerson, R. R., S. Kondragunta, G. Stenchikov, K. L. Civerolo, B. G. Doddridge, and B. N. Holben (1997), The Impact of Aerosols on Solar Ultraviolet Radiation and Photochemical Smog, *Science*, 278, 827–830, doi:10.1126/science.278.5339.827.

Edwards, G. D. and P. S. Monks (2003), Performance of a single-monochromator diode array spectroradiometer for the determination of actinic flux and atmospheric photolysis frequencies, *J. Geophys. Res*., 108, 8546, doi:10.1029/2002JD002844, D16.

Fine, R.; Miller, M.B.; Yates, E.L.; Iraci, L.T.; Gustin, M.S. (2015a), Investigating the influence of long-range transport on surface O_3 in Nevada, USA, using observations from multiple measurement platforms. *Science of the Total Environment* 530-531, 493-504.

Fine, R., Miller, M.B., Burley, J., Jaffe, D.A., Pierce, R.B., Lin, M., Gustin, M.S. (2015b), Variability and sources of surface ozone at rural sites in Nevada, USA: Results from two years of the Nevada Rural Ozone Initiative. *Science of the Total Environment* 530-531, 471–482, doi: 10.1016/j.scitotenv.2014.12.027.

Finlayson-Pitts, B.J., Pitts, J.N., (1986), *Atmospheric Chemistry: Fundamentals and Experimental Techniques*. John Wiley and Sons, New York, NY.

Fiore, A., Jacob, D. J., Liu, H., Yantosca, R. M., Fairlie, T. D., and Li, Q. B. (2003), Variability in surface ozone background over the United States: Implications for air quality policy, *J. Geophys. Res*., 108, 4787, doi:10.1029/2003jd003855.

Fiore, A. M., Dentener, F. J., Wild, O., et al. (2009), Multimodel estimates of intercontinental source-receptor relationships for ozone pollution, *J. Geophys. Res*., 114, D04301, doi:10.1029/2008jd010816.

Fiore, A.M.; Pierce, R.B.; Dickerson, R.D.; Lin, M. Detecting and Attributing Episodic High Background Ozone Events, *AQAST Special Issue of Environmental Manager*, Feb **2014**, a publication of the Air & Waste Management Association (A&WMA; www.awma.org)

Fischer, E.V., Hsu, N.C., Jaffe, D.A., Jeong, M.-J., and Gong, J.C. (2009), A decade of dust: Asian dust and springtime aerosol load in the U.S. Pacific Northwest. *Geophysical Research Letters* 36, L03821, doi: 10.1029/2008GL0364.

Fischer, E.V., Jaffe, D.A., Reidmiller, D.R., and Jaeglé, L. (2010), Meteorological controls on observed peroxyacetyl nitrate at Mount Bachelor during the spring of 2008. *Journal of Geophysical Research* 115, D03302, doi: 10.1029/2009JD012776.

Fischer, E.V., Jaffe, D.A., Marley, N.A., Gaffney, J.S., and Marchany-Rivera, A. (2010), Optical properties of aged Asian aerosols observed over the U.S. Pacific Northwest. *Journal of Geophysical Research* 115, D20209, doi: 10.1029/2010JD013943.

Fischer, E.V., Perry, K.D., and Jaffe, D.A. (2011a), Optical and chemical properties of aerosols transported to Mount Bachelor during spring 2010. *Journal of Geophysical Research* 116, D18202, doi: 10.1029/2011JD015932.

Fischer, E.V., Jaffe, D.A., and Weatherhead, E.C. (2011b), Free tropospheric peroxyacetyl nitrate (PAN) and ozone at Mount Bachelor: Potential causes of variability and timescale for trend detection. *Atmospheric Chemistry and Physics* 11, 5641–5654, doi: 10.5194/acp-11-5641-2011.

Fiscus, E.L.; Booker, F.L.; Burkey, K.O. (2005), Crop responses to ozone: uptake, modes of action, carbon assimilation and partitioning. *Plant, Cell and Environment*, *28*, 997-1011.

Flynn, J., B. Lefer, B. Rappengluck, M. Leuchner, R. Perna, J. Dibb, L. Ziemba, C. Anderson, J. Stutz, W. Brune, X. Ren, J. Mao, W. Luke, J. Olson, G. Chen, and J. Crawford (2010), Impact of clouds and aerosols on ozone production in Southeast Texas, *Atmos. Environ*., 44, 4126-4133, doi:10.1016/j.atmosenv.2009.09.005.

Granier, C., Bessagnet, B., Bond, T., D'Angiola, A., van der Gon, H. D., Frost, G. J., Heil, A., Kaiser, J. W., Kinne, S., Klimont, Z., Kloster, S., Lamarque, J.-F., Liousse, C., Masui, T., Meleux, F., Mieville, A., Ohara, T., Raut, J.-C., Riahi, K., Schultz, M. G., Smith, S. J., Thompson, A., van Aardenne, J., van der Werf, G. R., and van Vuuren, D. P. (2011), Evolution of anthropogenic and biomass burning emissions of air pollutants at global and regional scales during the 1980–2010 period, *Climatic Change*, 109, 163–190, doi:10.1007/s10584-011-0154-1.

Gratz, L.E.; Jaffe, D.A.; Hee, J.R. (2015), Causes of increasing ozone and decreasing carbon monoxide in springtime at the Mt. Bachelor Observatory from 2004 to 2013. *Atmos. Environ. 109*, 323-330, DOI: 10.1016/j.atmosenv.2014.05.076.

Griffin, R. J., Beckman, P. J., Talbot, R. W., Sive, B. C., and Varner, R. K. (2007), Deviations from ozone photostationary state during the International Consortium for Atmospheric Research on Transport and Transformation 2004 campaign: Use of measurements and photochemical modeling to assess potential causes, J. *Geophys. Res*., 112, D10S07, doi:10.1029/2006JD007604.

Gryparis, A.; Forsberg, B.; Katsouyanni, K.; Analitis, A.; Touloumi, G.; Schwartz, J. (2004), Acute effects of ozone on mortality from the 'Air Pollution and Health: A European Approach' project. *Am. J. Respir. Crit. Care Med.* 170, 1080–1087.

Gustin, M.S.; Fine, R.; Miller, M.; Jaffe, D.; Burley, J. (2015), The Nevada Rural Ozone Initiative (NVROI): Insights to understanding air pollution in complex terrain. *Science of The Total Environment* 530-531, 455-470.

Henderson, B. H., Pinder, R. W., Crooks, J., Cohen, R. C., Carlton, A. G., Pye, H. O. T., and Vizuete, W. (2012), Combining Bayesian methods and aircraft observations to constrain the $HO^{\cdot} + NO_2$ reaction rate, *Atmos. Chem. Phys*., 12, 653-667, doi:10.5194/acp-12-653-2012.

Herron-Thorpe, F.L., Mount, G.H., Emmons, L.K., Lamb, B.K., Jaffe, D.A., Wigder, N.L. Chung, S.H., Zhang, R., Woelfle, M.D., and Vaughan, J.K. (2014), Air quality simulations of wildfires in the Pacific Northwest evaluated with surface and satellite observations during the summers of 2007 and 2008. *Atmospheric Chemistry & Physics* 14, 11103–11152, doi: 10.5194/acpd-14-11103-2014.

Hilboll, A., Richter, A., and Burrows, J. P. (2013), Long-term changes of tropospheric over megacities derived from multiple satellite instruments, *Atmos. Chem. Phys.* 13, 4145-4169, doi:10.5194/acp-13-4145-2013.

Hodnebrog, Ø., S. Solberg, F. Stordal, T. M. Svendby, D. Simpson, M. Gauss, A. Hilboll, G. G. Pfister, S. Turquety, A. Richter, J. P. Burrows, and H. A. C. Denier van der Gon (2012), Impact of forest fires, biogenic emissions and high temperatures on the elevated Eastern Mediterranean

ozone levels during the hot summer of 2007, *Atmos. Chem. Phys*., 12, 8727-8750, doi:10.5194/acp-12-8727-2012.

Huang, M., Carmichael, G.R., Chai, T., Pierce, R.B., Oltmans, S.J., Jaffe, D.A., Bowman, K.W., Kaduwela, A., Cai, C., Spak, S.N., Weinheimer, A.J., Huey, L.G., and Diskin, G.S. (2013), Impacts of transported background pollutants on summertime western US air quality: model evaluation, sensitivity analysis and data assimilation. *Atmospheric Chemistry and Physics* 13, 359–391, doi:10.5194/acp-13-359-2013.

Hubbell BJ, Hallberg A, McCubbin DR, Post E. (2005), Health- related benefits of attaining the 8-hr ozone standard. *Environ Health Perspect* 113:73–82.

Jacob, D. (1999), *Introduction to Atmospheric Chemistry*, Princeton University Press.

Jacob, D. J. (2000), Heterogeneous chemistry and tropospheric ozone, *Atmos. Environ*., 34, 2131-2159, doi:10.1016/S1352-2310(99)00462-8.

Jacobson, M. Z. (1998), Studying the effects of aerosols on vertical photolysis rate coefficient and temperature profiles over an urban airshed, *J. Geophys. Res*., 103, 10593–10604, doi:10.1029/98JD00287.

Jaeglé, L., C. R. Webster, R. D. May, D. W. Fahey, E. L. Woodbridge, E. R. Keim, R. S. Gao, M. H. Proffitt, R. M. Stimpfle, R. J. Salawitch, S. C. Wofsy, and L. Pfister (1994), In situ measurements of the NO_2/NO ratio for testing atmospheric photochemical models, *Geophys. Res. Lett*., 21, 2555–2558, doi:10.1029/94GL02717.

Jaegle, L.; Jaffe, D.A.; Price, H.U.; Weiss-Penzias, P.; Palmer, P.I.; Evans, M.J.; Jacob, D.J.; Bey, I. (2003), Sources and budgets for CO and O_3 in the northeastern Pacific during the spring of 2001: results from the PHOBEA-II Experiment. *J. Geophys. Res. 108* (D20), 8802, DOI:10.1029/2002JD003121.

Jaffe, D. (2011), Relationship between surface and free tropospheric ozone in the western U.S. *Environ. Sci. Technol. 45*, 432-438.

Jaffe, D., Snow, J., and Cooper, O. (2003a), The April 2001 Asian dust events: Transport and impact on surface aerosol concentrations in the U.S. *EOS Transactions* 84, 501–516, doi: 10.1029/2003EO460001.

Jaffe D., McKendry I., Anderson, T., and Price, H. (2003b), Six 'new' episodes of trans-Pacific transport of air pollutants. *Atmospheric Environment* 37, 391–404, doi: 10.1016/S1352-2310(02)00862-2.

Jaffe, D.A., and Strode, S. (2008), Sources, fate and transport of atmospheric mercury from Asia. *Environmental Chemistry* 5, 121–26, doi: 10.1071/EN08010.

Jaffe, D. and Ray, J. (2007), Increase in surface ozone at rural sites in the Western US. *Atmospheric Environment* 41, 5452–5463, doi: 10.1016/j.atmosenv.2007.02.034.

Jaffe, D.A., Anderson, T., Covert, D., Kotchenruther, R., Trost, B., Danielson, J., Simpson, W., Berntsen, T., Karlsdottir, S., Blake, D., Harris, J., Carmichael, G., and Uno, I. (1999), Transport of Asian air pollution to North America. *Geophysical Research Letters* 26, 711–714, doi: 10.1029/1999GL900100.

Jaffe, D., Prestbo, E., Swartzendruber, P., Weiss-Penzias, P., Kato, S., Takami, A., Hatakeyama, S., and Kajii, Y. (2005), Export of atmospheric mercury from Asia. *Atmos. Environ.* 39, 3029–3038, doi: 10.1016/j.atmosenv.2005.01.030.

Jaffe, D.A.; Chand, D.; Hafner, W.; Westerling, A.; Spracklen, D. (2008a), Influence of fires on O_3 concentrations in the western U.S. *Environ. Sci. Technol.* 42, 5885-5891.

Jaffe, D.A., Hafner, W., Chand, D., Westerling, A., and Spracklen, D. (2008b), Interannual variations in PM2.5 due to wildfires in the Western United States. *Environmental Science & Technology* 42, 2812–2818, doi: 10.1021/es702755v.

Jaffe, D. and N. Wigder (2012), Ozone production from wildfires: A critical review, *Atmospheric Environment*, doi:10.1016/j.atmosenv.2011.11.063.

Jaffe, D., I. Bertschi, L. Jaegle´, P. Novelli, J. S. Reid, H. Tanimoto, R. Vingarzan, and D. L. Westphal (2004), Long-range transport of Siberian biomass burning emissions and impact on

surface ozone in western North America, *Geophys. Res. Lett*., 31, L16106, doi:10.1029/2004GL020093.

Jaffe, D.A., and Zhang, L. (2017), Meteorological anomalies lead to elevated O_3 in the western U.S. in June 2015. *Geophysical Research Letters* 44, doi: 10.1002/2016GL072010.

Jäkel, E., M. Wendisch, A. Kniffka, and T. Trautmann (2005), Airborne system for fast measurements of upwelling and downwelling actinic flux densities, *Appl. Opt.* 44, 434–444.

Jäkel, E., M. Wendisch, and B.L. Lefer (2006), Parameterization of ozone photolysis frequency in the lower troposphere using data from photodiode array detector spectrometers, *J. Atmos. Chem.*, 54, 67-87, doi:10.1007/s10874-006-9014-1.

Jiang, X., C. Wiedinmyer, and A.G. Carlton (2012), Aerosols from Fires: An Examination of the Effects on Ozone Photochemistry in the Western United States, *Environ. Sci. Technol.* 46, 11878-11886.

Kanaya, Y., Y. Kajii, and H. Akimoto (2003), Solar actinic flux and photolysis frequency determinations by radiometers and a radiative transfer model at Rishiri Island: comparisons, cloud effects, and detection of an aerosol plume from Russian forest fires, *Atmos. Environ*., 37, 2463-2475, doi:10.1016/S1352-2310(03)00183-3.

Keating, T., West, J., and Jaffe, D.A. (2005), Air Quality Impacts of Intercontinental Transport, EM The Magazine for Environmental Managers, Air & Waste Management Association, October, 28–30.

Klein, A.M., Bohannan, B.J.M., Jaffe, D.A., Levin, D.A., and Green, J.L. (2016), Molecular evidence for metabolically active bacteria in the atmosphere. *Frontiers in Microbiology* 7, doi: 10.3389/fmicb.2016.00772.

Kleinman, L., Y. N. Lee, S. Springston, L. Nunnermacker, X. Zhou, R. Brown, K. Hallock, P. Klotz, D. Leahy, J. Lee and L. Newman. (1994), Ozone Formation at a Rural Site in the Southeastern United States. *J. Geophys. Res*., 99, 3469-3482.

Kondo, Y., Morino, Y., Takegawa, N., Koike, M., Kita, K., Miyazaki, Y., Sachse, G., Vay, S., Avery, M., Flocke, F., Weinheimer, A., Eisele, F., Zondlo, M., Weber, R., Singh, H., Chen, G., Crawford, J., Blake, D., Fuelberg, H., Clarke, A., Talbot, R. Sandholm, S., Browell, E., Streets, D., Liley, B. (2004), Impacts of biomass burning in Southeast Asia on ozone and reactive nitrogen over the western Pacific in spring. *J. Geophys. Res.-Atmos.* 109, D15S12.

Kotchenruther R.A., Jaffe, D.A. and Jaeglé L. (2001), Ozone Photochemistry and the Role of PAN in the Springtime Northeastern Pacific Troposphere: Results from the PHOBEA Campaign. *J. Geophys. Res.* 106, 28,731-28,741.

Laing, J.R., Jaffe, D.A., and Hee, J.R. (2016), Physical and optical properties of aged biomass burning aerosol from wildfires in Siberia and the Western USA at the Mt. Bachelor Observatory. *Atmospheric Chemistry and Physics* 16, 15185–15197, doi: 10.5194/acp-16-15185-2016.

Langford, A.O.; Aikin, K.C.; Eubank, C.S.; Williams, E.J. (2009), Stratospheric contribution to high surface ozone in Colorado during spring. *Geophys. Res. Lett*. 36, DOI:10.1029/2009GL038367.

Langford, A.O.; Senff, C.J.; Alvarez, R.R.; Cooper, O.R.; Holloway, J.S.; Lin, M.Y.; Marchbanks, R.D.; Pierce, R.B.; Sandberg, S.P.; Weickmann, A.M.; Williams, E.J. (2015a), An overview of the 2013 Las Vegas Ozone Study (LVOS): Impact of stratospheric intrusions and long-range transport on surface air quality. *Atmos. Environ.* 109, 305-322.

Langford, A.O.; Pierce, R.B.; Schultz, P.J. (2015b), Stratospheric intrusions, the Santa Ana winds, and wildland fires in Southern California, *Geophys. Res. Lett*. 42, 6091–6097, doi:10.1002/2015GL064964.

Langford, A. O., R.J. Alvarez, J. Brioude, R. Fine, M.S. Gustin, M.Y. Lin, R.D. Marchbanks, R.B. Pierce, S.P. Sandberg, C.J. Senff, A.M. Weickmann, and E.J. Williams (2017), Entrainment of stratospheric air and Asian pollution by the convective boundary layer in the southwestern U.S., *J. Geophys. Res. Atmos*., 122, 1312– 1337, doi:10.1002/2016JD025987.

Lee, K. H., J. E. Kim, Y. J. Kim, J. Kim, and W. Hoyningen-Huene (2005), Impact of the smoke aerosol from Russian forest fires on the atmospheric environment over Korea during May 2003, *Atmos. Environ*. 39, 85-99, doi:10.1016/j.atmosenv.2004.09.032.

Lefer, B. L., R. E. Shetter, S. R. Hall, J. H. Crawford, and J. R. Olson (2003), Impact of clouds and aerosols on photolysis frequencies and photochemistry during TRACE-P: 1. Analysis using radiative transfer and photochemical box models, *J. Geophys. Res*., 108, 8821, doi:10.1029/2002JD003171, D21.

Lefohn, A.S.; Oltmans, S.J.; Dann, T.; Singh, H.B. (2001), Present-day variability of background ozone in the lower troposphere. *J. Geophys. Res.* 106 (D9), 9945-9958.

Leighton, P.A. (1961), Photochemistry of Air Pollution, Academic Press, New York.

Lerner, B. M., Gilman, J. B., Aikin, K. C., Atlas, E. L., Goldan, P. D., Graus, M., Hendershot, R., Isaacman-VanWertz, G. A., Koss, A., Kuster, W. C., Lueb, R. A., McLaughlin, R. J., Peischl, J., Sueper, D., Ryerson, T. B., Tokarek, T. W., Warneke, C., Yuan, B., and de Gouw, J. A. (2017), An improved, automated whole air sampler and gas chromatography mass spectrometry analysis system for volatile organic compounds in the atmosphere, *Atmos. Meas. Tech*., 10, 291-313, doi:10.5194/amt-10-291-2017.

Li, J., Z. Wang, X. Wang, K. Yamaji, M. Takigawa, Y. Kanaya, P. Pochanart, Y. Liu, H. Irie, B. Hu, H. Tanimoto, and H. Akimoto (2011), Impacts of aerosols on summertime tropospheric photolysis frequencies and photochemistry over Central Eastern China, *Atmos. Environ*. 45, 1817–1829.

Liang, Q., Jaegle, L., Jaffe, D.A., Weiss-Penzias, P., Heckman, A., and Snow, J.A. (2004), Long-range transport of Asian pollution to the northeast Pacific: Seasonal variations and transport pathways of carbon monoxide. *Journal of Geophysical Research-Atmospheres* 109, D23S07, doi: 10.1029/2003JD004402.

Liao, H., Y. L. Yung, and J. H. Seinfeld (1999), Effects of aerosols on tropospheric photolysis rates in clear and cloudy atmospheres, *J. Geophys. Res*., 104(D19), 23697–23707, doi:10.1029/1999JD900409.

Lin, X., M. Trainer, and S. C. Liu, (1988), On the Nonlinearity of the Tropospheric Ozone Production. *J. Geophys. Res*., 93, 15879-15888.

Lin, M.; Fiore, A.M.; Cooper, O.R.; Horowitz, L.W.; Langford, A.O.; Levy II, H.; Johnson, B.J.; Naik, V.; Oltmans, S.J.; Senff, C.J. (2012a), Springtime high surface ozone events over the western United States: quantifying the role of stratospheric intrusions. *J. Geophys. Res*. 117 (D21), DOI: 10.1029/2012JD018151.

Lin, M., Fiore, A. M., Horowitz, L. W., Cooper, O. R., Naik, V., Holloway, J., Johnson, B. J., Middlebrook, A. M., Oltmans, S. J., Pollack, I. B., Ryerson, T. B., Warner, J. X., Wiedinmyer, C., Wilson, J., and Wyman, B. (2012b), Transport of Asian ozone pollution into surface air over the western United States in spring, *J. Geophys. Res*., 117, D00V07, doi:10.1029/2011jd016961.

Lin, M., L.W. Horowitz, R. Payton, A.M. Fiore, and G. Tonnese, (2017), US surface ozone trnends and extremes from 1980 to 2014: quantifying the roles of rising Asian emissions, domestic controls, wildfires, and climate, *Atmos. Chem. Phys*., 17, 2943–2970, 2017, doi:10.5194/acp-17-2943-2017.

Liu, G.; Tarasick, D.W.; Fioletov, V.E.; Sioris, C.E.; Rochon, Y.J. (2009), Ozone correlation lengths and measurement uncertainties from analysis of historical ozonesonde data in North America and Europe. *J. Geophys. Res.* 114, D04112, doi:10.1029/2008JD010576.

Liu, S.C., Trainer, M., Fehsenfeld, F.C., Parrish, D.D., Williams, E.J., Fahey, D.W., Hubler, G. and Murphy, P.C. (1987), Ozone production in the rural troposphere and the implications for regional and global ozone distributions. *J. Geophys. Res.* 92(D4), 4191- 4207.

Lu, X., Zhang, L., Yue, X., Zhang, J., Jaffe, D., Stohl, A., Zhao, Y., and Shao, J. (2016), Wildfire influences on the variability and trend of summer surface ozone in the mountainous western United States. *Atmospheric Chemistry and Physics* 16, 14687–14702, doi: 10.5194/acp-16-14687-2016.

Madronich, S. (1987), Photodissociation in the atmosphere: 1. Actinic flux and the effects of ground reflections and clouds, *J. Geophys. Res*., 92(D8), 9740–9752, doi:10.1029/JD092iD08p09740.

Madronich, S. and S. Flocke (1999), The role of solar radiation in atmospheric chemistry, in Environmental Photochemistry, edited by P. Boule, pp. 1 –26, Springer-Verlag, New York.

Madronich, S., and G. Weller (1990), Numerical integration errors in calculated tropospheric photodissociation rate coefficients, *J. Atmos Chem*., 10, 289–300.

Malicet, J., D. Daumont, J. Charbonnier, C. Parisse, A. Chakir, and J. Brion (1995), Ozone UV spectroscopy. II. Absorption cross-sections and temperature dependence, *J. Atmos. Chem.* 21, 263–273, doi:10.1007/BF00696758.

Martins, V., A. Miranda, A. Carvalho, M. Schaap, C. Borrego, and E. Sa (2012), Impact of forest fires on particulate matter and ozone levels during the 2003, 2004 and 2005 fire seasons in Portugal, *Sci. Total Environ*., 414, 53-62. doi: 10.1016/j.scitotenv.2011.10.007.

Mason, S.A., Field, R.J., Yokelson, R.J., Kochivar, M.A., and Tinsley, M.R. (2001), Complex effects arising in smoke plume simulations due to inclusion of direct emissions of oxygenated organic species from biomass combustion, *J. Geophys. Res*. 106, 12527-12539.

Matthijsen, J., P. J. H. Builtjes, E. W. Meijer, and G. Boersen (1997), Modelling cloud effects on ozone on a regional scale: A case study, *Atmos. Environ*., 31(19), 3227-3238, doi:10.1016/S1352-2310(97)00064-2.

Mauzerall, D. L., Jacob, D. J., Fan, S.-M., Bradshaw, J. D., Gregory, G. L., Sachse, G. W., and Blake, D. R. (1996), Origin of tropospheric ozone at remote high northern latitudes in summer, *J. Geophys. Res*., 101, 4175–4188.

Mauzerall, D. L., Logan, J. A., Jacob, D. J., Anderson, B. E., Blake, D. R., Bradshaw, J. D., Heikes, B., Sachse, G. W., Singh, H., and Talbot, B. (1998), Photochemistry in biomass burning plumes and implications for tropospheric ozone over the tropical South Atlantic, *J. Geophys. Res*., 103, 8401–8423.

McClure, C.D., Jaffe, D.A., and Gao, H. (2016), Carbon dioxide in the free troposphere and boundary layer at the Mt. Bachelor Observatory. *Aerosol and Air Quality Research* 16, 717–728, doi: 10.4209/aaqr.2015.05.0323.

McDonald-Buller, E.C.; Allen, D.T.; Brown, N.; Jacob, D.J.; Jaffe, D.A.; Kolb, C.E.; Lefohn, A.S.; Oltmans, S.; Parrish, D.D.; Yarwood, G.; Zhang, L. (2011), Establishing policy relevant background (PRB) ozone concentrations in the United States. *Environ. Sci. Technol*. 45 (22), 9484-9497.

McKeen, S. A., G. Wotawa, D. D. Parrish, J. S. Holloway, M. P. Buhr, G. Hübler, F. C. Fehsenfeld, and J. F. Meagher (2002), Ozone production from Canadian wildfires during June and July of 1995, *J. Geophys. Res*., 107(D14), doi:10.1029/2001JD000697

Mebust, A. K., A. R. Russell, R. C. Hudman, L. C. Valin, R. C. Cohen (2011), Characterization of wildfire NOx emissions using MODIS fire radiative power and OMI tropospheric NO_2 columns, *Atmos. Chem. Phys*., 11, 5839-5851, doi:10.5194/acp-11-5839-2011.

Mok, J., N.A. Krotkov, A. Arola, O. Torres, H. Jethva, M. Andrade, G. Labow, T.F. Eck, Z. Li, R.R. Dicekrson, G.L. Stenchikov, S. Osipov, and X. Ren, (2016), Impacts of brown carbon from biomass burning on surface UV and ozone photochemistry in the Amazon Basin, *Nature Scientific Reports* 6:36940, DOI: 10.1038/srep36940.

Monks, P.S.; Granier, C.; Fuzzi, S.; Stohl, A.; Williams, M.L.; Akimoto, H.; Amann, M.; Baklanov, A.; Baltensperger, U.; Bey, I.; Blake, N.; Blake, R.S.; Carslaw, K.; Cooper, O.R.; Dentener, F.; Fowler, D.; Fragkou, E.; Frost, G.J.; Generoso, S.; Ginoux, P.; Grewe, V.; Guenther, A.; Hansson, H.C.; Henne, S.; Hjorth, J.; Hofzumahaus, A.; Huntrieser, H.; Isaksen, I.S.A.; Jenkin, M.E.; Kaiser, J.; Kanakidou, M.; Klimont, Z.; Kulmala, M.; Laj, P.; Lawrence, M.G.; Lee, J.D.; Liousse, C.; Maione, M.; McFiggans, G. (2009), Atmospheric composition change – global and regional air quality. *Atmos. Environ*. 43 (33), 5268-5350.

Nunnermacker, L.J., R.R. Dickerson, A. Fried and R. Sams, (1989), A New Gas-Phase Nitric Acid Calibration System, *Environ. Sci. Technol.* 23, 106-110.

Olszyna, K. J., E. M. Bailey, R. Simonaitis and J. F. Meagher. (1994), O_3 and NO_y Relationships at a Rural Site. *J. Geophys. Res*., 99, 14557-14563.

Palancar, G. G., B. L. Lefer, S. R. Hall, W. J. Shaw, C. A. Corr, S. C. Herndon, J. R. Slusser, and S. Madronich (2013), Effect of aerosols and NO_2 concentration on ultraviolet actinic flux near

Mexico City during MILAGRO: measurements and model calculations, *Atmos. Chem. Phys.*, 13, 1011–1022, doi:10.5194/acp-13-1011-2013.

Palancar, G. G., R. E. Shetter, S. R. Hall, B. M. Toselli, and S. Madronich (2011), Ultraviolet actinic flux in clear and cloudy atmosphere: model calculations and aircraft-based measurements, *Atmos. Chem. Phys*., 11, 5457-5469, doi:10.5194/acp-11-5457-2011.

Parrington, M., Palmer, P. I., Lewis, A. C., Lee, J. D., Rickard, A. R., Di Carlo, P., Taylor, J. W., Hopkins, J. R., Punjabi, S., Oram, D. E., Forster, G., Aruffo, E., Moller, S. J., Bauguitte, S. J.-B., Allan, J. D., Coe, H., and Leigh, R. J. (2013), Ozone photochemistry in boreal biomass burning plumes, *Atmos. Chem. Phys*., 13, 7321– 7341, doi:10.5194/acp-13-7321-2013.

Parrish, D. D., M. Trainer, E. J. Williams, D. W. Fahey, G. Hübler, C. S. Eubank, S. C. Liu, P. C. Murphy, D. L. Albritton, and F. C. Fehsenfeld (1986), Measurements of the NOx-O_3 photostationary state at Niwot Ridge, Colorado, *J. Geophys. Res*. 91(D5), 5361–5370, doi:10.1029/JD091iD05p05361.

Parrish, D.D.; Law, K.S.; Staehelin, J.; Derwent, R.; Cooper, O.R.; Tanimoto, H.; Volz-Thomas, A.; Gilge, S.; Scheel, H.E.; Steinbacher, M.; Chan, E. (2012), Long-term changes in lower tropospheric baseline ozone concentration at northern mid-latitudes. *Atmos. Chem. Phys*. 12, 11485-11504.

Pfister, G. G., Emmons, L. K., Hess, P. G., Honrath, R., Lamarque, J.F., Martin, M., Val and Owen, R. C., Avery, M. A., Browell, E. V., Holloway, J. S., Nedelec, P., Purvis, R., Ryerson, T. B., Sachse, G. W., and Schlager, H. (2006), Ozone production from the 2004 North American boreal fires, *J. Geophys. Res*. 111, D24S07, doi:10.1029/2006JD007695.

Pfister, G. G., C. Wiedinmyer, and L. K. Emmons (2008), Impacts of the fall 2007 California wildfires on surface ozone: Integrating local observations with global model simulations, *Geophys. Res. Lett*., 35, L19814, doi:10.1029/2008GL034747.

Pierce, R. B.; Al-Saadi, J.A.; Schaack, T.; Lenzen, A.; Zapotocny, T.; Johnson, D.; Kittaka, C.; Buker, M.; Hitchman, M.H.; Tripoli, G.; Fairlie, T.D.; Olson, J.R.; Natarajan, M.; Crawford, J.; Fishman, J.; Avery, M.; Browell, E.V.; Creilson, J.; Kondo, Y.; Sandholm, S.T. (2003), Regional

Air Quality Modeling System (RAQMS) predictions of the tropospheric ozone budget over East Asia. *J. Geophys. Res.* 108 (D21), 8825, DOI:10.1029/2002JD003176.

Pierce, R. B.; Schaack, T. K.; Al-Saadi, J.; Fairlie, T. D.; Kittaka, C.; Lingenfelser, G.; Natarajan, M.; Olson, J.; Soja, A.; Zapotocny, T. H.; Lenzen, A.; Stobie, J.; Johnson, D. R.; Avery, M.; Sachse, G.; Thompson, A.; Cohen, R.; Dibb, J.; Crawford, J.; Rault, D.; Martin, R.; Szykman, J.; Fishman, J. (2007), Chemical data assimilation estimates of continental US ozone and nitrogen budgets during the Intercontinental Chemical Transport Experiment – North America. *J. Geophys. Res*. 112, D12S21, DOI:10.1029/2006JD007722.

Pierce, R. B.; Al-Saadi, J.; Kittaka, C.; Schaack, T.; Lenzen, A.; Bowman, K.; Szykman, J.; Soja, A.; Ryerson, T.; Thompson, A.M.; Bhartia, P.; Morris, G.A. (2009), Impacts of background ozone production on Houston and Dallas, Texas, air quality during the Second Texas Air Quality Study field mission, *J. Geophys. Res.* 114, D00F09, doi:10.1029/2008JD011337.

Price, H.U., Jaffe, D.A., Cooper, O.R., and Doskey, P.V. (2004), Photochemistry, ozone production, and dilution during long-range transport episodes from Eurasia to the northwest United States. *Journal of Geophysical Research* 109, D23S13, doi: 10.1029/2003JD004400.

Primbs, T., Simonich, S., Schmedding, D., Wilson, G., Jaffe, D., Takami, A., Kato, S., Hatakeyama, S., Kajii, Y. (2007), Atmospheric outflow of anthropogenic semivolatile organic compounds from East Asia in spring 2004. *Environmental Science & Technology* 41, 3551–3558.

Real, E., K. S. Law, B. Weinzierl, M. Fiebig, A. Petzold, O. Wild, J. Methven, S. Arnold, A. Stohl, H. Huntrieser, A. Roiger, H. Schlager, D. Stewart, M. Avery, G. Sachse, E. Browell, R. Ferrare, and D. Blake (2007), Processes influencing ozone levels in Alaskan forest fire plumes during long-range transport over the North Atlantic, *J. Geophys. Res.*, 112, D10S41, doi:10.1029/2006JD007576.

Real, E. and K. Sartelet (2011), Modeling of photolysis rates over Europe: impact on chemical gaseous species and aerosols, *Atmos. Chem. Phys*., 11, 1711-1727, doi:10.5194/acp-11-1711-2011.

Reid, J. S., Koppmann, R., Eck, T. F., and Eleuterio, D. P. (2005), A review of biomass burning emissions part II: intensive physical proper- ties of biomass burning particles, *Atmos. Chem. Phys*., 5, 799– 825, doi:10.5194/acp-5-799-2005.

Reidmiller, D.R., Fiore, A.M., Jaffe, D.A., Bergmann, D., Cuvelier, C., Dentener, F.J., Duncan, B.N., Folberth, G., Gauss, M., Gong, S., Hess, P., Jonson, J.E., Keating, T., Lupu, A., Marmer, E., Park, R., Schultz, M.G., Shindell, D.T., Szopa, S., Vivanco, M.G., Wild, O., and Zuber, A., (2009a), The influence of foreign vs. North American emissions on surface ozone in the US. *Atmospheric Chemistry and Physics* 9, 5027–5042, doi: 10.5194/acp-9-5027-2009.

Reidmiller, D.R., Jaffe, D.A., Chand, D., Strode, S., Swartzendruber, P., Wolfe, G.M., and Thornton, J.A. (2009b), Interannual variability of long-range transport as seen at the Mt. Bachelor Observatory. *Atmospheric Chemistry and Physics* 9, 557–572, doi:10.5194/acp-9-557-2009.

Reidmiller, D.R., Jaffe, D. A., Fischer, E. V. and Finley, V., (2010), Nitrogen oxides in the boundary later and free troposphere at the Mt. Bachelor Observatory, *Atmos. Chem. Phys.* 10, 6043-6062.

Ridley, B. A., F. E. Grahek, (1990), A Small, Low Flow, High Sensitivity Reaction Vessel for NO Chemiluminescence Detectors. *J. Atmos. Oceanic Technol.* 7, 307–311.

Rubio, M. A., E. Lissi, E. Gramsch, and R. D. Garreaud (2015), Effect of nearby forest fires on ground level ozone concentrations in Santiago, Chile, *Atmosphere*, 6, 1926–1938, doi:10.3390/atmos6121838.

Ryerson, T. B., et al. (2001), Observations of ozone formation in power plant plumes and implications for ozone control strategies, *Science* 292, 719–723.

Ryerson, T. B., Buhr, M. P., Frost, G. J., Goldan, P. D., Hol- loway, J. S., Hu ̈bler, G., Jobson, B. T., Kuster, W. C., McKeen, S. A., Parrish, D. D., Roberts, J. M., Sueper, D. T., Trainer, M., Williams, J., and Fehsenfeld, F. C. (1998), Emissions lifetimes and ozone formation in power plant plumes, J. *Geophys. Res*., 103, 22569–22583.

Seinfeld, J. H. and S. N. Pandis (1998), *Atmospheric Chemistry and Physics*, Wiley-Interscience, New York, 1326 pp.

Shetter, R. E., W. Junkermann, W. H. Swartz, G. J. Frost, J. H. Crawford, B. L. Lefer, J. D. Barrick, S. R. Hall, A. Hofzumahaus, A. Bias, J. G. Calvert, C. A. Cantrell, S. Madronich, M. Muller, A. Kraus, P. S. Monks, G. D. Edwards, R. McKenzie, P. Johnston, R. Schmitt, E. Griffioen, M. Krol, A. Kylling, R. R. Dickerson, S. A. Lloyd, T. Martin, B. Gardiner, B. Mayer, G. Pfister, E. P. Roth, P. Koepke, A. Ruggaber, H. Schwander, and M. van Weele (2003), Photolysis frequency of NO2: Measurement and modeling during the International Photolysis Frequency Measurement and Modeling Intercomparison (IPMMI), *J. Geophys. Res*., 108, 8544, doi:10.1029/2002JD002932, D16.

Shon, Z.-H., Madronich, S., Song, S.-K., Flocke, F. M., Knapp, D. J., Anderson, R. S., Shetter, R. E., Cantrell, C. A., Hall, S. R., and Tie, X. (2008), Characteristics of the NO-NO2-O3 system in different chemical regimes during the MIRAGE-Mex field campaign, *Atmos. Chem. Phys*., 8, 7153–7164, doi:10.5194/acp-8-7153-2008.

Sillman, S. (1999), The relation between ozone, NOx and hydrocarbons in urban and polluted rural environments, *Atmos. Environ*. 33, 1821-1845.

Sillman, S. (2000), Ozone production efficiency and loss of NO_X in power plant plumes: Photochemical model and interpretation of measurements in Tennessee, *J. Geophys. Res*., 105, 9189–9202.

Singh, H. B., Anderson, B. E., Brune, W. H., Cai, C., Cohen, R. C., Crawford, J. H., Cubison, M. J., Czech, E. P., Emmons, L., Fu- elberg, H. E., Huey, G., Jacob, D. J., Jimenez, J. L., Kaduwela, A., Kondo, Y., Mao, J., Olson, J. R., Sachse, G. W., Vay, S. A., Weinheimer, A., Wennberg, P. O., Wisthaler, A., and the ARC- TAS Science Team. (2010), Pollution influences on atmospheric compo- sition and chemistry at high northern latitudes: Boreal and California forest fire emissions, *Atmos. Environ*., 44, 4553–4564, doi:10.1016/j.atmosenv.2010.08.026.

Singh, H. B., Cai, C., Kaduwela, A., Weinheimer, A., and Wisthaler, A. (2012), Interactions of fire emissions and urban pollution over California: Ozone formation and air quality simulations, *Atmos. Environ*., 56, 45–51, doi:10.1016/j.atmosenv.2012.03.046.

Smith, D.J., Griffin, D.W., and Jaffe, D.A. (2011), The high life: Transport of microbes in the atmosphere. *EOS,Transactions American Geophysical Union* 92, No. 30, 249–250, doi: 10.1029/2011EO300001.

Smith, D.J., Jaffe, D.A., Birmele, M.N., Griffin, D.W., Schuerger, A.C., Hee, J., and Roberts, M.S. (2012), Free tropospheric transport of microorganisms from Asia to North America. *Microbial Ecology* 64, 973–985, doi: 10.1007/s00248-012-0088-9.

Smith, D.J., Timonen, H.J., Jaffe, D.A., Griffin, D.W., Birmele, M.N., Perry, K.D., Ward, P.D., and Roberts, M.S. (2013), Intercontinental Dispersal of Bacteria and Archaea in Transpacific Winds. *Applied and Environmental Microbiology* 79, 1134–1139, doi: 10.1128/AEM.03029-12.

Stobie, J. M., et al. (1985), The use of optimum interpolation at AFGWC, Proc., 7th Conference on Numerical Weather Prediction, Montreal, *Amer. Meteor. Soc*. 43-49.

Stobie, J. M. (2000), Algorithm Theoretical Basis Document for Statistical Digital Filter (SDF) Analysis System (Stretch-Grid Version), Data Assimilation Office, NASA Goddard Space Flight Center, Greenbelt, MD, 20771.

Strode, S., Jaeglé, L., Jaffe, D., Swartzendruber, P., Selin, N., Holmes, C., and Yantosca, R. (2008), Trans-Pacific transport of mercury. *Journal of Geophysical Research* 113, D15305, doi: 10.1029/2007JD009428.

Suthawaree, J., Kato, S., Takami, A., Hatakeyama, S., Kadena, H., Togushi, M., Tomoyose, N., Yogi, K., Jaffe, D.A., Swartzendruber, P., Prestbo, E., and Yoshizumi, K. (2007), Influence from long-range transport of Asian outflow on O3, CO and VOCs concentrations during an intensive measurement campaign at Cape Hedo, Okinawa, in spring 2004. *Journal of Japan Society for Atmospheric Environment* 42, 350–361.

Swartzendruber, P.C., Chand, D., Jaffe, D.A., Smith, J., Reidmiller, D., Gratz, L., Keeler, J., Strode, S., Jaeglé, L., and Talbot R. (2008), The vertical distribution of mercury, CO, ozone, and aerosol scattering coefficient in the Pacific Northwest during the spring 2006 INTEX-B campaign. *Journal of Geophysical Research-Atmospheres* 113, D10305, doi: 10.1029/2007JD009579.

Takahashi, K., N. Taniguchi, Y. Matsumi, M. Kawasaki, and M. N. R. Ashfold (1998), Wavelength and temperature dependence of the absolute O(^{1}D) production yield from the 305 – 329 nm photodissociation of ozone, *J. Chem. Phys., 108*, 7161 – 7172.

Tang, Y., G. R. Carmichael, I. Uno, J. H. Woo, G. Kurata, B. Lefer, R. E. Shetter, H. Huang, B. E. Anderson, M. A. Avery, A. D. Clarke, and D. R. Blake (2003), Impacts of aerosols and clouds on photolysis frequencies and photochemistry during TRACE-P: 2. Three-dimensional study using a regional chemical transport model, *J. Geophys. Res*., 108, 8822, doi:10.1029/2002JD003100, D21.

Teakles, A.D., So, R., Ainslie, B., Nissen, R., Schiller, C., Vingarzan, R., McKendry, I., Macdonald, A.M., Jaffe, D.A., et al. (2017), Impacts of the July 2012 Siberian fire plume on air quality in the Pacific Northwest. *Atmospheric Chemistry and Physics* 17, 2593–2611, doi: 10.5194/acp-17-2593-2017.

Thompson, A. M. (1984), The effect of clouds on photolysis rates and ozone formation in the unpolluted troposphere, *J. Geophys. Res*., 89(D1), 1341–1349, doi:10.1029/JD089iD01p01341.

Timonen, H., Wigder, N., and Jaffe, D.A. (2013), Influence of background particulate matter (PM) on urban air quality in the Pacific Northwest. *Journal of Environmental Management* 129, 333–340, doi:10.1016/j.jenvman.2013.07.023.

Timonen, H., Jaffe, D.A., Wigder, N., Hee, J., Gao, H., Pitzman, L., and Cary, R.A. (2014), Sources of carbonaceous aerosol in the free troposphere. *Atmospheric Environment* 92, 146–153, doi: 10.1016/j.atmosenv.2014.04.014.

Trainer, M. et al. (1993), Correlation of Ozone with NO_y in Photochemically Aged Air. *J. Geophys. Res*. 98, 2917-2925.

U.S. Environmental Protection Agency, Office of Research and Development, Washington DC (EPA-600/R-05/004aF-cF), Air quality criteria for ozone and related photochemical oxidants, 2006; http://cfpub.epa.gov/ncea/cfm/recordisplay.cfm?deid¼149923.

U.S. Environmental Protection Agency (EPA), National Emissions Inventory (NEI) air pollutant emissions trends data, 2012; http://www.epa.gov/ttnchie1/trends/.

U.S. Environmental Protection Agency (EPA). National ambient air quality standards for ozone, Final rule, 2015.

Vakkari, V., Kerminen, V. M., Beukes, J. P., Tiitta, P., van Zyl, P. G., Josipovic, M., Venter, A. D., Jaars, K., Worsnop, D. R., Kulmala, M., and Laakso, L. (2014), Rapid changes in biomass burning aerosols by atmospheric oxidation, *Geophys. Res. Lett*., 41, 2644–2651, doi:10.1002/2014gl059396.

Val Martín, M., R. E. Honrath, R. C. Owen, G. Pfister, P. Fialho, and F. Barata (2006), Significant enhancements of nitrogen oxides, black carbon, and ozone in the North Atlantic lower free troposphere resulting from North American boreal wildfires, *J. Geophys. Res.*, *111*, D23S60, doi:10.1029/2006JD007530.

Val Martin, M.; Honrath, R.; Owen, R.C.; Pfister, G.; Fialho, P.; and Barata, F. (2006), Significant enhancements of nitrogen oxides, ozone and aerosol black carbon in the North Atlantic lower free troposphere resulting from North American boreal wildfires. *J. Geophys. Res.* 111, D23S60, DOI:10.1029/2006JD007530.

Val Martin, M., Honrath, R.E., Owen, R.C., Lapina, K., (2008), Large-scale impacts of anthropogenic pollution and boreal wildfires on the nitrogen oxides over the central North Atlantic region. *Journal of Geophysical Research-Atmospheres* 113, D17308.

Verstraeten, W. W., J. L. Neu, J. Williams, K. W. Bowman, J. R. Worden, and K. F. Boersma (2015), Rapid increases in tropospheric ozone production and export from China, *Nat. Geosci*. 8, 690–695, doi:10.1038/ngeo2493.

Voulgarakis, A., O. Wild, N. H. Savage, G. D. Carver, J. A. Pyle (2009), Clouds, photolysis and regional tropospheric ozone budgets, *Atmos. Chem. Phys*., 9, 8235-8246, doi:10.5194/acp-9-8235-2009.

Wai, K.M., Wu, S., Li, X., Jaffe, D.A., and Perry, K.D. (2016), Global atmospheric transport and source-receptor relationships for arsenic. *Environmental Science & Technology* 50, 3714–3720, doi: 10.1021/acs.est.5b05549.

Weiss-Penzias, P., Jaffe, D.A., Swartzendruber, P., Dennison, J.B., Chand, D., Hafner, W., and Prestbo, E. (2006), Observations of Asian air pollution in the free troposphere at Mt. Bachelor Observatory in the spring of 2004. *Journal of Geophysical Research* 111, D10304, doi: 10.1029/2005JD006522.

Weiss-Penzias, P., Jaffe, D.A., Swartzendruber, P., Hafner, W., Chand, D., and Prestbo, E. (2007), Quantifying Asian biomass burning sources of mercury using the Hg/CO ratio in pollution plumes observed at the Mount Bachelor Observatory. *Atmospheric Environment* 41, 4366–4379, doi: 10.1016/j.atmosenv.2007.01.058.

Wigder, N.L.; Jaffe, D.A.; Saketa, F.A. (2013a), Ozone and particulate matter enhancements from regional wildfires observed at Mount Bachelor during 2004–2011. *Atmos. Environ.* 75, 24–31, DOI: 10.1016/j.atmosenv.2013.04.026.

Wigder, N.L.; Jaffe, D.A.; Herron-Thorpe, F.L.; Vaughan, J.K. (2013b), Influence of daily variations in baseline ozone on urban air quality in the United States Pacific Northwest. *J. Geophys. Res. Atmos.* 118, 3343–3354, DOI: 10.1029/2012JD018738.

Wolfe, G.M., Thornton, J.A., McNeill, V.F., Jaffe, D.A., Reidmiller, D., Chand, D., Smith, J., Swartzendruber, P., Flocke, F., and Zheng, W. (2007), Influence of trans-Pacific pollution transport on acyl peroxy nitrate abundances and speciation at Mount Bachelor Observatory during INTEX-B. *Atmospheric Chemistry and Physics* 7, 5309–5325, doi: 10.5194/acp-7-5309-2007.

Yates, E.L.; Iraci, L.T; Roby, M.C.; Pierce, R.B.; Johnson, M.S.; Reddy, P.J.; Tadic, J.M.; Loewenstein, M.; Gore, W. (2013), Airborne observations and modeling of springtime stratosphere-to-troposphere transport over California. *Atmos. Chem. Phys*. 13, 12481–12494, doi:10.5194/acp-13-12481-2013.

Ying, Z., X. Tie, S. Madronich, G. Li, and S. Massie (2011), Simulation of regional dust and its effect on photochemistry in the Mexico City area during MILAGRO experiment, *Atmos. Environ*., 45, 2549-2558.

Yokelson, R. J., J. G. Goode, D. E. Ward, R. A. Susott, R. E. Babbitt, D. D. Wade, I. Bertschi, D. W. T. Griffith, and W. M. Hao (1999), Emissions of formaldehyde, acetic acid, methanol, and other trace gases from biomass fires in North Carolina measured by airborne Fourier transform infrared spectroscopy, *J. Geophys. Res.*, *104*(D23), 30,109–30,125, doi:10.1029/1999JD900817.

Yokelson, R.J., Christian, T.J., Karl, T.G., Guenther, A., (2008), The tropical forest and fire emissions experiment: laboratory fire measurements and synthesis of campaign data. *Atmospheric Chemistry and Physics* 8, 3509e3527.

Yokelson, R.J., Burling, I.R., Urbanski, S.P., Atlas, E.L., Adachi, K., Buseck, P.R., Wiedinmyer, C., Akagi, S.K., Toohey, D.W., Wold, C.E., (2011), Trace gas and particle emissions from open biomass burning in Mexico. *Atmospheric Chemistry and Physics* 11, 6787e6808.

Zhang, L., Jacob, D.J., Boersma, K.F., Jaffe, D.A., Olson, J.R., Bowman, K.W., Worden, J.R., Thompson, A.M., Avery, M.A., Cohen, R.C., Dibb, J.E., Flock, F.M., Fuelberg, H.E., Huey, L.G., McMillan, W.W., Singh, H.B., and Weinheimer, A.J. (2008), Transpacific transport of ozone pollution and the effect of recent Asian emission increases on air quality in North America: an integrated analysis using satellite, aircraft, ozonesonde, and surface observations. *Atmospheric Chemistry and Physics* 8, 6117–6136.

Zhang, L., Jacob, D.J., Kopacz, M., Henze, D.K., Singh, K., and Jaffe, D.A. (2009), Intercontinental source attribution of ozone pollution at western U.S. sites using an adjoint method. *Geophysical Research Letters* 36, L11810, doi: 10.1029/2009GL037950.

Zhao, T.L., Gong, S.L., Zhang, X.Y., and Jaffe, D.A. (2008), Asian dust storm influence on North American ambient PM levels: observational evidence and controlling factors, *Atmospheric Chemistry & Physics* 8, 2717–2728.

Zhou, S., Collier, S., Jaffe, D.A., Briggs, N.L., Hee, J., Sedlacek, A.G., III, Kleinman, L., Onasch, T.B., and Zhang, Q. (2017), Regional influence of wildfires on aerosol chemistry in the western US and insights into atmospheric aging of biomass burning organic aerosol. *Atmospheric Chemistry and Physics* 17, 2477–2493, doi: 10.5194/acp-17-2477-2017.

APPENDIX A

CO-AUTHORS AND CONTRIBUTIONS

Chapter 2 was previously published with the following co-authors:

Daniel A. Jaffe[1,2], R. Bradley Pierce[3], Mae S. Gustin[4]

R. Bradley Pierce performed Real-time Air Quality Modeling System (RAQMS) runs and helped in the analysis. Mae S. Gustin provided ozone measurements for the South Fork State Recreation Area, NV (SFSR) and Berlin-Ichthyosaur State Park, NV (BISP) sites through the Nevada Rural Ozone network. The authors thank Jonathan Hee for preparing the final datasets at MBO. Funding for research at MBO was supported by the National Science Foundation (grant number: 1447832). The MBO is also supported by a grant from the NOAA Earth System Research Laboratory.

Chapter 3 was developed in consultation with:

Daniel A. Jaffe[1,2], Samuel R. Hall[5], Kirk Ulmann[5], Barry Lefer[6]

Samuel R. Hall and Kirk Ulmann assisted in the calibration of the Diode Array Actinic Flux Spectroradiometer (DAFS) at NCAR, conversion of the actinic flux data into photolysis rates, and in proofreading the manuscript. Barry Lefer loaned us the DAFS. The authors like to thank the MBO ski area for their support and assistance. Funding for research at MBO was supported by the National Science Foundation (grant number: 1447832). The MBO is also supported by a grant from the NOAA Earth System Research Laboratory.

Chapter 4 was developed in consultation with:

Daniel A. Jaffe[1,2], Joost de Gouw[7], Carsten Warneke[7]

Joost de Gouw and Carsten Warneke helped in the analysis of the SONGNEX aircraft data. We thank John Holloway for the CO data; Charles Brock for the aerosol scattering data; Tom Ryerson for the ozone and NOy data; Patrick Veres for the PAN data; Andy Neuman for the HNO_3 data; and Robert Wild for the NOx data. We thank Jonathan Hee for finalizing the MBO datasets. We also thank the MBO staff for their support and assistance. Funding for research at MBO was supported by the National Science Foundation (grant number: 1447832) and the NOAA Earth System Research Laboratory.

[1] Department of Atmospheric Sciences, University of Washington, 408 Atmospheric Sciences–Geophysics Building, Seattle, Washington 98195, United States.

[2] School of Science, Technology, Engineering and Mathematics, University of Washington Bothell, 18115 Campus Way NE, Bothell, Washington 98011, United States.

[3] NOAA/NESDIS, Center for Satellite Applications and Research, Advanced Satellite Products Branch, 1225 West Dayton Street, Madison, Wisconsin 53705, United States.

[4] Department of Natural Resources and Environmental Science, University of Nevada–Reno, Reno, Nevada 89557, United States.

[5] Atmospheric Chemistry Division, National Center for Atmospheric Research, 3090 Center Green Drive, Boulder, Colorado 80301, United States.

[6] NASA Earth Science Division, 300 E Street SW, Washington, DC 20546, United States.

[7] NOAA Earth System Research Laboratory, 325 Broadway, Boulder, CO 80305, United States.

APPENDIX B

SATELLITE IMAGES FROM GOES-WEST ON AUGUST 2015

These are retrievals from the GOES-WEST geostationary satellite on August 18, 2015 over Mt. Bachelor Observatory (MBO) (red star).

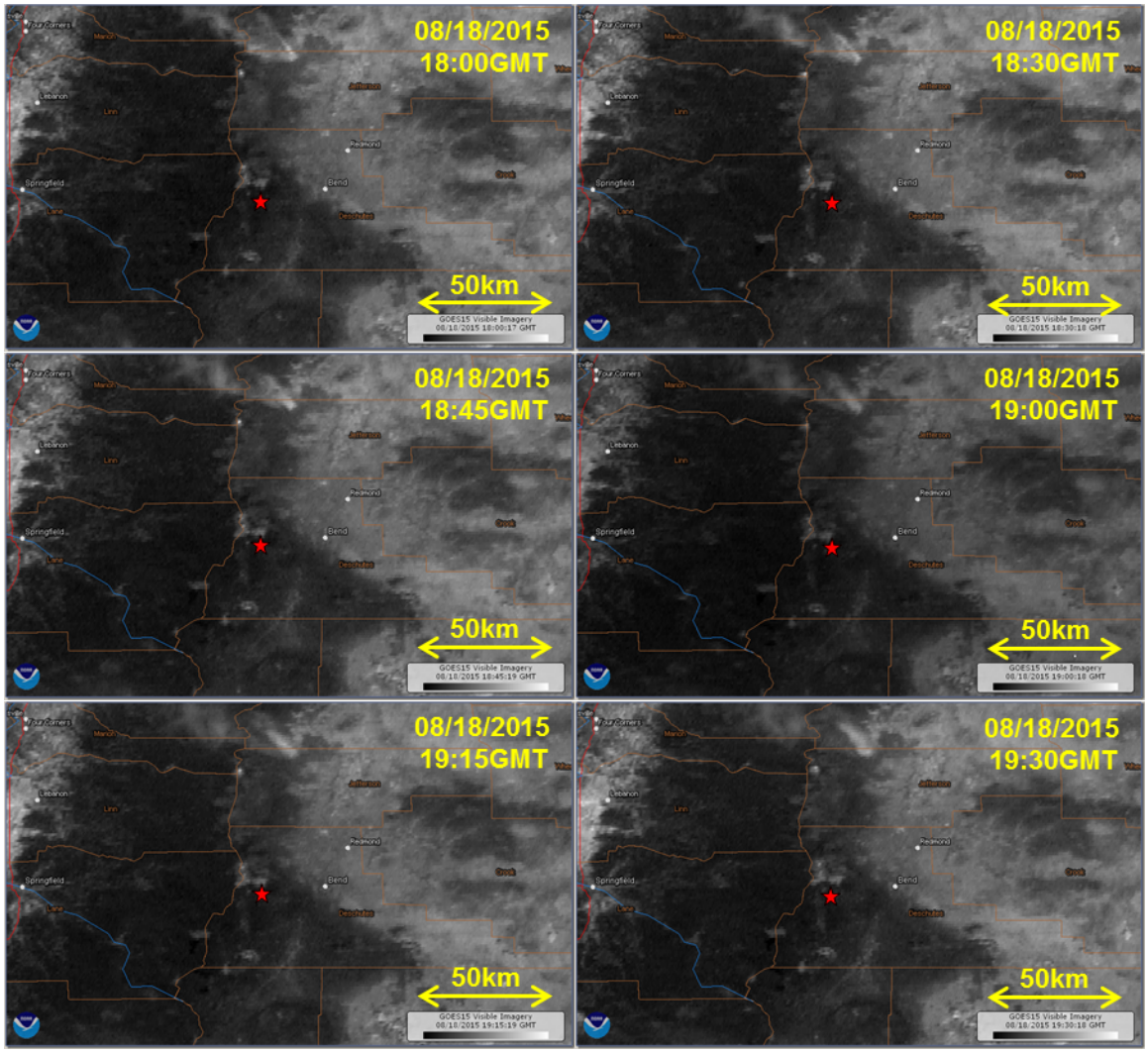

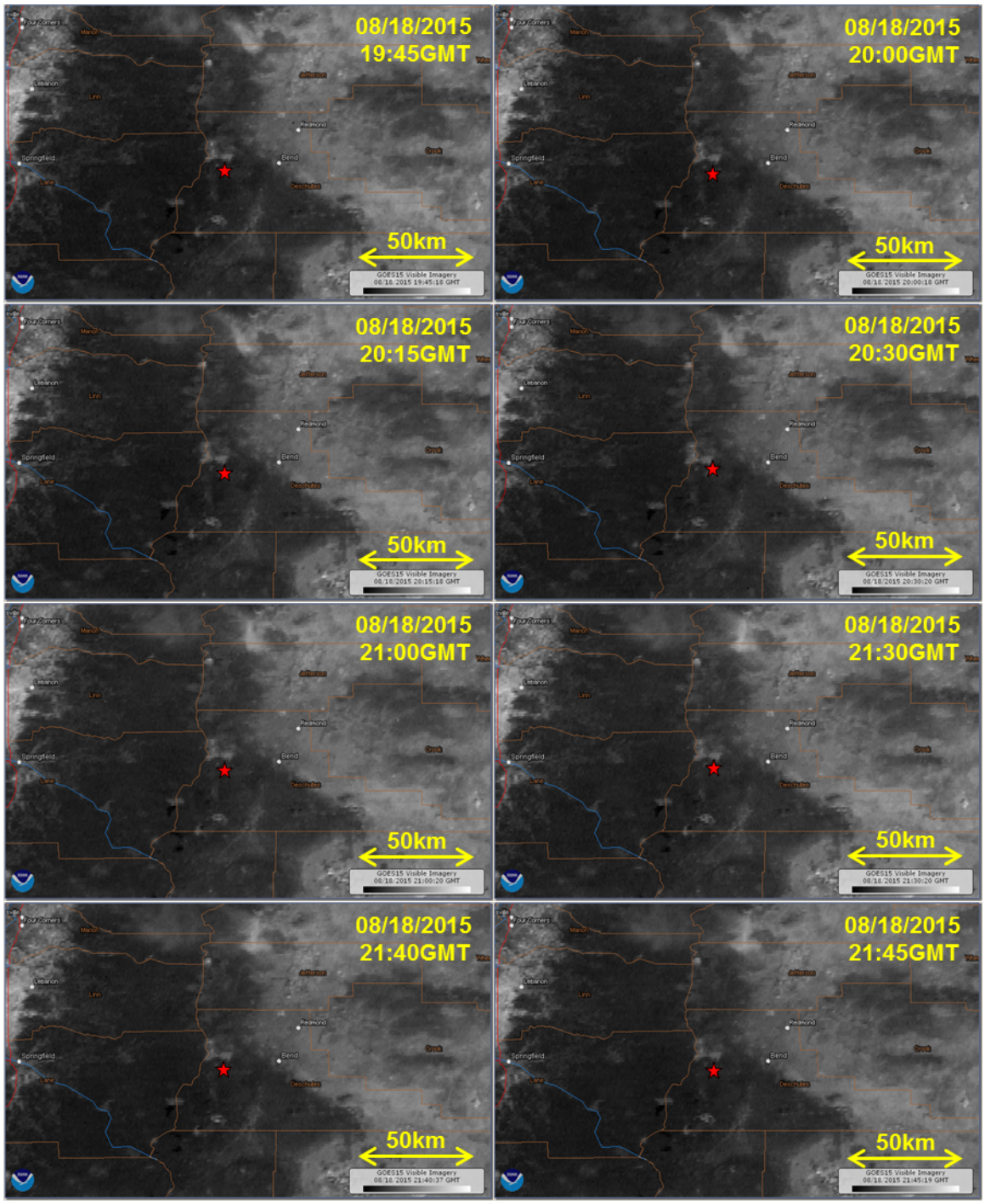

These are retrievals from the GOES-WEST geostationary satellite on August 25, 2015 over MBO (red star).

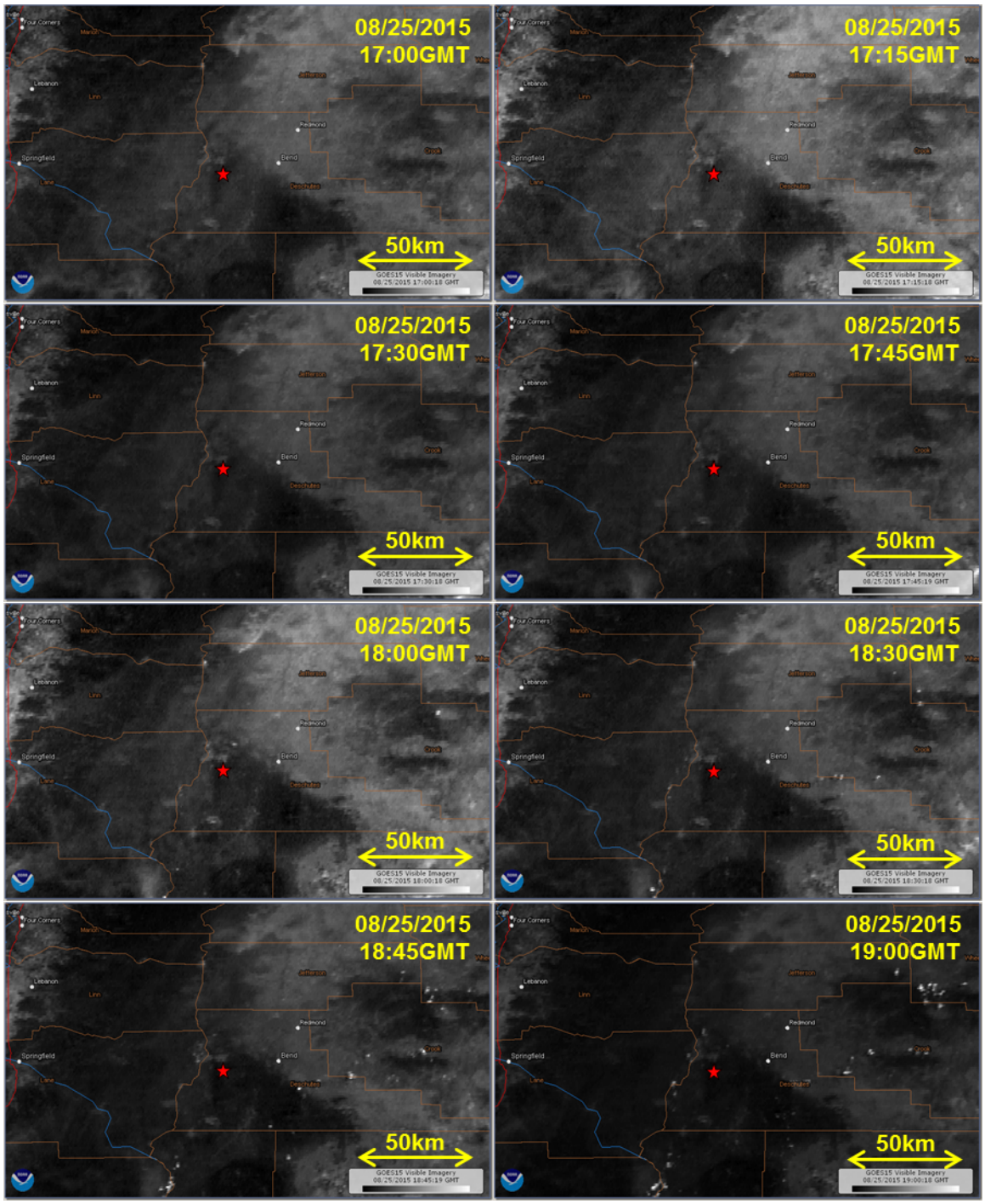
08/25/2015
17:00GMT
50km
08/25/2015
17:15GMT
50km
08/25/2015
17:30GMT
50km
08/25/2015
17:45GMT
50km
08/25/2015
18:00GMT
50km
08/25/2015
18:30GMT
50km
08/25/2015
18:45GMT
50km
08/25/2015
19:00GMT
50km

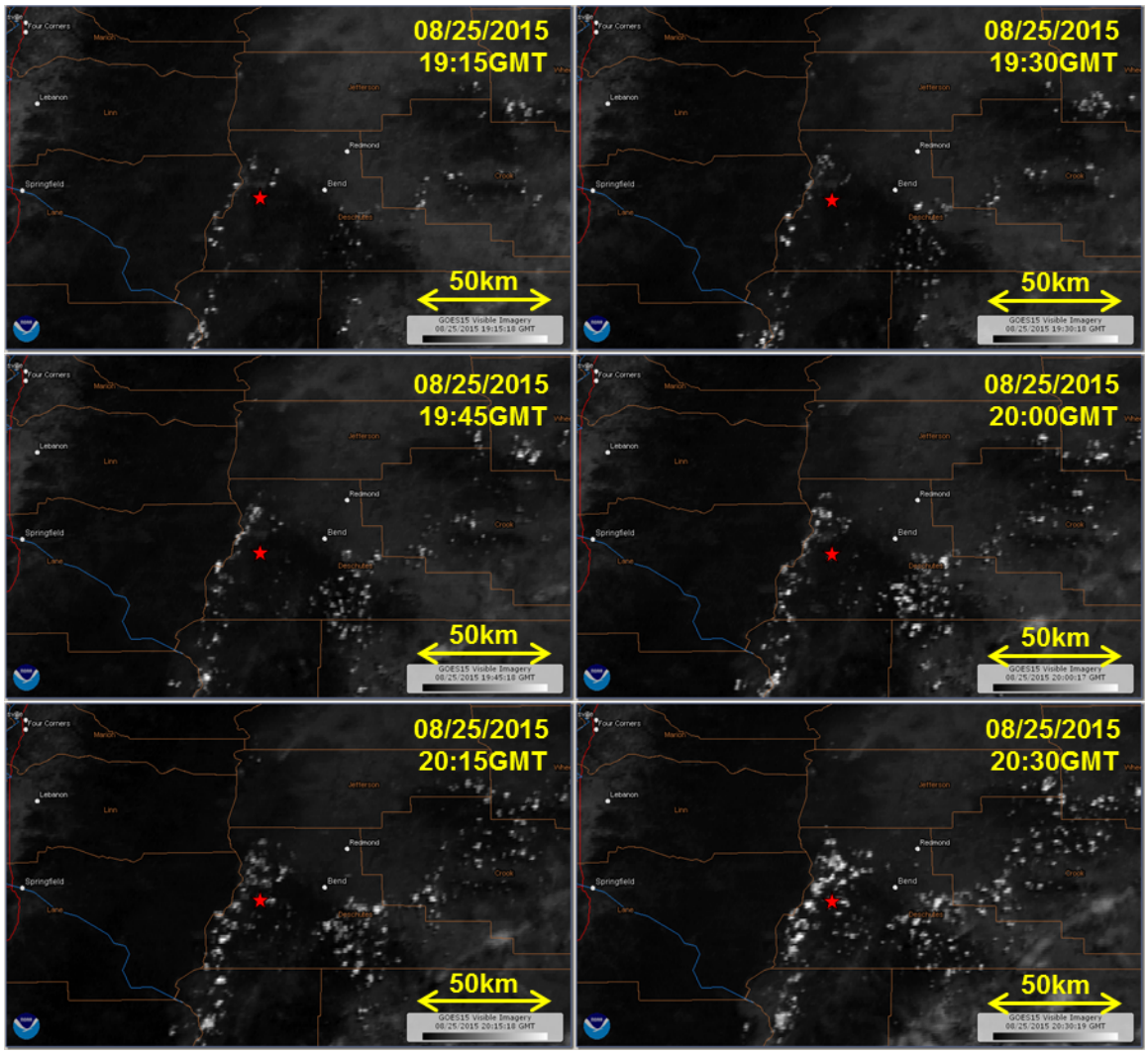
08/25/2015
19:15GMT
50km
08/25/2015
19:30GMT
50km
08/25/2015
19:45GMT
50km
08/25/2015
20:00GMT
50km
08/25/2015
20:15GMT
50km
08/25/2015
20:30GMT
50km

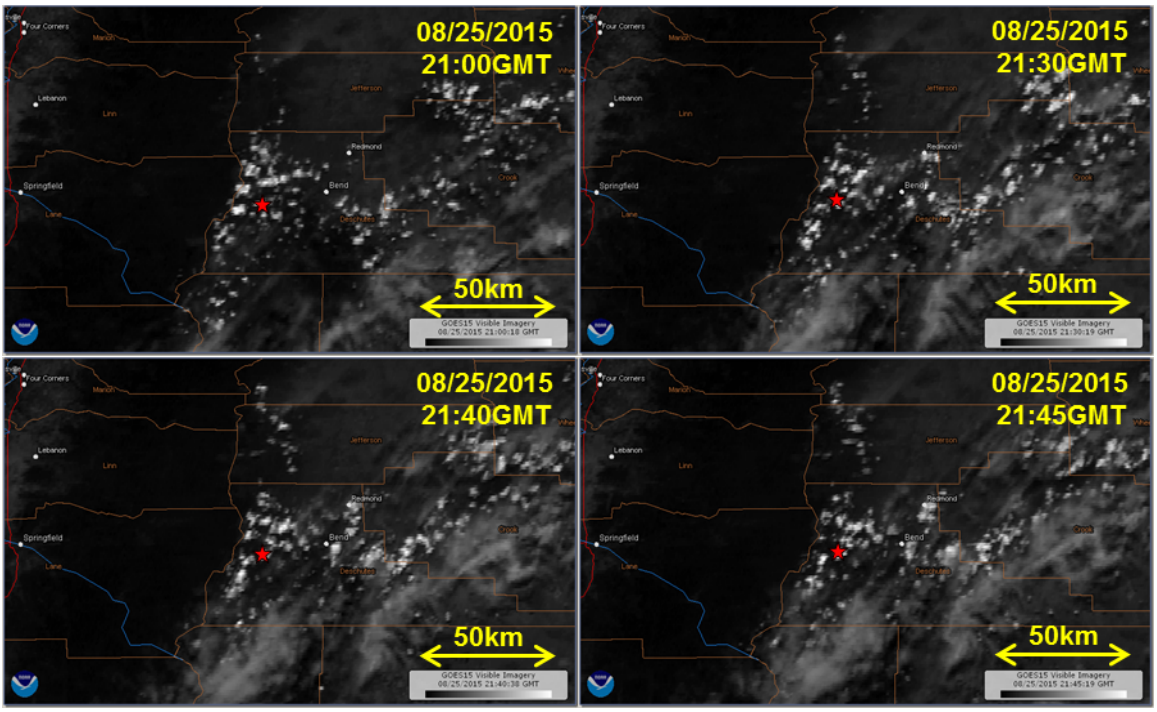

These are retrievals from the GOES-WEST geostationary satellite on August 29, 2015 over MBO (red star).

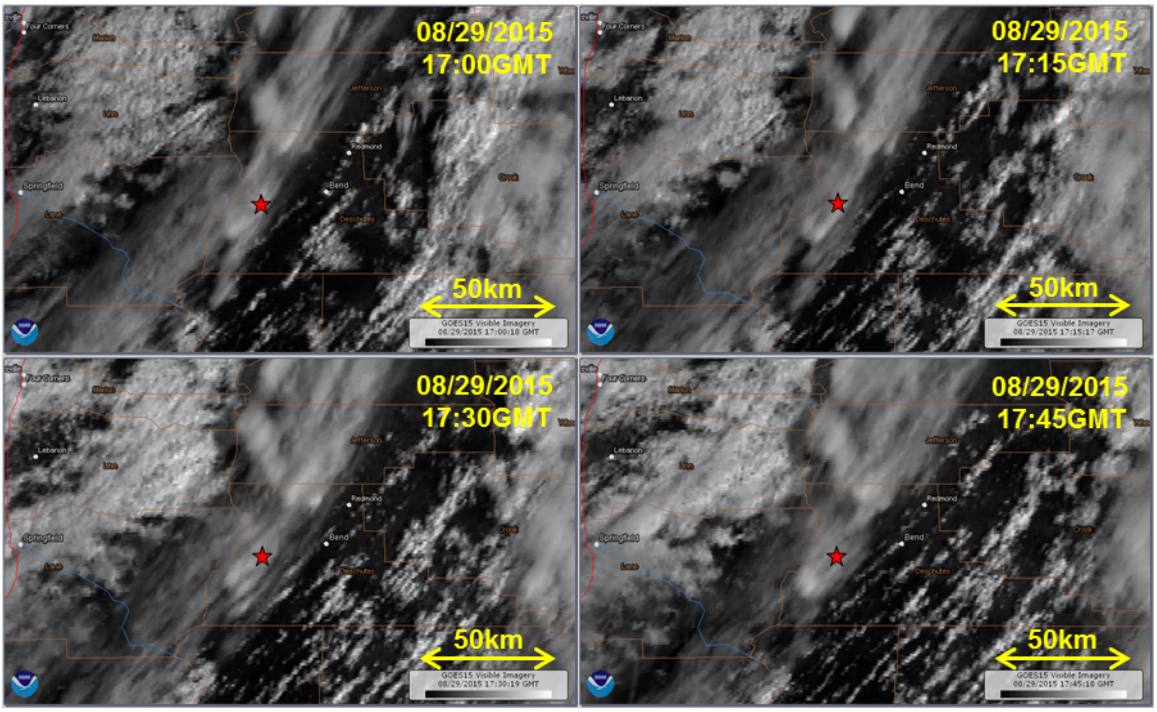

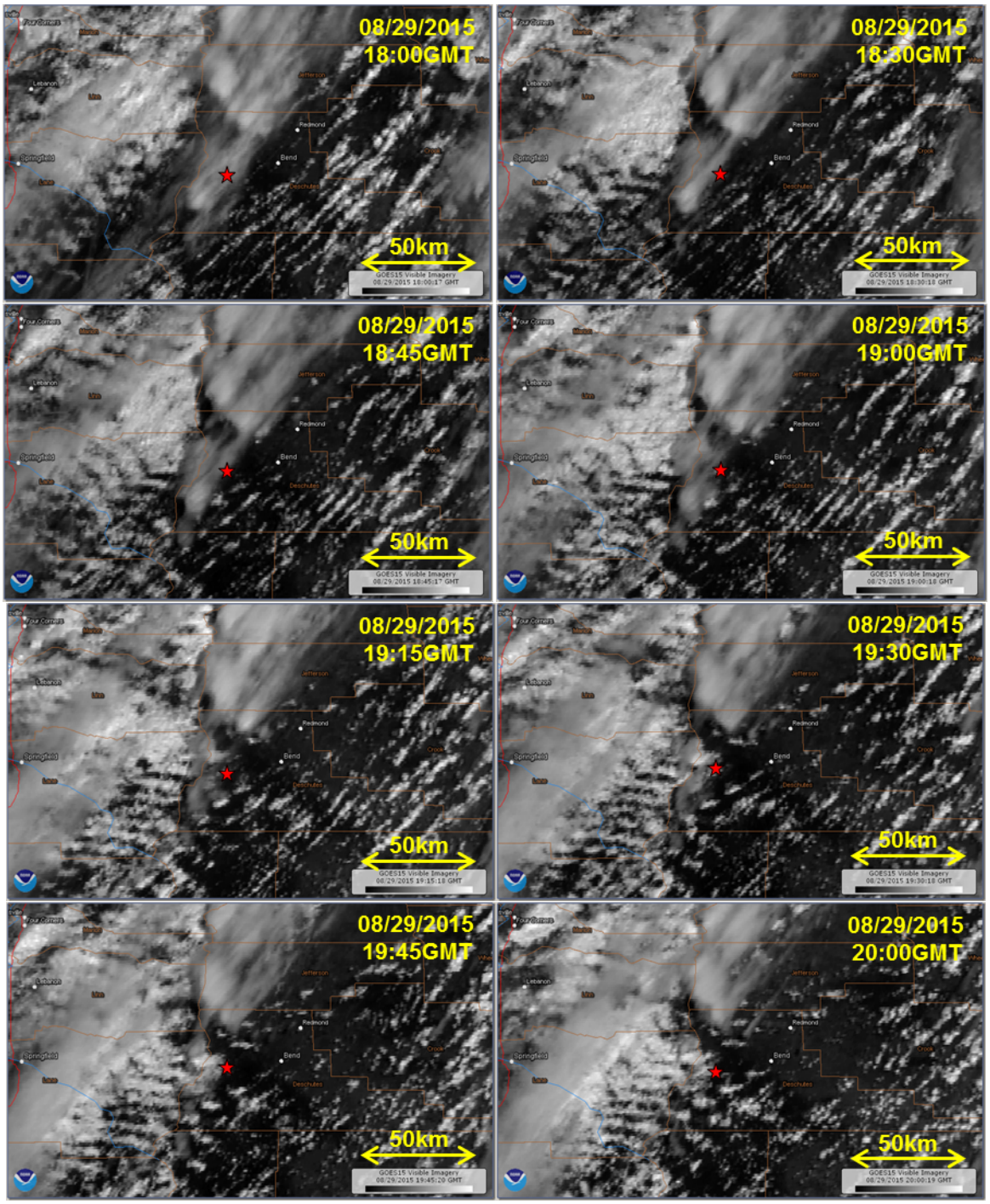
08/29/2015
18:00GMT
50km
08/29/2015
18:30GMT
50km
08/29/2015
18:45GMT
50km
08/29/2015
19:00GMT
50km
08/29/2015
19:15GMT
50km
08/29/2015
19:30GMT
50km
08/29/2015
19:45GMT
50km
08/29/2015
20:00GMT
50km

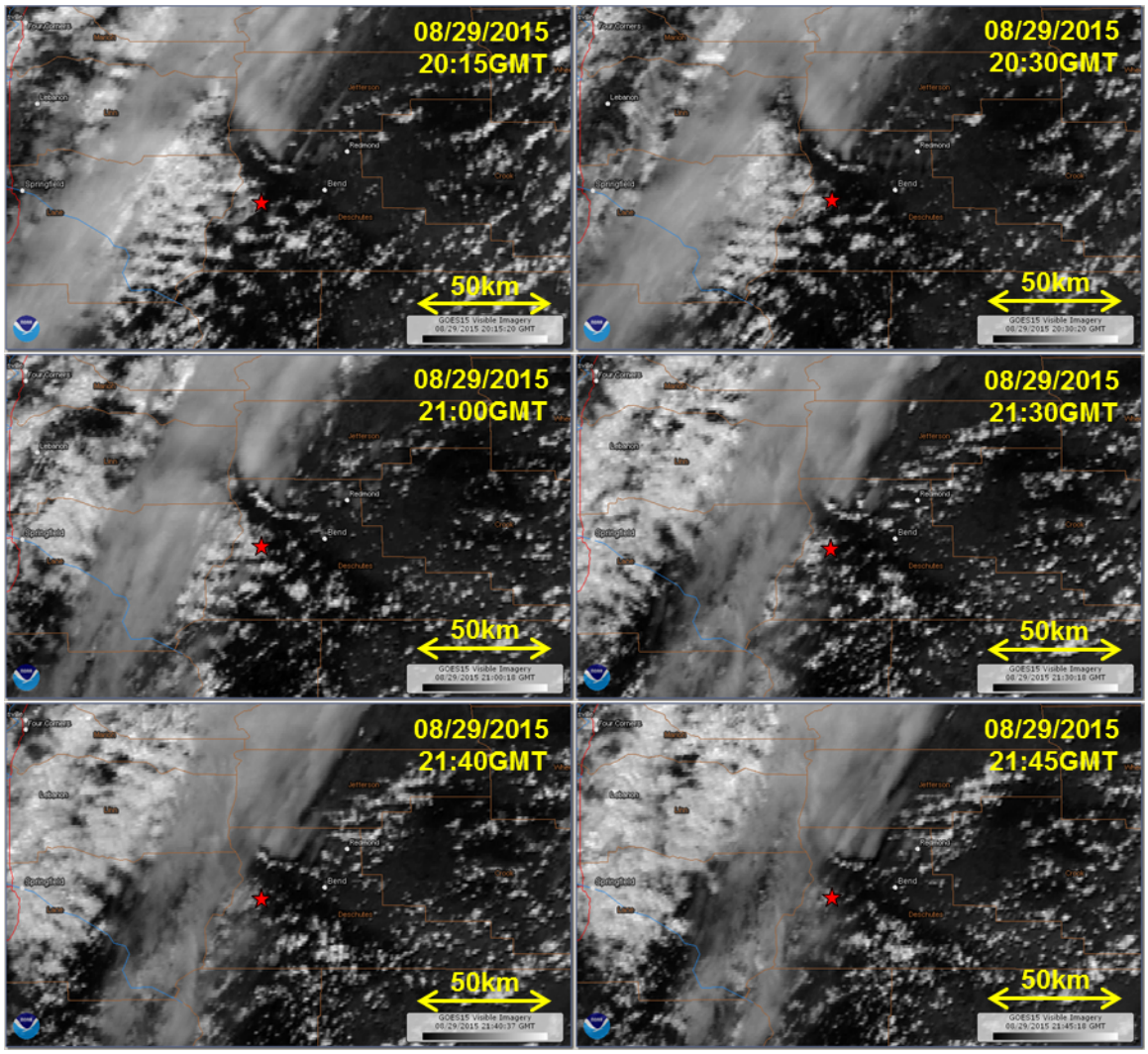
08/29/2015
20:15GMT
50km
08/29/2015
20:30GMT
50km
08/29/2015
21:00GMT
50km
08/29/2015
21:30GMT
50km
08/29/2015
21:40GMT
50km
08/29/2015
21:45GMT
50km

APPENDIX C

FORWARD DISPERSION RUNS FROM HYSPLIT ON APRIL 2015

These are HYSPLIT forward dispersion runs initiated on April 20, 2015 at MBO (43.979N, 121.687W) using meteorology obtained from GDAS. Release top: 6000 m a.g.l.; release bottom: 2000 m a.g.l.

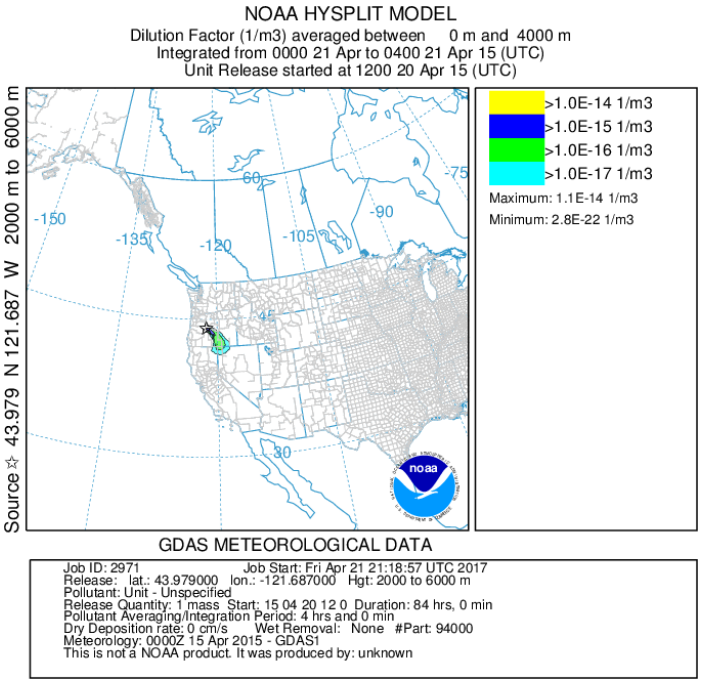

NOAA HYSPLIT MODEL
Dilution Factor (1/m3) averaged between 0 m and 4000 m
Integrated from 0800 21 Apr to 1200 21 Apr 15 (UTC)
Unit Release started at 1200 20 Apr 15 (UTC)

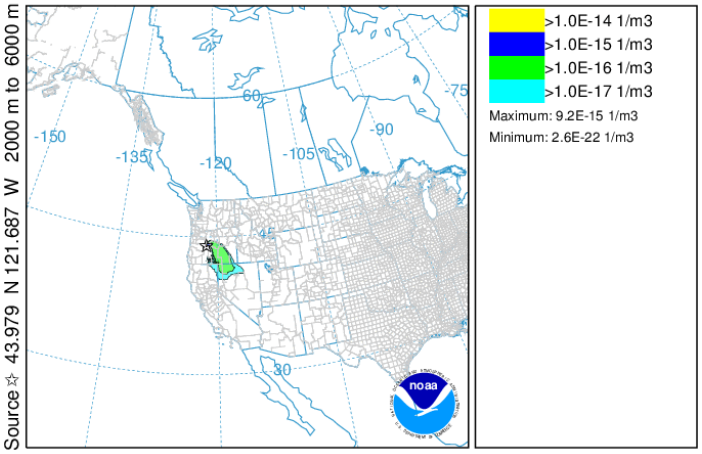

GDAS METEOROLOGICAL DATA

Job ID: 2971 Job Start: Fri Apr 21 21:18:57 UTC 2017
Release: lat.: 43.979000 lon.: -121.687000 Hgt: 2000 to 6000 m
Pollutant: Unit - Unspecified
Release Quantity: 1 mass Start: 15 04 20 12 0 Duration: 84 hrs, 0 min
Pollutant Averaging/Integration Period: 4 hrs and 0 min
Dry Deposition rate: 0 cm/s Wet Removal: None #Part: 94000
Meteorology: 0000Z 15 Apr 2015 - GDAS1
This is not a NOAA product. It was produced by: unknown

NOAA HYSPLIT MODEL
Dilution Factor (1/m3) averaged between 0 m and 4000 m
Integrated from 1600 21 Apr to 2000 21 Apr 15 (UTC)
Unit Release started at 1200 20 Apr 15 (UTC)

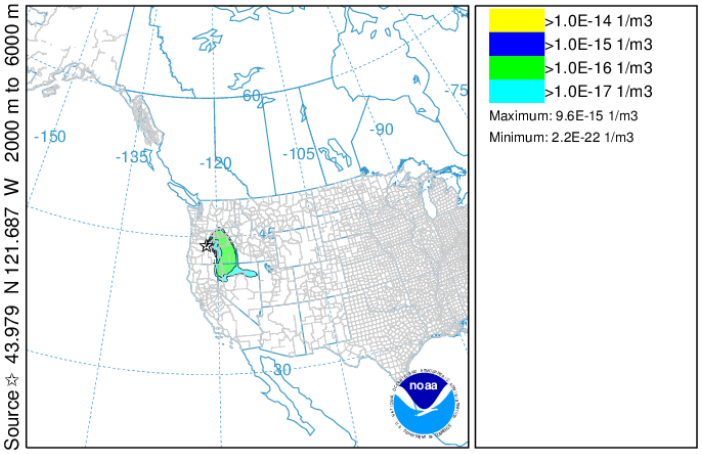

GDAS METEOROLOGICAL DATA

Job ID: 2971 Job Start: Fri Apr 21 21:18:57 UTC 2017
Release: lat.: 43.979000 lon.: -121.687000 Hgt: 2000 to 6000 m
Pollutant: Unit - Unspecified
Release Quantity: 1 mass Start: 15 04 20 12 0 Duration: 84 hrs, 0 min
Pollutant Averaging/Integration Period: 4 hrs and 0 min
Dry Deposition rate: 0 cm/s Wet Removal: None #Part: 94000
Meteorology: 0000Z 15 Apr 2015 - GDAS1
This is not a NOAA product. It was produced by: unknown

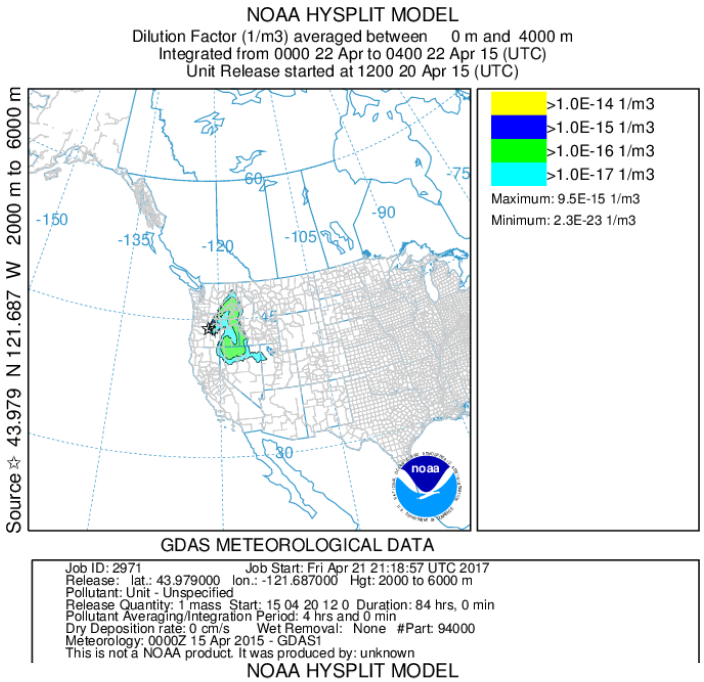
NOAA HYSPLIT MODEL
Dilution Factor (1/m3) averaged between 0 m and 4000 m
Integrated from 0000 22 Apr to 0400 22 Apr 15 (UTC)
Unit Release started at 1200 20 Apr 15 (UTC)
Source ☆ 43.979 N 121.687 W 2000 m to 6000 m
>1.0E-14 1/m3
>1.0E-15 1/m3
>1.0E-16 1/m3
>1.0E-17 1/m3
Maximum: 9.5E-15 1/m3
Minimum: 2.3E-23 1/m3
GDAS METEOROLOGICAL DATA
Job ID: 2971 Job Start: Fri Apr 21 21:18:57 UTC 2017
Release: lat.: 43.979000 lon.: -121.687000 Hgt: 2000 to 6000 m
Pollutant: Unit - Unspecified
Release Quantity: 1 mass Start: 15 04 20 12 0 Duration: 84 hrs, 0 min
Pollutant Averaging/Integration Period: 4 hrs and 0 min
Dry Deposition rate: 0 cm/s Wet Removal: None #Part: 94000
Meteorology: 0000Z 15 Apr 2015 - GDAS1
This is not a NOAA product. It was produced by: unknown

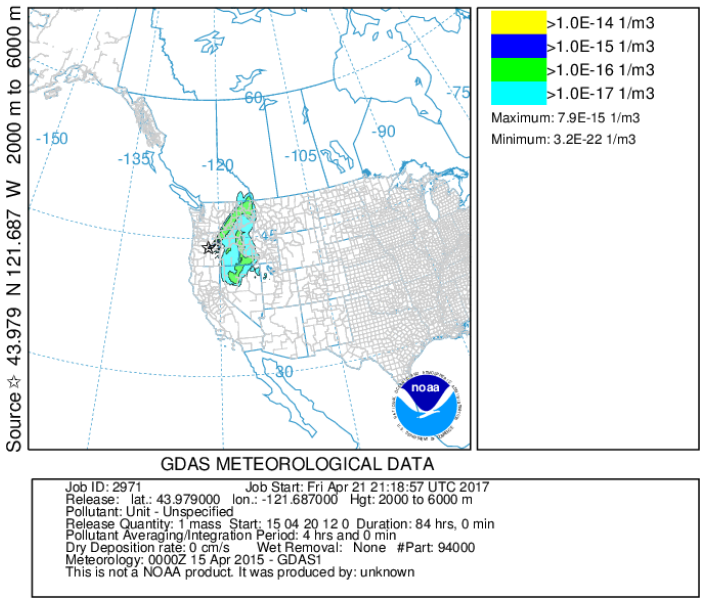
NOAA HYSPLIT MODEL
Dilution Factor (1/m3) averaged between 0 m and 4000 m
Integrated from 0800 22 Apr to 1200 22 Apr 15 (UTC)
Unit Release started at 1200 20 Apr 15 (UTC)
Source ☆ 43.979 N 121.687 W 2000 m to 6000 m
>1.0E-14 1/m3
>1.0E-15 1/m3
>1.0E-16 1/m3
>1.0E-17 1/m3
Maximum: 7.9E-15 1/m3
Minimum: 3.2E-22 1/m3
GDAS METEOROLOGICAL DATA
Job ID: 2971 Job Start: Fri Apr 21 21:18:57 UTC 2017
Release: lat.: 43.979000 lon.: -121.687000 Hgt: 2000 to 6000 m
Pollutant: Unit - Unspecified
Release Quantity: 1 mass Start: 15 04 20 12 0 Duration: 84 hrs, 0 min
Pollutant Averaging/Integration Period: 4 hrs and 0 min
Dry Deposition rate: 0 cm/s Wet Removal: None #Part: 94000
Meteorology: 0000Z 15 Apr 2015 - GDAS1
This is not a NOAA product. It was produced by: unknown

NOAA HYSPLIT MODEL
Dilution Factor (1/m3) averaged between 0 m and 4000 m
Integrated from 1600 22 Apr to 2000 22 Apr 15 (UTC)
Unit Release started at 1200 20 Apr 15 (UTC)

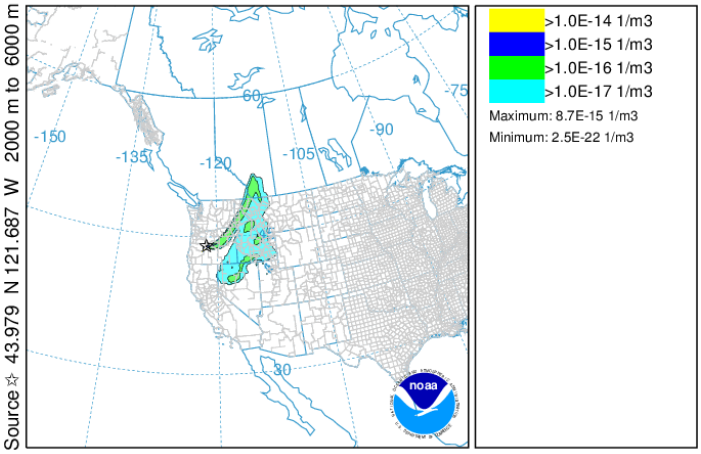

GDAS METEOROLOGICAL DATA

Job ID: 2971 Job Start: Fri Apr 21 21:18:57 UTC 2017
Release: lat.: 43.979000 lon.: -121.687000 Hgt: 2000 to 6000 m
Pollutant: Unit - Unspecified
Release Quantity: 1 mass Start: 15 04 20 12 0 Duration: 84 hrs, 0 min
Pollutant Averaging/Integration Period: 4 hrs and 0 min
Dry Deposition rate: 0 cm/s Wet Removal: None #Part: 94000
Meteorology: 0000Z 15 Apr 2015 - GDAS1
This is not a NOAA product. It was produced by: unknown

NOAA HYSPLIT MODEL
Dilution Factor (1/m3) averaged between 0 m and 4000 m
Integrated from 0000 23 Apr to 0400 23 Apr 15 (UTC)
Unit Release started at 1200 20 Apr 15 (UTC)

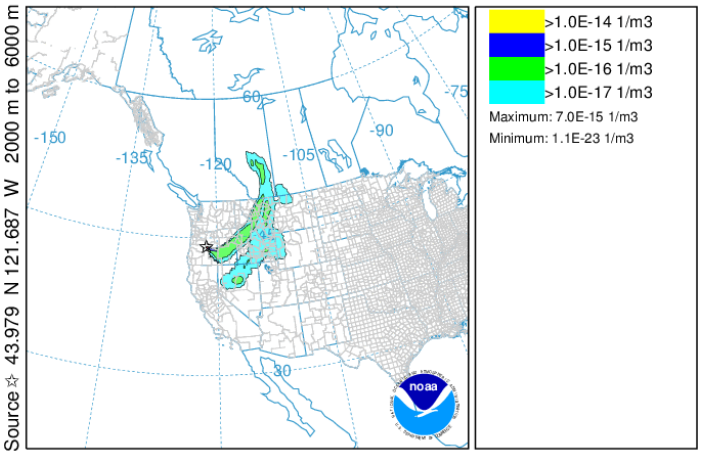

GDAS METEOROLOGICAL DATA

Job ID: 2971 Job Start: Fri Apr 21 21:18:57 UTC 2017
Release: lat.: 43.979000 lon.: -121.687000 Hgt: 2000 to 6000 m
Pollutant: Unit - Unspecified
Release Quantity: 1 mass Start: 15 04 20 12 0 Duration: 84 hrs, 0 min
Pollutant Averaging/Integration Period: 4 hrs and 0 min
Dry Deposition rate: 0 cm/s Wet Removal: None #Part: 94000
Meteorology: 0000Z 15 Apr 2015 - GDAS1
This is not a NOAA product. It was produced by: unknown

NOAA HYSPLIT MODEL
Dilution Factor (1/m3) averaged between 0 m and 4000 m
Integrated from 0800 23 Apr to 1200 23 Apr 15 (UTC)
Unit Release started at 1200 20 Apr 15 (UTC)

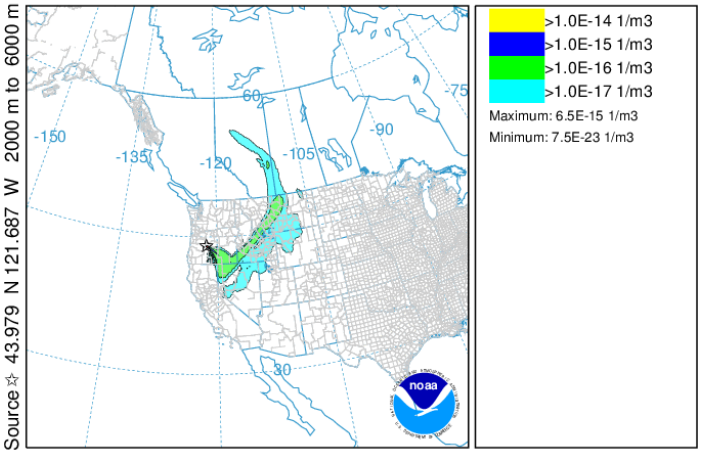

GDAS METEOROLOGICAL DATA

Job ID: 2971 Job Start: Fri Apr 21 21:18:57 UTC 2017
Release: lat.: 43.979000 lon.: -121.687000 Hgt: 2000 to 6000 m
Pollutant: Unit - Unspecified
Release Quantity: 1 mass Start: 15 04 20 12 0 Duration: 84 hrs, 0 min
Pollutant Averaging/Integration Period: 4 hrs and 0 min
Dry Deposition rate: 0 cm/s Wet Removal: None #Part: 94000
Meteorology: 0000Z 15 Apr 2015 - GDAS1
This is not a NOAA product. It was produced by: unknown

NOAA HYSPLIT MODEL
Dilution Factor (1/m3) averaged between 0 m and 4000 m
Integrated from 1600 23 Apr to 2000 23 Apr 15 (UTC)
Unit Release started at 1200 20 Apr 15 (UTC)

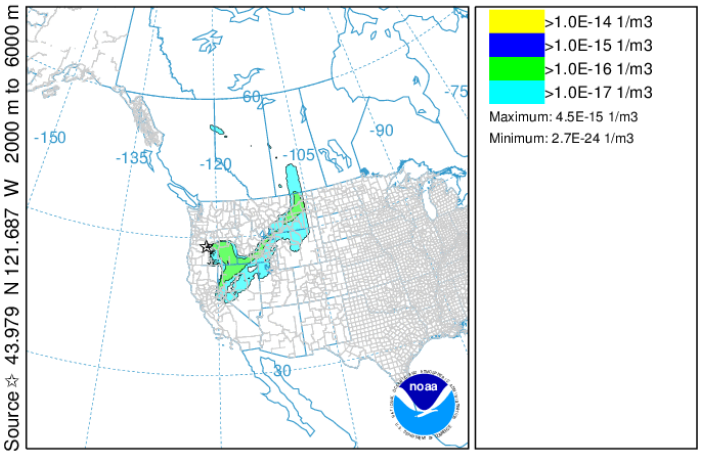

GDAS METEOROLOGICAL DATA

Job ID: 2971 Job Start: Fri Apr 21 21:18:57 UTC 2017
Release: lat.: 43.979000 lon.: -121.687000 Hgt: 2000 to 6000 m
Pollutant: Unit - Unspecified
Release Quantity: 1 mass Start: 15 04 20 12 0 Duration: 84 hrs, 0 min
Pollutant Averaging/Integration Period: 4 hrs and 0 min
Dry Deposition rate: 0 cm/s Wet Removal: None #Part: 94000
Meteorology: 0000Z 15 Apr 2015 - GDAS1
This is not a NOAA product. It was produced by: unknown

APPENDIX D

NAAPS GLOBAL AEROSOL MODEL FOR APRIL 2015

These are results from the Navy Aerosol Analysis and Prediction System (NAAPS) Global Aerosol Model (https://www.nrlmry.navy.mil/aerosol/) from 17-24 April 2015. Plots are presented in a 4-panel format, each 6 hours apart. Upper-left image is the total optical depth at a wavelength of 0.55μm for all NAAPS components: sulfate, dust, and smoke. Upper-right, lower-left, and lower-right images are the sulfate mass mixing ratio, dust mass mixing ratio, and smoke mass mixing ratio, respectively, (all in $\mu g/m^3$) at the surface.

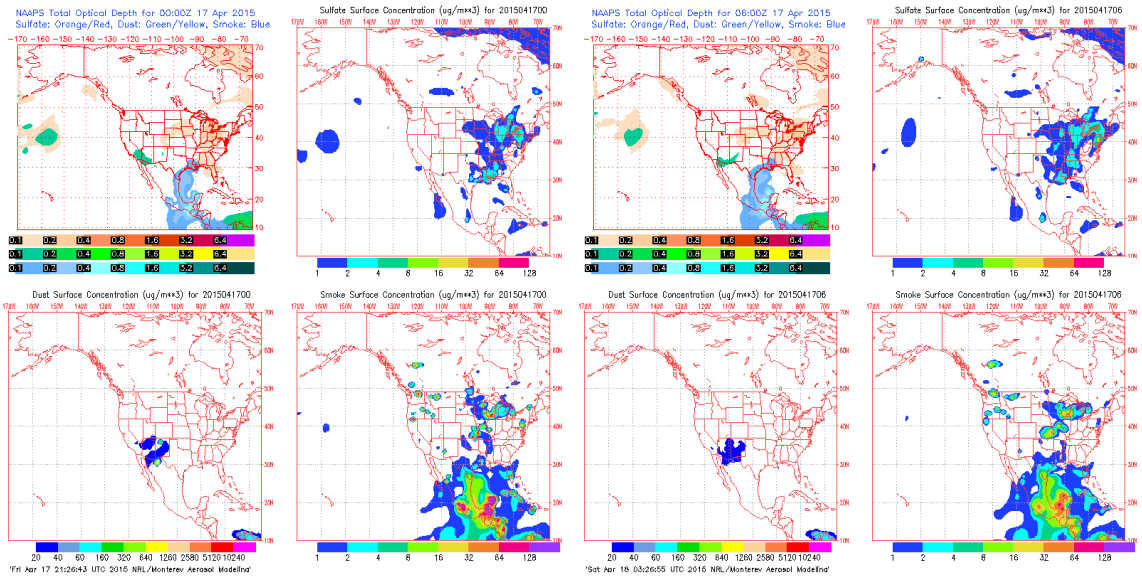

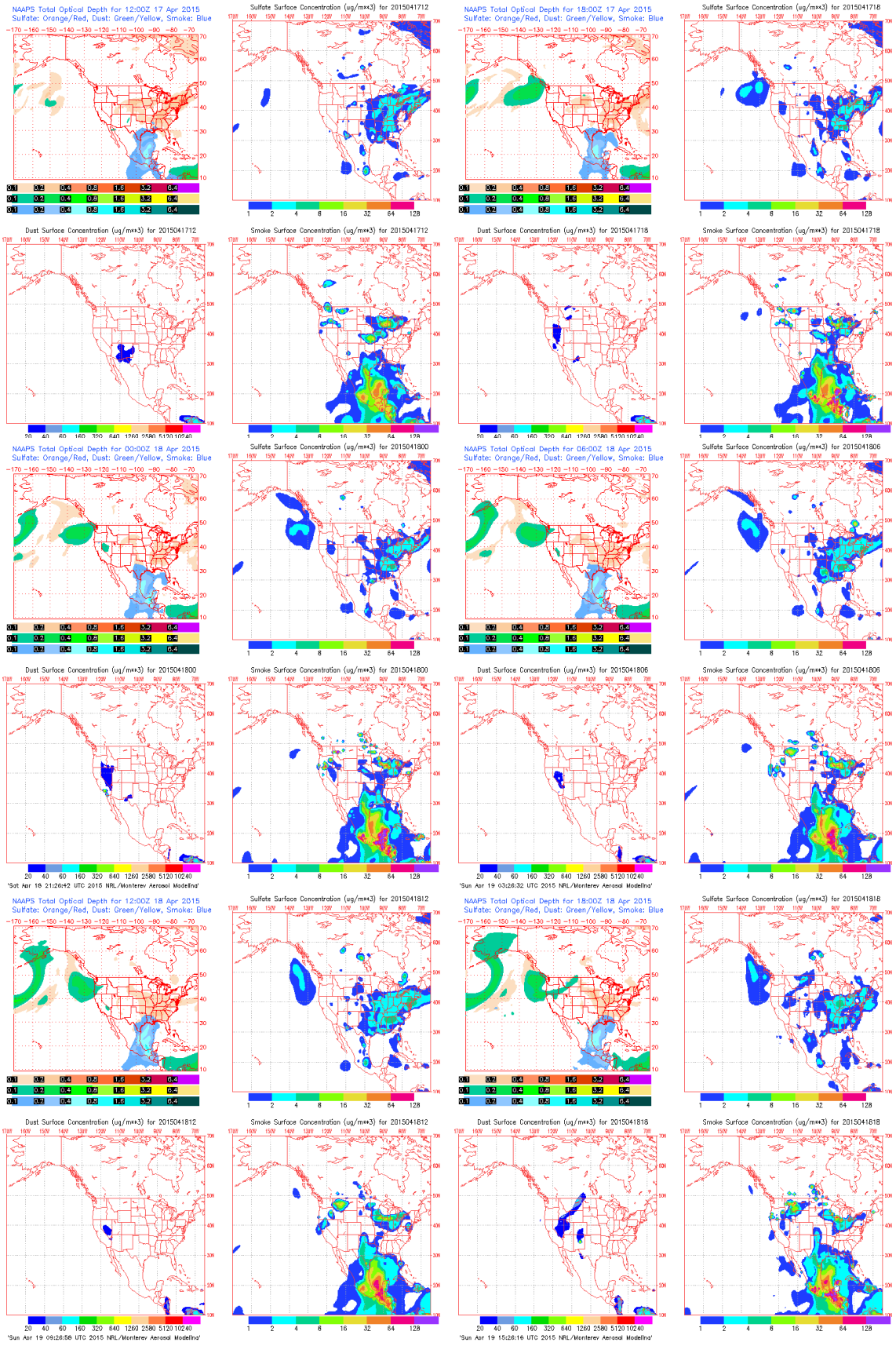
NAAPS Total Optical Depth for 12:00Z 17 Apr 2015
Sulfate: Orange/Red, Dust: Green/Yellow, Smoke: Blue
Sulfate Surface Concentration (ug/m**3) for 2015041712
NAAPS Total Optical Depth for 18:00Z 17 Apr 2015
Sulfate: Orange/Red, Dust: Green/Yellow, Smoke: Blue
Sulfate Surface Concentration (ug/m**3) for 2015041718
Dust Surface Concentration (ug/m**3) for 2015041712
Smoke Surface Concentration (ug/m**3) for 2015041712
Dust Surface Concentration (ug/m**3) for 2015041718
Smoke Surface Concentration (ug/m**3) for 2015041718
NAAPS Total Optical Depth for 00:00Z 18 Apr 2015
Sulfate: Orange/Red, Dust: Green/Yellow, Smoke: Blue
Sulfate Surface Concentration (ug/m**3) for 2015041800
NAAPS Total Optical Depth for 06:00Z 18 Apr 2015
Sulfate: Orange/Red, Dust: Green/Yellow, Smoke: Blue
Sulfate Surface Concentration (ug/m**3) for 2015041806
Dust Surface Concentration (ug/m**3) for 2015041800
Smoke Surface Concentration (ug/m**3) for 2015041800
Dust Surface Concentration (ug/m**3) for 2015041806
Smoke Surface Concentration (ug/m**3) for 2015041806
'Sat Apr 18 21:26:42 UTC 2015 NRL/Monterey Aerosol Modelina'
'Sun Apr 19 03:26:32 UTC 2015 NRL/Monterey Aerosol Modelina'
NAAPS Total Optical Depth for 12:00Z 18 Apr 2015
Sulfate: Orange/Red, Dust: Green/Yellow, Smoke: Blue
Sulfate Surface Concentration (ug/m**3) for 2015041812
NAAPS Total Optical Depth for 18:00Z 18 Apr 2015
Sulfate: Orange/Red, Dust: Green/Yellow, Smoke: Blue
Sulfate Surface Concentration (ug/m**3) for 2015041818
Dust Surface Concentration (ug/m**3) for 2015041812
Smoke Surface Concentration (ug/m**3) for 2015041812
Dust Surface Concentration (ug/m**3) for 2015041818
Smoke Surface Concentration (ug/m**3) for 2015041818
'Sun Apr 19 09:26:58 UTC 2015 NRL/Monterey Aerosol Modelina'
'Sun Apr 19 15:26:16 UTC 2015 NRL/Monterey Aerosol Modelina'

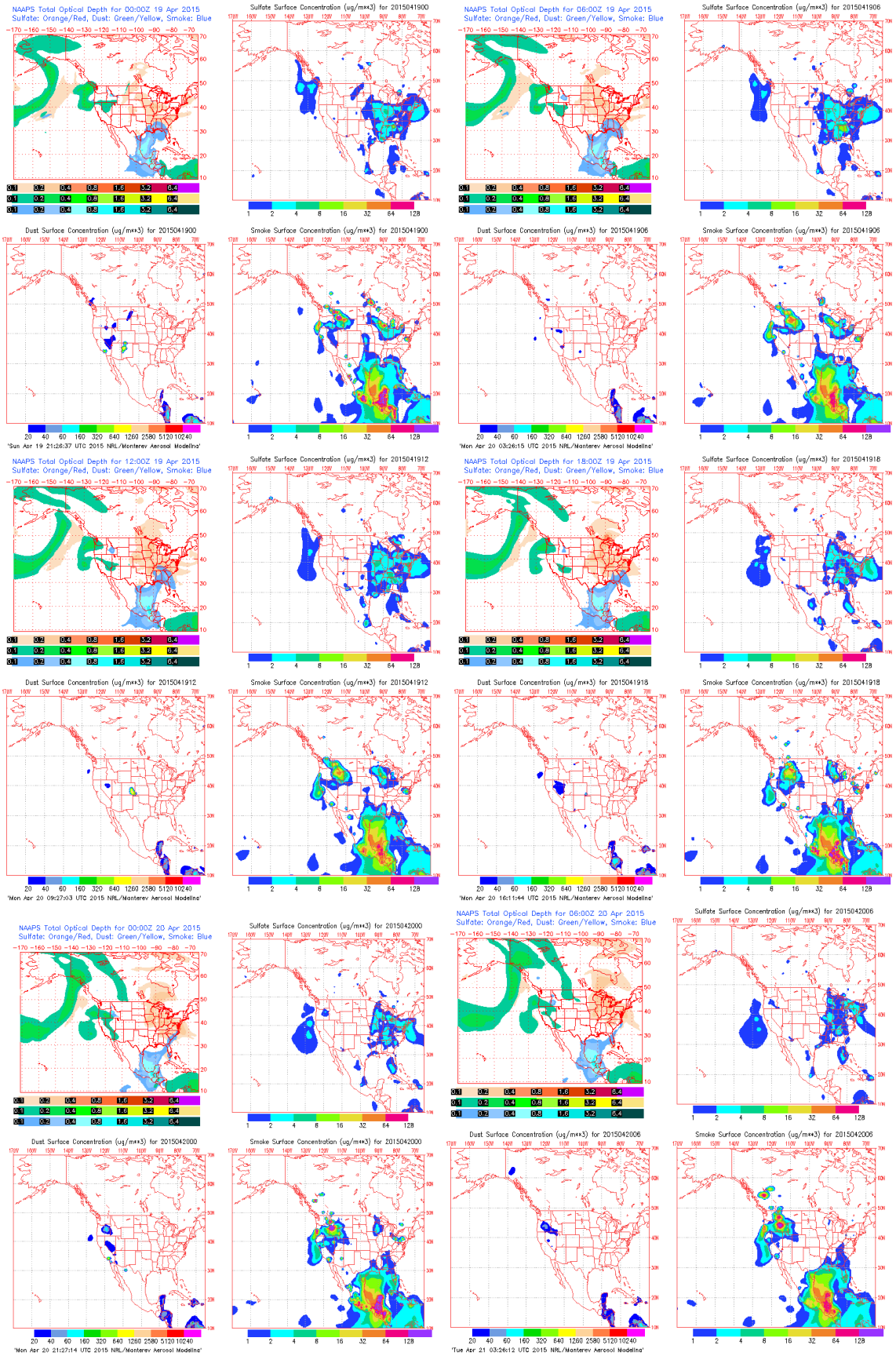
NAAPS Total Optical Depth for 00:00Z 19 Apr 2015
Sulfate: Orange/Red, Dust: Green/Yellow, Smoke: Blue
Sulfate Surface Concentration (ug/m**3) for 2015041900
NAAPS Total Optical Depth for 06:00Z 19 Apr 2015
Sulfate: Orange/Red, Dust: Green/Yellow, Smoke: Blue
Sulfate Surface Concentration (ug/m**3) for 2015041906
Dust Surface Concentration (ug/m**3) for 2015041900
Smoke Surface Concentration (ug/m**3) for 2015041900
Dust Surface Concentration (ug/m**3) for 2015041906
'Sun Apr 19 21:26:37 UTC 2015 NRL/Monterey Aerosol Modelina'
'Mon Apr 20 03:26:15 UTC 2015 NRL/Monterey Aerosol Modelina'
Smoke Surface Concentration (ug/m**3) for 2015041906
NAAPS Total Optical Depth for 12:00Z 19 Apr 2015
Sulfate: Orange/Red, Dust: Green/Yellow, Smoke: Blue
Sulfate Surface Concentration (ug/m**3) for 2015041912
NAAPS Total Optical Depth for 18:00Z 19 Apr 2015
Sulfate: Orange/Red, Dust: Green/Yellow, Smoke: Blue
Sulfate Surface Concentration (ug/m**3) for 2015041918
Dust Surface Concentration (ug/m**3) for 2015041912
Smoke Surface Concentration (ug/m**3) for 2015041912
Dust Surface Concentration (ug/m**3) for 2015041918
'Mon Apr 20 09:27:03 UTC 2015 NRL/Monterey Aerosol Modelina'
'Mon Apr 20 16:11:44 UTC 2015 NRL/Monterey Aerosol Modelina'
Smoke Surface Concentration (ug/m**3) for 2015041918
NAAPS Total Optical Depth for 00:00Z 20 Apr 2015
Sulfate: Orange/Red, Dust: Green/Yellow, Smoke: Blue
Sulfate Surface Concentration (ug/m**3) for 2015042000
NAAPS Total Optical Depth for 06:00Z 20 Apr 2015
Sulfate: Orange/Red, Dust: Green/Yellow, Smoke: Blue
Sulfate Surface Concentration (ug/m**3) for 2015042006
Dust Surface Concentration (ug/m**3) for 2015042000
Smoke Surface Concentration (ug/m**3) for 2015042000
Dust Surface Concentration (ug/m**3) for 2015042006
'Mon Apr 20 21:27:14 UTC 2015 NRL/Monterey Aerosol Modelina'
'Tue Apr 21 03:26:12 UTC 2015 NRL/Monterey Aerosol Modelina'
Smoke Surface Concentration (ug/m**3) for 2015042006

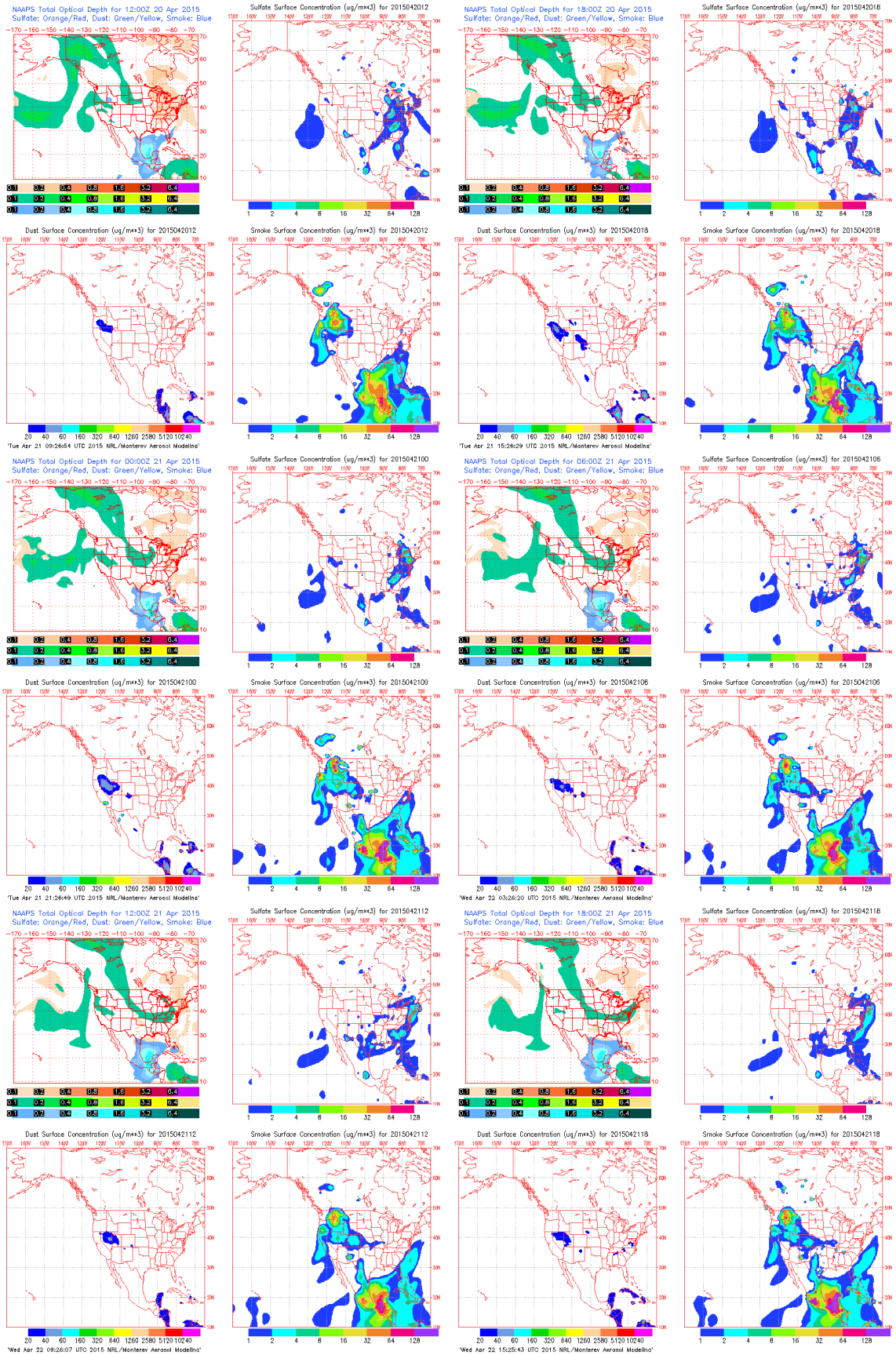
NAAPS Total Optical Depth for 12:00Z 20 Apr 2015
Sulfate: Orange/Red, Dust: Green/Yellow, Smoke: Blue
Sulfate Surface Concentration (ug/m**3) for 2015042012
NAAPS Total Optical Depth for 18:00Z 20 Apr 2015
Sulfate: Orange/Red, Dust: Green/Yellow, Smoke: Blue
Sulfate Surface Concentration (ug/m**3) for 2015042018
Dust Surface Concentration (ug/m**3) for 2015042012
'Tue Apr 21 09:26:54 UTC 2015 NRL/Monterey Aerosol Modelina'
Smoke Surface Concentration (ug/m**3) for 2015042012
Dust Surface Concentration (ug/m**3) for 2015042018
'Tue Apr 21 15:26:29 UTC 2015 NRL/Monterey Aerosol Modelina'
Smoke Surface Concentration (ug/m**3) for 2015042018
NAAPS Total Optical Depth for 00:00Z 21 Apr 2015
Sulfate: Orange/Red, Dust: Green/Yellow, Smoke: Blue
Sulfate Surface Concentration (ug/m**3) for 2015042100
NAAPS Total Optical Depth for 06:00Z 21 Apr 2015
Sulfate: Orange/Red, Dust: Green/Yellow, Smoke: Blue
Sulfate Surface Concentration (ug/m**3) for 2015042106
Dust Surface Concentration (ug/m**3) for 2015042100
'Tue Apr 21 21:26:49 UTC 2015 NRL/Monterey Aerosol Modelina'
Smoke Surface Concentration (ug/m**3) for 2015042100
Dust Surface Concentration (ug/m**3) for 2015042106
'Wed Apr 22 03:26:20 UTC 2015 NRL/Monterey Aerosol Modelina'
Smoke Surface Concentration (ug/m**3) for 2015042106
NAAPS Total Optical Depth for 12:00Z 21 Apr 2015
Sulfate: Orange/Red, Dust: Green/Yellow, Smoke: Blue
Sulfate Surface Concentration (ug/m**3) for 2015042112
NAAPS Total Optical Depth for 18:00Z 21 Apr 2015
Sulfate: Orange/Red, Dust: Green/Yellow, Smoke: Blue
Sulfate Surface Concentration (ug/m**3) for 2015042118
Dust Surface Concentration (ug/m**3) for 2015042112
'Wed Apr 22 09:26:07 UTC 2015 NRL/Monterey Aerosol Modelina'
Smoke Surface Concentration (ug/m**3) for 2015042112
Dust Surface Concentration (ug/m**3) for 2015042118
'Wed Apr 22 15:25:43 UTC 2015 NRL/Monterey Aerosol Modelina'
Smoke Surface Concentration (ug/m**3) for 2015042118

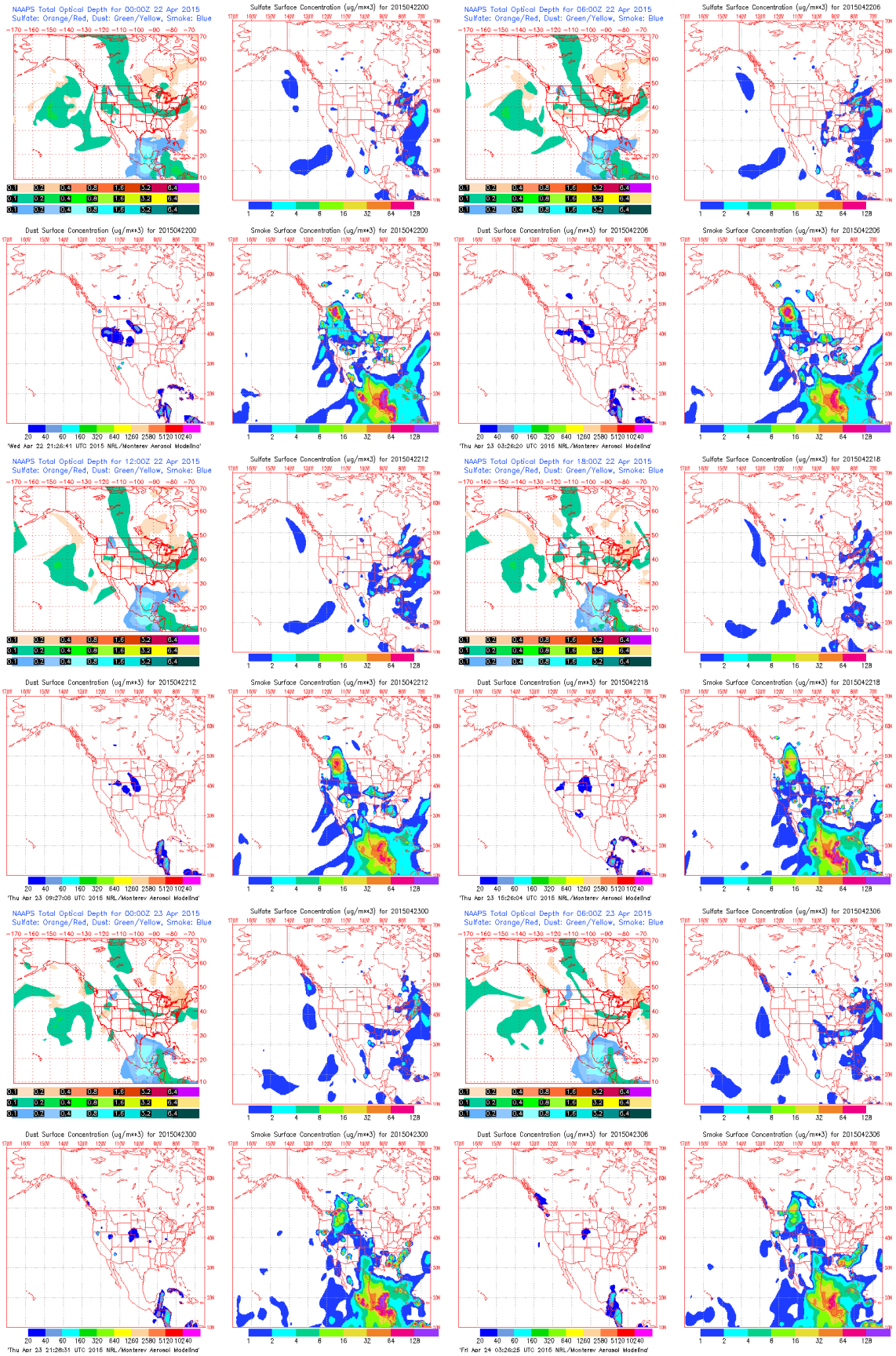
NAAPS Total Optical Depth for 00:00Z 22 Apr 2015
Sulfate: Orange/Red, Dust: Green/Yellow, Smoke: Blue
Sulfate Surface Concentration (ug/m**3) for 2015042200
NAAPS Total Optical Depth for 06:00Z 22 Apr 2015
Sulfate: Orange/Red, Dust: Green/Yellow, Smoke: Blue
Sulfate Surface Concentration (ug/m**3) for 2015042206
Dust Surface Concentration (ug/m**3) for 2015042200
'Wed Apr 22 21:26:41 UTC 2015 NRL/Monterey Aerosol Modelina'
Smoke Surface Concentration (ug/m**3) for 2015042200
Dust Surface Concentration (ug/m**3) for 2015042206
'Thu Apr 23 03:26:20 UTC 2015 NRL/Monterey Aerosol Modelina'
Smoke Surface Concentration (ug/m**3) for 2015042206
NAAPS Total Optical Depth for 12:00Z 22 Apr 2015
Sulfate: Orange/Red, Dust: Green/Yellow, Smoke: Blue
Sulfate Surface Concentration (ug/m**3) for 2015042212
NAAPS Total Optical Depth for 18:00Z 22 Apr 2015
Sulfate: Orange/Red, Dust: Green/Yellow, Smoke: Blue
Sulfate Surface Concentration (ug/m**3) for 2015042218
Dust Surface Concentration (ug/m**3) for 2015042212
'Thu Apr 23 09:27:08 UTC 2015 NRL/Monterey Aerosol Modelina'
Smoke Surface Concentration (ug/m**3) for 2015042212
Dust Surface Concentration (ug/m**3) for 2015042218
'Thu Apr 23 15:26:04 UTC 2015 NRL/Monterey Aerosol Modelina'
Smoke Surface Concentration (ug/m**3) for 2015042218
NAAPS Total Optical Depth for 00:00Z 23 Apr 2015
Sulfate: Orange/Red, Dust: Green/Yellow, Smoke: Blue
Sulfate Surface Concentration (ug/m**3) for 2015042300
NAAPS Total Optical Depth for 06:00Z 23 Apr 2015
Sulfate: Orange/Red, Dust: Green/Yellow, Smoke: Blue
Sulfate Surface Concentration (ug/m**3) for 2015042306
Dust Surface Concentration (ug/m**3) for 2015042300
'Thu Apr 23 21:26:31 UTC 2015 NRL/Monterey Aerosol Modelina'
Smoke Surface Concentration (ug/m**3) for 2015042300
Dust Surface Concentration (ug/m**3) for 2015042306
'Fri Apr 24 03:26:25 UTC 2015 NRL/Monterey Aerosol Modelina'
Smoke Surface Concentration (ug/m**3) for 2015042306

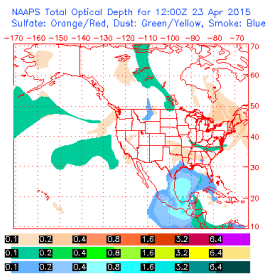
NAAPS Total Optical Depth for 12:00Z 23 Apr 2015
Sulfate: Orange/Red, Dust: Green/Yellow, Smoke: Blue

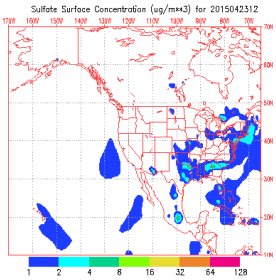
Sulfate Surface Concentration (ug/m**3) for 2015042312

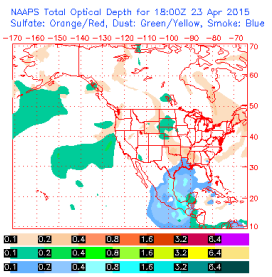
NAAPS Total Optical Depth for 18:00Z 23 Apr 2015
Sulfate: Orange/Red, Dust: Green/Yellow, Smoke: Blue

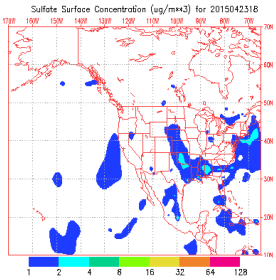
Sulfate Surface Concentration (ug/m**3) for 2015042318

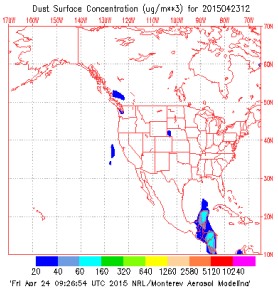
Dust Surface Concentration (ug/m**3) for 2015042312
'Fri Apr 24 09:26:54 UTC 2015 NRL/Monterey Aerosol Modeling'

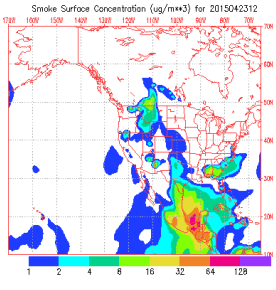
Smoke Surface Concentration (ug/m**3) for 2015042312

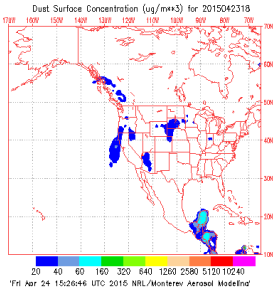
Dust Surface Concentration (ug/m**3) for 2015042318
'Fri Apr 24 15:26:46 UTC 2015 NRL/Monterey Aerosol Modeling'

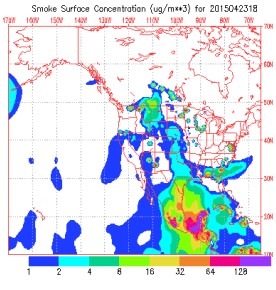
Smoke Surface Concentration (ug/m**3) for 2015042318

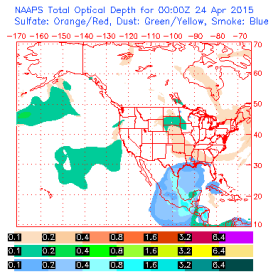
NAAPS Total Optical Depth for 00:00Z 24 Apr 2015
Sulfate: Orange/Red, Dust: Green/Yellow, Smoke: Blue

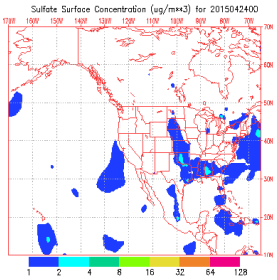
Sulfate Surface Concentration (ug/m**3) for 2015042400

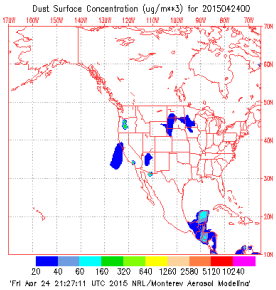
Dust Surface Concentration (ug/m**3) for 2015042400
'Fri Apr 24 21:27:11 UTC 2015 NRL/Monterey Aerosol Modeling'

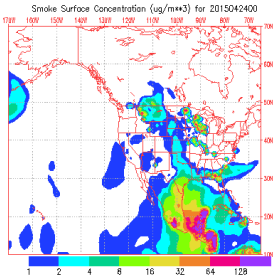
Smoke Surface Concentration (ug/m**3) for 2015042400

VITA

Pao Baylon was born in Tacloban City, Philippines. He finished his BS Physics degree from Ateneo de Manila University in 2010 and then pursued a one-year postgraduate diploma in Earth System Physics at the Abdus Salam International Center for Theoretical Physics in Trieste, Italy. He moved to Seattle in 2011 to start his graduate studies at the University of Washington's Atmospheric Sciences department. Pao is passionate about photography, traveling, volleyball, teaching, and cooking. He likes to hike, to eat out with his friends, and to learn about different cultures. He cares about the following causes: education, environment, and poverty alleviation.